Innovative antifouling technologies: microtexture and metal

Thesis submitted by
Matthew John Vučko BSc, MSc
In June 2014

for the degree of Doctor of Philosophy
in the Centre for Sustainable Tropical Fisheries and Aquaculture
School of Marine and Tropical Biology
James Cook University

Statement on the contribution of others

Financial support for this research was provided by the School of Marine and Tropical Biology and the Graduate Research School of James Cook University (JCU), and the Commonwealth Scientific and Industrial Research Organisation (CSIRO). Stipend support was provided by JCU with a Postgraduate Research Scholarship and by CSIRO with a Postgraduate Studentship.

My primary supervisor Rocky de Nys (JCU, Townsville, Queensland, Australia) and secondary supervisors Andrew Poole (CSIRO, Waurn Ponds, Victoria, Australia) and Peter King (CSIRO, Clayton, Victoria, Australia) provided intellectual guidance, financial support and editorial assistance.

Mathew Vickers and Nicholas Paul (JCU, Townsville, Queensland, Australia) provided statistical support. Christina Carl (JCU, Townsville, Queensland, Australia) and Steve Whalan (Southern Cross University, Lismore, New South Wales, Australia) provided editorial assistance and helped with the culture of animals and with experimental assays (Chapters 2 and 3).

Fiona Glenn and Brett Sexton (CSIRO, Clayton, Victoria, Australia) provided microtextured surfaces (Chapter 2) and Sue Horne provided photocatalytic matrices (Chapter 3).

All work involving scanning electron microscopy, energy dispersive X-ray spectroscopy and atomic force microscopy was performed at the Advanced Analytical Centre (AAC) of JCU (Chapters 2 and 4).

The work involving the focused ion beam scanning electron microscope was performed at the Melbourne Centre for Nanofabrication, which is the Victorian node of the Australian National Fabrication Facility, an initiative partly funded by the Commonwealth of Australia and the Victorian Government (Chapter 4).

Peter King and Mahnaz Jahedi (CSIRO, Clayton, Victoria, Australia) produced all cold spray metal-embedded surfaces (Chapters 4, 5, 6 and 7).

Yi Hu (AAC of JCU, Townsville, Queensland, Australia) analysed all water samples obtained for release rate measurements (Chapters 6 and 7).

Finally, the Townsville Yacht Club provided their facilities for all field trials done throughout this research.

Acknowledgements

Many amazing people have supported me and contributed to the success of this thesis and I have been very lucky to have such a great supervisory team, always enthusiastic and ready to help, each with strengths that complement the others.

First and foremost, I would like to thank my primary supervisor Rocky de Nys. You have an unwavering ability to make the worst situation seem like a walk in the park. One meeting with you and my faith in research is restored. You have given me the skills and confidence to write effectively and become a scientist and no matter how busy you get, you always had time to meet, discuss and read whatever it is I had for you. I will forever be indebted and am very grateful to have been your student.

Thank you to Andrew and Peter, my associate supervisors. They too have provided invaluable advice and support throughout this thesis. Andrew, you were always able to see things in a different perspective, while Peter, you helped me see the smaller side of things and taught me that sometimes the overall picture isn't as important as is the miniscule details.

Thank you to Tine, Hugh, Scott, Sarah, Pedro, Zou Zou, Ian, Marie, Kerri, Vero, Boer, Andrew and the ever changing de Nys lab group who have always been supportive. Special thanks to Michelle Condy for passing the reigns over to me and teaching me everything I needed to know to get started in this field.

I would also like to thank many of the amazing people at James Cook University for helping me along the way. Ross Barrett from the workshop, Vince Pullella and Gordon Bailey ffrom IT, Simon Wever and Ben Lawes from MARFU, Stratis Manolis and Greg Jameson from the biological store, Julie Fedorniak from vehicles and Karen Wood

from the finance office. Many thanks to the team at the Advanced Analytical Centre, Shane Askew, Kevin Blake and Yi Hu, for their expertise and help over the past three years. They have been essential to the success of the research found in this thesis.

I would like to thank Mark Cruickshank, Jo Hassett and Kerri Hauser from the Townsville Yacht Club for their continued support over the years and Kevin Tilbrook from the Museum of Tropical Queensland for his invertebrate expertise. Thank you to Susan McGrath and Kristin Nunn for years of support and always having answers to my questions. I would also like to thank Lin Schwarzkopf for introducing me to Rocky. Without your recommendation I never would have started down this path.

Thank you to all of the anonymous reviewers whose comments, criticisms and expertise in the field of biofouling improved each one of the manuscripts published from this thesis.

Thank you to my family, especially my parents Mary and Steve, who have always been supportive throughout my postgraduate studies and my time away from Canada. Thank you to all my friends, from Australia and Canada, for years of friendship, good times and support through the not so good times. A special thanks to Betsy for her battery.

Lastly, but certainly not least, thank you to my wife Anne. Having a child together while doing a PhD might seem like a challenge, but it has made me work harder than ever before never knowing what the next day will bring. Who knew something so small could have such a profound effect on one's life, thanks for the good times Littleman. Anne, you have been by my side through it all and only you will know what I have truly gone through to accomplish this. Thank you for your love, support and encouragement, I could not have done it without you.

Abstract

Fouling causes negative economic impacts to the major marine industries of shipping, aquaculture and geophysical exploration. Currently, the most widely used method to prevent the accumulation of fouling is copper-based biocidal antifouling paints. However, their deleterious impact on the marine environment and non-target organisms is driving the need to develop environmentally-sustainable antifouling technologies. Innovative antifouling technologies employing microtexture, photocatalysts and cold spray metal embedment are promising alternatives to current antifouling paints. This thesis investigates these alternative technologies to identify their efficacy across both niche and broad spectrum antifouling applications.

In Chapter 2, a series of 18 textured (0.4–1,000 μm) and non-textured (0 μm) polydimethylsiloxane (PDMS) surfaces with round- and square-wave linear grating profiles were tested for their antifouling potential against the settlement of fouling organisms in the laboratory and in the field against the recruitment of a multi-species fouling community. In laboratory assays, *Nitzschia closterium* and *Amphora* sp. were deterred by all surface topographies regardless of texture periodicity. Settlement of *Ulva* sp. was lower on texture sizes less than propagule size, and settlement of *Saccostrea glomerata* and *Bugula neritina* was lower on texture sizes closest to, but less than, larval sizes. After the six month field trials, all textured surfaces lost their deterrent effect, however, the foul-release capabilities of textures were still present. High initial attachment was correlated with more fouling remaining after removal trials, indicating that fouling recruited in higher numbers to surfaces upon which they attached most strongly.

In Chapter 3, the potential for a photocatalyst to enhance the antifouling properties of microtexture was examined. PDMS surfaces, textured with a square-wave linear grating profile (0, 20, 200, 300 and 600 μm), were embedded with a range of photocatalytic titanium dioxide (TiO_2) nanoparticle loadings (3.75, 7.5, 11.25 and 15 wt%). The resulting surfaces were used to test the combined efficacy of these technologies as antifouling materials in the laboratory and in the field against the common fouling bryozoan, *B. neritina*. Settlement of *B. neritina* was quantified in the laboratory under two intensities of ultraviolet light. The lowest settlement rates were observed on 20 μm surfaces. However, texture effects were not as critical to larval settlement as the presence of TiO_2. TiO_2, in conjunction with ultraviolet light, completely inhibited larval metamorphosis even at the lowest loading (3.75 wt%) and the lowest intensity of ultraviolet light (24 W m^{-2}). Recruitment of *B. neritina* during field trials showed similar results to laboratory assays. The lowest recruitment occurred on 20 and 200 μm surfaces, with recruitment being significantly lower on all surfaces containing TiO_2. Therefore for *B. neritina*, although all TiO_2 loadings were effective, 3.75 wt% can be used as a minimum inhibitory concentration to deter larval settlement and the addition of a 20 μm texture further increases the deterrent effect.

In Chapter 4, the use of cold spray technology to give antifouling properties to thermoplastic polymers (polymers) by embedding metals known to prevent fouling was investigated. Two polymers, high-density polyethylene (HDPE) and nylon were metallised with copper powder using cold spray technology. After 250 days in the field, copper-embedded HDPE and copper plate controls were completely free of hard foulers compared to copper-embedded nylon and polymer controls which were heavily fouled with both soft and hard fouling. The success of copper-embedded polymers is related to the interaction between the properties of the polymers (elastic modulus and hardness) and the cold spray process which affect particle embedment depth, and subsequently, the release of copper ions as determined by analytical techniques. This chapter demonstrates that embedding metal particles using cold spray equipment is an effective antifouling technology for polymers, in particular those that are difficult to treat with standard copper-based biocide paints.

Furthermore, efficacy is a function of the interaction between the cold spray metal and the polymer recipient.

In Chapter 5, cold spray metal embedment was used to determine the effects of loading densities of metal particles on fouling. Antifouling efficacy under field conditions was quantified for low (22.1 ± 4.8 g m^{-2}) and high (101.1 ± 10.8 g m^{-2}) densities of copper particles embedded into polyurethane seismic streamer skins, which are used in geophysical exploration. Failure of each copper-embedded treatment was defined as settlement of hard foulers. Low-density streamers failed after 42 days while high-density streamers failed after 210 days. Most importantly, the high-density streamers were completely free of hard foulers including the barnacle *Amphibalanus reticulatus* during this time. In conclusion, cold spray metal embedment is an effective antifouling technology for polyurethane seismic streamer skins, under intense fouling conditions. Higher copper particle densities enhance antifouling longevity and the effect of density provides a tool to extend efficacy and enhance antifouling performance for specific polymers.

Finally, in Chapter 6, loading density gradients of metal particles were investigated. Particles of copper, bronze and zinc metal were embedded into a polymer using cold spray technology to produce loading density gradients. The gradients were used to identify the species with the highest tolerance to the release of copper and zinc ions. The gradients also established the minimum effective release rates (MERRs) of copper and zinc ions needed to prevent the recruitment of fouling under field conditions. *Watersipora* sp. and *Simplaria pseudomilitaris* had the highest tolerance to the release of metal ions. Copper and bronze gradient tubes were similar in their MERRs of copper ions against *Watersipora* sp. (0.058 g m^{-2} h^{-1} and 0.054 g m^{-2} h^{-1}, respectively) and against *S. pseudomilitaris* (0.030 g m^{-2} h^{-1} and 0.025 g m^{-2} h^{-1}, respectively). Zinc was not an effective antifouling material with failure within two weeks. The cold spray gradients were effective in determining MERRs and these outcomes provide the basis for the development of cold spray surfaces with pre-determined life-spans using controlled MERRs.

In summary, the research presented throughout this thesis describes innovative antifouling technologies that can be used as alternatives to current antifouling paints. In addition, this thesis identifies the efficacy of these technologies across niche and broad spectrum antifouling applications, while highlighting the importance of field-based trials. The incorporation of microtexture and a photocatalyst to already successful foul-release coatings, allows for further improvement of those materials. In addition, the use of cold spray technology as an innovative method to give antifouling properties to thermoplastic polymers has been thoroughly investigated and provides a promising avenue for future research and commercialisation. In conclusion, this thesis provides a significant contribution to the relatively new field of environmentally-sustainable antifouling technologies and provides an innovative method to give antifouling properties to materials that previously, could not be protected against fouling.

Table of contents

Vucko MJ, Poole AJ, Carl C, Sexton BA, Glenn FL, Whalan S and de Nys R (2014). Using textured PDMS to prevent settlement and enhance release of marine fouling organisms. *Biofouling* 30: 1-16.

Vucko MJ, Poole AJ, Sexton BA, Glenn FL, Carl C and de Nys R (2013). Combining a photocatalyst with microtopography to develop effective antifouling materials. *Biofouling* 29: 751-762.

Vucko MJ, King PC, Poole AJ, Carl C, Jahedi MZ and de Nys R (2012). Cold spray metal embedment: an innovative antifouling technology. *Biofouling* 28: 239-248.

Vucko MJ, King PC, Poole AJ, Jahedi MZ and de Nys R (2013). Polyurethane seismic streamer skins: an application of cold spray metal embedment. *Biofouling* 29: 1-9.

Vucko MJ, King PC, Poole AJ, Hu Y, Jahedi MZ and de Nys R (2014). Assessing the antifouling properties of cold spray metal embedment using loading density gradients of metal particles. *Biofouling* 30: 651-666.

List of tables

Chapter 5

Chapter 6

List of figures

Chapter 2

Chapter 3

Chapter 4

Chapter 5

Chapter 6

Chapter 1

General introduction

1.1 The progression of marine biofouling and its economic impact

Marine biofouling (fouling) is characterised by the accumulation of biological communities on surfaces submerged in seawater (Briand 2009). These communities include soft fouling species such as bacteria, diatoms and algae, and hard fouling species such as bryozoans, tubeworms, barnacles and mussels (Prendergast 2010). A variety of factors and processes facilitate the settlement (attachment of fouling larvae) and recruitment (any stage after settlement) of marine fouling. They include surface texture (Aldred and Clare 2008; Scardino et al. 2008; Long et al. 2010; Scardino and de Nys 2011), surface wettability (Dahlström et al. 2004; Zhang et al. 2005; Bennett et al. 2010), elastic modulus of the surface (Chaudhury et al. 2005), submersion depth of the surface (Cowie 2010), surface colour (Swain et al. 2006; Carl et al. 2011), physical, chemical and biological surface-associated cues (Pawlik 1992; Huang and Hadfield 2003; Dahlström et al. 2004; Qian, Xu, and Fusetani 2010), species availability depending on geographic location (Canning-Clode and Wahl 2010), the presence of conspecifics (Elbourne et al. 2008), seasonality (Jenkins and Martins 2010) and environmental conditions such as salinity, flow rate, temperature, ultraviolet irradiation and nutrient availability (Prendergast 2010). The process of fouling in a natural environment results in a complex three-dimensional community that will continue to develop and change, with ongoing settlement and recruitment of fouling, until the surface is removed from the water. Regardless of this complexity one thing remains consistent, fouling in the marine environment causes substantial negative impacts when it occurs on artificial structures made by humans.

Fouling causes negative effects on water intakes for power stations and desalination plants (Henderson 2010) as well as offshore oil and gas platforms (Page et al. 2010) and the deep sea structures associated with them (Apolinario and Coutinho 2009). Fouling also impedes the functional capacity of vessels (Edyvean 2010; Schultz et al. 2011), aquatic infrastructure associated with aquaculture (de Nys and Guenther 2009; Fitridge et al. 2012) and structures used within the geophysical exploration industry (Vignaux 2010; Harrick and Stenzel 2011; Poole et al. 2012). Fouling on the hull of a ship will increase roughness which will subsequently increase hydrodynamic drag and therefore fuel consumption and lateness penalties (Townsin 2003; Schultz et al. 2011). Fouling on cages and netting used in aquaculture causes decreases in cage volume, flow and buoyancy while it increases physical damage and deformation as well as cage weight and therefore mooring stress (Braithwaite and McEvoy 2005; Fredriksson et al. 2007; Moe et al. 2009; Fitridge et al. 2012). Finally, fouling on seismic streamers skins, used to protect sensitive electronic equipment in geophysical exploration, causes reductions in seismic data quality and increases in equipment failure, feedback noise, hydrodynamic drag and therefore fuel consumption (Harper 1995; Vignaux 2010; Harrick and Stenzel 2011). The negative impacts associated with fouling have existed for thousands of years; for as long as humans have been using the marine environment. Consequently, attempts to deter and control the problem of fouling using antifouling technologies have also existed from the first uses of the marine environment.

1.2 Past antifouling technologies

Written records exist from as early as the 5th century B.C. citing treatments to mitigate the negative effects of fouling on ships, however, the search for suitable antifouling solutions most likely began even earlier (reviewed in WHOI 1952a; Yebra et al. 2004). Early treatments used to prevent fouling consisted of coating the bottoms of ships in pitch, wax, tar and asphalt as well as arsenic and sulphur mixed with oil (reviewed in Callow 1990). Lead sheathing was introduced in the 3rd century B.C., and between the

16th and 18th centuries was the most common form of ship cladding, even though it was not an effective deterrent against fouling in general, but mainly protected against marine borers (Yebra et al. 2004). The first successful form of antifouling was copper sheathing, and its use brought an end to earlier, unsuccessful antifouling treatments. Although copper was suggested as an antifoulant in 1625 in a patent presenting a mixture of a copper substance, cement and powdered iron, the first trial properly documenting the deterrent effect of copper, in the form of sheathing, was in 1758 on a warship in the British Navy (WHOI 1952a). After the success of that trial, copper sheathing was widely used in the British Navy for the next 40 years. At the end of the 18th century, the increasing use of iron ships led to the cessation of the use of copper sheathing due to its corrosive effects on iron, as well as a renewed necessity to find effective antifouling treatments (WHOI 1952a). Many alternatives were suggested, the most promising of which were paints consisting of an antifoulant such as copper oxide or mercury oxide, and a solvent such as turpentine or benzene which were bound together using resin or shellac varnish (Yebra et al. 2004). These formulations led to the production of modern-day antifouling paints, which were able to prevent fouling for up to 18 months by the early 1900's (WHOI 1952a). In the 1950's, these paints were further improved by the incorporation of organotins, within which the tri-butyl-tin (TBT) functional group was extremely effective at preventing fouling due to its strong biocidal activity towards a range of fouling organisms (Dubey and Roy 2003; Yebra et al. 2004).

Initially, TBT was only available within an insoluble polymer matrix which lasted for 18 months prior to failure with the recruitment of fouling. The introduction of TBT within a soluble polymer matrix improved the paint as an antifoulant; but it was not efficient under low flow conditions, and the solubility of the paint caused it to erode too quickly at high speeds (Yebra et al. 2004). This led to the formulation of a TBT self-polishing copolymer which allowed a controlled release of TBT, where pigment particles eroded to continually expose the surface underneath, producing a polishing effect (Kiil et al. 2001; Chambers et al. 2006). The result of this polishing was a reduction in the roughness of the hull which led to a reduction in fuel consumption

and emissions as well as direct savings of more than two billion USD a year globally (Abbott et al. 2000; Champ 2000; Almeida et al. 2007). By the 1980's, the TBT self-polishing copolymer was used on more than 80% of the world's commercial fleet (Abbott et al. 2000). The TBT self-polishing copolymer was one of the most successful antifouling coatings in history with the caveat that it was extremely toxic towards non-target organisms and the broader environment, both of which have been widely documented (reviewed in Champ 2000; Terlizzi et al. 2001). For example, in addition to TBT's acute toxicity to fouling organisms and fish (Martin et al. 1989; Dubey and Roy 2003), it is also persistent in sediment (MacGuire 2000), causes sterilization, imposex, reduced reproduction and deformations in molluscs (Bryan et al. 1987; Alzieu 1991), and has a high affinity for bioaccumulation in non-target organisms (Weidenhaupt et al. 1997; MacGuire 2000). These negative effects forced a total ban of TBT on ships < 25 m in length and a restriction on the release rates of compounds containing TBT by 2008 (Champ 2001; Yebra et al. 2004). Consequently, there was a renewed urgency to find a suitable alternative in the form of a tin-free antifouling coating.

1.3 Present-day antifouling technologies

Presently, the most widely used antifouling products are paint formulations that consist of copper oxide, which is soluble in seawater, combined with an organic booster biocide (Brooks and Waldock 2009; Finnie and Williams 2010). The toxicity of copper in marine invertebrates occurs directly through the absorption of waterborne free Cu^{+} and Cu^{2+} ions, arguably the most toxic form of the metal (Pinho et al. 2007; Brooks and Waldock 2009; Thomas and Brooks 2010). The mechanism of toxicity of copper is associated with the inhibition of the activity of the carbonic anhydrase enzyme, impairing gas exchange and acid–base regulation, and the inhibition of Na^{+}- and K^{+}-ATPase activity, causing intracellular ion imbalances (Grosell et al. 2007; Lopes et al. 2011). However, copper is only effective within the boundary layers of the antifouling surface, and is less toxic when released into the environment as a result of

the complexation of copper with dissolved organic carbon in the water column and a low bioavailability of copper within sediments (Voulvoulis et al. 1999; Lu and Allen 2001; Brooks et al. 2008; Brooks and Waldock 2009; Thomas and Brooks 2010). In addition, the leaching of copper from antifouling coatings into the natural environment comprises only ~1% of the total influx, the rest of which comes from natural weathering of the land (Brooks and Waldock 2009). Therefore, apart from enclosed harbours where the release of copper from many stationary vessels may reach unacceptable levels, the use of copper alone is acceptable for the purposes of antifouling.

Copper ions are effective against a broad range of fouling organisms, though hard fouling species such as barnacles and tubeworms are more susceptible to the toxicity of copper than soft fouling species such as diatoms and algae (Finnie and Williams 2010). Therefore, to prevent species which may be tolerant to lower release rates of copper ions, paint formulations have been improved by incorporating booster biocides (Voulvoulis et al. 1999). Currently, approximately 18 biocidal compounds are in use worldwide but for many of these compounds, especially those that are not readily available, there is limited data describing their long-term effects on the aquatic environment (Thomas 2009). For biocides that are most commonly used, there is substantial variation in the chemical and physical properties surrounding their toxicity to fouling, toxicity to non-target organisms, leaching rates, solubility and persistence in the environment (reviewed in Thomas 2009). For example, Irgarol 1051 and Diuron both disrupt the photosynthetic process in algae and are toxic to non-target organisms (Liu et al. 1999; Voulvoulis et al. 1999; Evans et al. 2000; Giacomazzi and Cochet 2004; Yebra et al. 2004). However, Irgarol 1051 has higher leaching rates with lower solubility, and a longer half-life in marine sediments compared to Diuron (Tóth et al. 1996; Thomas 2009). The diversity in initial chemical properties and deleterious effects on the marine environment and non-target organisms has resulted in restrictions and bans which vary for each of the 18 biocides depending on geographic location and legislation of the accompanying country (Thomas 2009).

In addition to the obvious concerns surrounding the booster biocides, a further drawback to copper-based biocide paints is their poor adhesion to thermoplastic polymers. Marine industries, including aquaculture and geophysical exploration, which rely on the use thermoplastic polymers, cannot employ copper-based biocide paints, which are designed for inflexible surfaces. Instead, cages and netting used in aquaculture, produced using high-density polyethylene and nylon are coated in flexible waxy emulsions incorporating copper. The typical life span of these waxy emulsions prior to failure is between 6 to 9 months, much shorter than copper-based biocide paints which have a lifespan of approximately 36 months (reviewed in Braithwaite and McEvoy 2005; Braithwaite et al. 2007; de Nys and Guenther 2009; Finnie and Williams 2010; Guenther et al. 2010). In addition, no functional coatings exist for seismic streamers where polyurethane, which is relatively soft, flexible and hydrophobic, is handled mechanically during operation on specialised exploration vessels (Poole et al. 2012).

1.4 Alternatives to present-day antifouling technologies

Issues with copper-based biocide paints have led to the conceptualisation and testing of many alternative environmentally-sustainable antifouling treatments (Omae 2003; Callow and Callow 2011). Here, microtexture, photocatalysts and cold spray metal embedment are introduced and examined for their potential as antifouling technologies, which are the focus of subsequent chapters of this thesis. The need for non-toxic alternatives to booster biocides has shifted the focus of antifouling technologies from examining the chemical properties of a surface to examining the physical properties of a surface. By manipulating the physical properties of a surface, it can be less desirable to fouling or reduce the attachment strength of fouling making it easier to remove (Callow and Callow 2009). These surface-based technologies are the most promising alternative (Webster and Chisholm 2010) and rely on the modification of structural, mechanical and polarization properties of a surface in an effort to maximise the antifouling or foul-release capabilities of the material (Rosenhahn et al.

2008). In addition, photocatalysis is a potential broad-spectrum alternative to enhance surface-based technologies. In the marine environment, photocatalysts can cause a decrease in larval adhesion strength and even mortality of the larvae of macrofouling organisms (Carl et al. 2012b). Although they have the potential to negatively affect settling organisms, they are not persistent in the environment and are unlikely to affect non-target organisms (Bhatkhande et al. 2002). Nevertheless, they are not currently used in marine antifouling and offer a promising avenue as a broad spectrum antifouling technology which can prevent the formation of biofilms and the settlement of a range of marine fouling organisms. Finally, the need to develop new antifouling treatments for thermoplastic polymers has led to the investigation of cold spray metal embedment, a relatively new innovation (Papyrin et al. 2007). Cold spray technology is used to embed small amounts of pure metal particles into thermoplastic polymers without compromising polymer properties (Poole et al. 2012; Vucko et al. 2012; Chapter 4). The use of metal to prevent fouling is not a new concept, as has been discussed previously however, by applying pure metal particles that are known to prevent fouling, thermoplastic polymers can be given antifouling properties while maximising longevity.

1.4.1 Microtextures

The manipulation of surfaces for the purpose of antifouling has been examined extensively with the modification of elastic modulus (Brady and Aronson 2003; Chaudhury et al. 2005), charge (Rasmussen and Østgaard 2001; Petrone et al. 2011), amphiphilicity (Joshi et al. 2009; Martinelli et al. 2012), wettability (Finlay et al. 2002; Aldred et al. 2006; Carman et al. 2006; Petrone et al. 2011; Carl et al. 2012a; Bloecher et al. 2013; Di Fino et al. 2014) and microtexture (Callow et al. 2002; Schumacher et al. 2007a; Schumacher et al. 2007b; Carl et al. 2012a). These studies have provided the foundation from which we can further advance our understanding of the parameters contributing to larval settlement. Ultimately, a combination of these properties will be needed to successfully develop materials that are effective. Yet isolating specific surface properties and investigating their effects alone is fundamental to

understanding their relative importance when combining properties for the ultimate antifouling or foul-release material.

Currently, foul-release coatings, which are being applied commercially (Townsin and Anderson 2009), are produced using materials with low surface energies such as silicone elastomers and fluoropolymers (Webster and Chisholm 2010). To date, the most successful of the foul-release materials is polydimethylsiloxane (PDMS; Anderson et al. 2003). Although, these coatings do not necessarily prevent the settlement of fouling, the low-surface energy of the material makes it easier to remove fouling after settlement with the use of hydrodynamic shear forces (Kavanagh et al. 2005; Wendt et al. 2006; Finnie and Williams 2010). However, these coatings are only effective for organisms that adhere poorly and are easily removed (Finlay et al. 2002; Bennett et al. 2010), while other organisms attach well, making removal more difficult (Finlay et al. 2002; Finlay et al. 2010). In addition, foul-release coatings are not suitable for slow-moving vessels or stationary marine structures due to their dependence on hydrodynamic forces. Therefore, to improve the efficacy of foul-release coatings, incorporating microtexture into a known foul-release material may enhance the antifouling and foul-release capabilities of that material.

Microtexture is a key element affecting the settlement of marine fouling invertebrates (Bers and Wahl 2004; Long et al. 2010; Scardino and de Nys 2011). The physical component of a surface provides contact points that facilitate attachment, settlement, and in many cases metamorphosis. There is a positive correlative effect between the number of attachment points available on a surface and the settling success of fouling organisms (Callow et al. 2002; Scardino et al. 2006; Scardino et al. 2008). This has been demonstrated for diatoms (Scardino et al. 2006), algae (Callow et al. 2002; Schumacher et al. 2007a; Schumacher et al. 2007b), bryozoans (Scardino et al. 2008), tubeworms (Scardino et al. 2008), barnacles (Berntsson et al. 2000; Schumacher et al. 2007b; Aldred et al. 2010; Chaw et al. 2011) and mussels (Carl et al. 2012a). Generally, fouling larvae are deterred by microtextures with widths that are slightly smaller than the smallest dimension of the fouling larvae. This results in a smaller area that the organism can interact with and a fewer number of attachment points (Callow et al. 2002; Scardino et

al. 2006; Scardino et al. 2008). A smaller interaction area means that larvae will not be in complete contact with the surface and consequently, will not be able to use the full potential of their adherence mechanism. Therefore, 'attachment point theory' provides an avenue to deter the settlement of fouling or enhance the foul-release capabilities of a surface by reducing the number of attachment points.

Conversely, the deterrent effect of surface-based technologies involving microtexture can be diminished when the number of available attachment points increases, occurring once the surface has become conditioned and overgrown by organisms that are too small to be affected (Molino and Wetherbee 2008; Molino et al. 2009a; Molino et al. 2009b; Bers et al. 2010; Terlizzi and Faimali 2010; Zargiel et al. 2011; Martinelli et al. 2012). Therefore, textured surfaces that work well against specific fouling organisms in laboratory assays can lose their deterrent effects in the field against the intense fouling pressures of a natural, multi-species fouling community. However, although the deterrent effect of those textures may be lost, their underlying foul-release capabilities may still be present. To date, a majority of the literature investigating the effects of microtexture focus on controlled, short-term laboratory assays (Schumacher et al. 2007b; Scardino et al. 2008; Aldred et al. 2010; Cooper et al. 2011; Carl et al. 2012a). In contrast, there is a paucity of comparisons between successful laboratory assays and the performance of textured surfaces exposed to natural fouling communities for longer periods (Thomason et al. 2002; Bers and Wahl 2004), highlighting the importance of field trials.

1.4.2 Photocatalysts

Phototcatalysis is a chemical oxidation process activated by light which generates reactive oxidising agents, including hydroxyl radicals (Fujishima et al. 2008). Hydroxyl radicals have an oxidising power greater than ozone and second only to fluorine (dos Santos et al. 2007) and are able to react with organic molecules and biological substrates at rates close to diffusion limits (Bhatkhande et al. 2002). Photocatalytic technology is used in antifouling membranes (Choi et al. 2007; Madaeni and Ghaemi 2007), heat exchange surfaces (Gopal et al. 2007), self-sterilising and self-cleaning

surfaces (Fujishima and Zhang 2006; Fujishima et al. 2008), as well as air and water remediation often with the mineralisation of toxic and recalcitrant organic compounds (Bhatkhande et al. 2002; Gogate and Pandit 2004; Choi et al. 2007; Demeestere et al. 2007). In addition, photocatalysts are lethal to bacteria, fungi, viruses, prions, protozoans, spores, oocysts and cancer cells due to non-specific decomposition and mineralisation (Watts et al. 1995; Lonnen et al. 2005; Xu et al. 2007; Paspaltsis et al. 2009; Zhao et al. 2009). In general, photocatalysts are semi-conductor metal oxides such as TiO_2, ZnO, WO_3, CdS, ZnS, $SrTiO_3$ and SnO_2 (Bhatkhande et al. 2002). Of these, titanium dioxide (TiO_2) is regarded as an ideal photocatalyst due to its low cost, high energy, abundance, corrosion resistance and chemical safety (Aprile et al. 2008). When TiO_2 is activated by light of sufficient energy, which in environmental applications is sunlight, a photo-excited electron in the valence band is promoted to the conduction band (Wang et al. 2007; Gaya and Abdullah 2008) resulting in the formation of a positive hole in the valence band and an electron in the conduction band creating a hole–electron pair (Fujishima et al. 2008). The conduction band electron reduces molecular oxygen to form superoxide radicals, which either react to form hydroxyl radicals or oxidise target compounds directly (Demeestere et al. 2007; Gaya and Abdullah 2008). In the absence of suitable electron and hole scavengers, the stored energy is dissipated within a few nanoseconds by recombination (Bhatkhande et al. 2002). Although human safety concerns have been raised about the nanoparticulate form (Long et al. 2007), the high reactivity of the radicals formed makes them safe for use, since the photokilling zone is restricted to the near-surface of the material, and they are not persistent in the environment and therefore unlikely to react with non-target organisms. Although photocatalysts have the potential to negatively affect fouling by degrading conditioning molecules, settlement cues and extracellular polysaccharide glues, they are currently not used as marine antifoulings. By introducing TiO_2 into a microtextured PDMS matrix, the combined efficacy of both technologies can be tested with the added advantage that the mechanical properties of silicone elastomers can be improved with the incorporation of the photocatalyst (Mirabedini et al. 2008).

1.4.3 Cold spray metal embedment

Cold spray is a metal spray process whereby solid metal particles (typically < 50 μm) are accelerated to supersonic velocities in an inert gas flow and deposited onto a substratum surface to form a coating (Stoltenhoff et al. 2002; Papyrin et al. 2007). Gas is accelerated using high pressure and heat (less than the melting point of the metal being used) and once stabilised, particles are injected into the gas flow and pass through a converging-diverging nozzle and onto the surface (Gärtner et al. 2006). Many factors can be manipulated during the cold spray process (nozzle type, nozzle dimensions, gas type, gas temperature, powder size, powder flow rate, powder insertion location and dimensions), and the appropriate balance depends largely on the type of metal powder being used and the substratum being sprayed (Pattison et al. 2007; Lupoi and O'Neill 2011). This balance must be maintained throughout the cold spray process in order to allow particles to surpass a critical velocity where, instead of rebounding off intended substratum at low velocity, or abrading at moderate velocity, particles embed or adhere to the surface. Heating of the gas not only increases velocity but also enhances plasticity of the metal particles, enabling effective deposition and heat transfer to the surface, which may improve embedment into the substratum. Applications of cold spray are very broad and include the formation of wear- and corrosion-resistant coatings, improvement of electrical and heat conductivity (Gärtner et al. 2006), freeform shape production without the use of moulds, and structure reinforcement (Pattison et al. 2007). Cold spray is ideal in these situations due to the dense nature of the deposits and the absence of defects such as material stress and warping, substandard mechanical properties, and changes in microstructure caused by excessive heating or melting of the particles, seen with competing thermal spray techniques (Amon et al. 1993; Gärtner et al. 2006; Pattison et al. 2007). The use of cold spray technology as a method to control fouling, by embedding metal particles known to prevent fouling (i.e. copper) into polymers, is an innovative approach and has the potential to deliver new antifouling materials.

1.5 Aims and chapter summaries

The overall aims for this thesis were to investigate innovative antifouling technologies using microtexture, photocatalysts and cold spray metal embedment as potential alternatives to present antifouling technologies. Microtexture, used in conjunction with a foul-release material, has been examined thoroughly in the past but generally in the context of laboratory assays alone. Here, laboratory assays are done in conjunction with field trials to establish links between the two. Furthermore, incorporating a photocatalyst into texture is examined in the context of antifouling to investigate the combined efficacy of both these technologies. Finally, although metals have been used in the past and are used presently in paints and emulsions, here, pure metal powders are embedded into thermoplastic polymers using cold spray technology, and examined as a potential antifouling alternative.

Chapter 2 examines the antifouling and foul-release efficacy of 18 textures (0–1,000 μm) incorporated into PDMS, against the settlement and recruitment of fouling organisms in the laboratory and in the field, respectively. Short-term laboratory assays were done to establish the settlement patterns of fouling taxa representing the spectrum of size ranges of settling organisms within a natural fouling community. Long-term field trials were done to examine the deterrence of recruitment of fouling organisms as well as the foul-release properties exhibited by the textures. The importance of conducting long-term field trials in conjunction with short-term laboratory assays, as well as the ability of a surface to maintain its foul-release properties, is discussed.

Chapter 3 investigates the potential to produce an effective antifouling technology by combining microtexture with a photocatalyst. PDMS incorporating five textures (0–600 μm) was combined with a range of photocatalytic TiO_2 nanoparticle loadings (0–15 wt%) and tested in the laboratory and in the field against a common fouling bryozoan. Laboratory assays examined the effects of summer versus winter ultraviolet radiation while field trials, undertaken when the bryozoans were most prevalent, quantified the effects of microtexture and TiO_2 in the natural environment. The

interaction between microtexture and TiO_2 loading, with respect to ultraviolet radiation strength, and the effects on the settlement and recruitment of the fouling bryozoan is discussed.

Chapter 4 examines for the first time, the embedment of metal powder into thermoplastic polymers using cold spray technology to determine the potential of this technology as an effective deterrent against fouling organisms. Two thermoplastic polymers embedded with copper powder were trialled for 250 days under field conditions to quantify their efficacy as antifouling materials. At the end of the field trial, analytical techniques were used to determine the differences in the structure of individual particles and the overall composition of the copper-embedded surfaces. The efficacy of antifouling, which is a function of the interaction between the metal powder and the thermoplastic polymer recipient, is discussed.

Chapter 5 examines an application of cold spray technology, where antifouling properties were given to polyurethane seismic streamer skins by embedding copper particles. The geophysical exploration industry uses seismic streamers to protect sensitive electronic equipment which measure seismic feedback data while being towed at moderate speeds (4–5.5 knots). There are no functional antifouling coatings for seismic streamer skins due to the technical constraints associated with application procedures and to the mechanical handling of the streamers during operation. Therefore, the streamers were embedded with copper powder using different loading densities of copper particles to determine antifouling longevity under field conditions. In addition, upon failure of the surfaces with the recruitment of fouling, streamers were exposed to realistic flow to establish whether they have foul-release capabilities. The effects of density loading of copper particles on antifouling efficacy are discussed.

Chapter 6 investigates the minimum effective release rates of copper and zinc ions from metal-embedded polymers needed to prevent the recruitment of fouling under field conditions. This Chapter also examines which species, from a natural fouling community, had the highest tolerance to copper and zinc ions and which species were most easily deterred by these metal ions. Minimum effective release rates were

established by producing copper-, bronze- and zinc-embedded thermoplastic polymer tubes, using cold spray technology, with a loading density gradient of metal particles ranging from low to high densities. In addition, the release rates of copper ions from copper- and bronze-embedded tubes were quantified to establish whether these metals could be used interchangeably. The use of gradients to determine minimum effective release rates as well as the effect of release rates of metal ions on the recruitment of fouling organisms is discussed.

Chapter 7 presents a summary and discussion of the results while examining future directions for the use of microtexture and photocatalytic materials as antifoulants and for the improvement of cold spray metal embedment technology for use with thermoplastic polymers.

Chapter 2

Using textured PDMS to prevent settlement and enhance foul-release of marine fouling organisms*

2.1 Introduction

Biofouling is the settlement of fouling organisms to submerged surfaces and results in significant economic and environmental problems. In the marine environment, it impedes the functional capacity of vessels (Edyvean 2010; Schultz et al. 2011) and aquatic infrastructure associated with aquaculture (de Nys and Guenther 2009; Fitridge et al. 2012), offshore oil and gas platforms (Page et al. 2010) geophysical exploration (Vignaux 2010; Harrick and Stenzel 2011) and water intakes for power stations and desalination plants (Henderson 2010). Larval settlement of marine fouling organisms onto these surfaces is an essential step towards the establishment of fouling communities and is facilitated by biological, physical and chemical surface-associated cues (Rittschof et al. 1998; Clare and Aldred 2009). The larval settlement phase is therefore a primary target in the development of effective antifouling solutions to mitigate the economic costs associated with biofouling.

Traditionally, successful antifouling technologies have incorporated metal or organic biocides to inhibit larval settlement, however, the deleterious effect to marine ecosystems resulting from their use has redirected effort to the development of environmentally-sustainable antifouling materials (Callow and Callow 2011). Many of these are produced by manipulating structural, mechanical and polarization properties in an effort to maximise the antifouling or foul-release capabilities of the material (Rosenhahn et al. 2008). Ultimately, a combination of these properties will be

*Chapter 2 adapted from Vucko MJ, Poole AJ, Carl C, Sexton BA, Glenn FL, Whalan S and de Nys R (2014). Using textured PDMS to prevent settlement and enhance release of marine fouling organisms. Biofouling 30: 1-16.

needed to successfully adopt materials that are effective. However, isolating specific surface properties and investigating their effects alone is fundamental to understanding their relative importance when combining properties for the ultimate antifouling or foul-release material.

The manipulation of surfaces for the purpose of antifouling has been approached extensively and includes the modification of elastic modulus (Brady and Aronson 2003; Chaudhury et al. 2005), charge (Rasmussen and Østgaard 2001; Petrone et al. 2011), amphiphilicity (Joshi et al. 2009; Martinelli et al. 2012), wettability (Aldred et al. 2006; Carl et al. 2012a; Bloecher et al. 2013) and microtexture (Callow et al. 2002; Schumacher et al. 2007a; Schumacher et al. 2007b; Carl et al. 2012a). These studies have provided the foundation from which we can further advance our understanding of some of the parameters contributing to larval settlement. Of these properties, microtexture is a key element affecting the settlement of marine fouling invertebrates (Bers and Wahl 2004; Long et al. 2010; Scardino and de Nys 2011). The physical component of a surface provides contact points that facilitate attachment, settlement, and in many cases metamorphosis. There is a positive correlative effect between the number of attachment points available on a surface and the settling success of fouling organisms (Callow et al. 2002; Scardino et al. 2006; Scardino et al. 2008). This 'attachment point theory' provides an avenue to enhance the antifouling and foul-release capabilities of a surface by reducing the number of attachment points.

Conversely, the deterrent effect of surface-based technologies involving microtexture can be diminished when the number of available attachment points increases, occurring once the surface has become conditioned and overgrown by organisms that are too small to be affected (Molino and Wetherbee 2008; Molino et al. 2009a; Molino et al. 2009b; Bers et al. 2010; Zargiel et al. 2011; Martinelli et al. 2012). Therefore, textured surfaces that work well against specific fouling organisms in laboratory assays can lose their deterrent effects in the field against the intense fouling pressures of a natural, multi-species fouling community. However, although the deterrent effect of those textures may be lost, their underlying foul-release capabilities may still be present. To date, a majority of the literature investigating the effects of microtexture

focus on controlled, short-term laboratory assays (Schumacher et al. 2007b; Scardino et al. 2008; Aldred et al. 2010; Cooper et al. 2011; Carl et al. 2012a). While these studies are essential, there is a paucity of comparisons between successful laboratory assays and the performance of textured surfaces exposed to natural fouling communities for longer periods (Thomason et al. 2002; Bers and Wahl 2004).

Therefore, this Chapter aims to investigate the short- and long-term deterrence, as well as the foul-release capabilities in a range of surface textures from nanometres to millimetres (micro to macro), using a known foul-release material, polydimethylsiloxane (PDMS; [Townsin and Anderson 2009]). Short-term, controlled laboratory assays were undertaken to examine the deterrence of settlement by common fouling taxa. Long-term field trials were undertaken to examine the deterrence of recruitment and the foul-release properties exhibited by textures, which were expected to become overgrown once exposed to the multitude of species of different sizes in a natural fouling community. The specific aims of this Chapter were to test the deterrent effects of surface textures ranging from 0.2 to 1,000 μm on the settlement of taxa commonly associated with fouling, including diatoms, algae, barnacles, oysters and bryozoans in laboratory assays. These species represent the spectrum of size ranges for settling organisms within a fouling community, and each should be deterred by specific textures based on their smallest larval dimension. In addition, textured surfaces were exposed to a natural fouling community for a fixed period of six months. The recruitment of fouling organisms to textured PDMS was examined, however, there was a focus on the retention of foul-release properties of those textures, quantified using a flow channel and high-pressure water jet.

2.2 Materials and methods

2.2.1 Production of textured PDMS surfaces

The antifouling efficacy of textured PDMS surfaces was tested against the settlement of fouling in the laboratory and recruitment of fouling in the field using non-textured

(0 μm; Figure 2.1) and textured (0.2, 0.5, 1, 2, 4, 10, 20, 40, 60, 80, 100, 200, 300, 400, 600, 800 and 1,000 μm; Figure 2.1) surfaces. Textured surfaces had parallel channel feature dimensions with a nominal 1:1 mark:space ratio (groove width = land area width). To produce the textured surfaces, PDMS (Sylgard 184, Dow Corning, USA) was cast onto corresponding master templates fabricated using either electron- (0.2–1 μm) or photo- (2–1,000 μm) lithography techniques according to the general method described in Carl et al. (2012a). Electron beam lithography (Leica EBMF10; 0.2–1 μm) and photolithography (2–20 μm) used ma-P1200 series spin-on photo-resists (micro resist technology GmbH, Berlin, Germany). The photo-resist thickness, for the fabrication of the smaller texture sizes (2–20 μm) was controlled by the spin-speed (1,756–500 rpm for resist thickness of 2–20 μm, respectively) and time. Since resists had a minimum depth of 2 μm, the depth of textured surfaces with a periodicity of 0.2–1 μm was controlled by reducing the resist exposure time, while textured surfaces with a periodicity of 2–20 μm used the full thickness of their respective resists for channel depths. Nickel casting shims were produced from textured resist samples so multiple castings of PDMS could be carried out without damaging the original surface. A physical vapour deposition unit was used to sputter-coat the plates with nickel (approximately 100 nm; 200 W DC for 7 min) and the plates were electroplated at 8.0 A for 7 h in a nickel sulphamate bath (pH, 4; temperature, 45°C) (Sexton and Marnock 2000). Multiple copies of the nickel master shims (250 μm thick) were then produced by electroplating and used for the casting of PDMS test surfaces.

Fabrication of the larger texture sizes (40–1,000 μm) used photolithography methods onto Nyloprint photopolymer plates. Nyloprint ST-43 (200 μm film thickness) was used to produce the 40–200 μm textured samples while Nyloprint ST-92 (600 μm film thickness) was used to produce the 300–1,000 μm textured samples. Textured surfaces with a periodicity of 200 and 600–1,000 μm used the full thickness of the Nyloprint sheets for channel depths, while the channel depth of textured surfaces with a periodicity of 40–100 and 300–400 μm was controlled by reducing the exposure time to the Nyloprint sheets.

Preparation of the templates for casting was done by spraying the nickel or Nyloprint master with a thin coating of release agent, wiping excess agent away and drying the template for 30 min at 75°C. A stainless steel square mold was fixed to the grating surface with removable tape to form a well. PDMS was prepared as a 10:1 ratio of base elastomer to curing agent and the two parts were thoroughly mixed and then degassed under vacuum to remove bubbles. The mixture was poured onto the surface and cured for up to 30 min at 75°C. Samples generated had an approximate thickness of 8 mm and measured 15 x 15 mm (0.2–1 μm), 75 x 75 mm (2–80 μm) and 125 x 125 mm (100–1,000 μm).

Surfaces were examined in detail to clearly observe pattern fidelity and determine relevant topographical dimensions including aspect ratio, overall texture shape (round or square) and the depth and width between each space and peak (Figure 2.1; Figure 2.2; Table 2.1). Textured surfaces were examined using two different methods depending on periodicity. Surfaces with 0–4 μm periodicity were examined using atomic force microscopy (NT-MDT NTEGRA). Surfaces with a 10–100 μm and 200–1,000 μm periodicity were examined using a compound microscope (Leica DM LB) at 40x and 5x magnification, respectively. Non-textured PDMS had an average area roughness (Sa) of 1.378 nm, while textured surfaces had either a round-wave linear grating profile (0.2, 0.5, 1, 40, 60, 80, 100, 300 and 400 μm; Figures 2.1B, C, D, I, J, K, L, N and O) or a square-wave linear grating profile (2, 4, 10, 20, 200, 600, 800 and 1,000 μm; Figures 2.1E, F, G, H, M, P, Q and R). The square-wave profile resulted when samples used the full thickness of the spin-resist or Nyloprint plate, while the round-wave profile resulted from varied exposure time to the spin-resist or Nyloprint plate required to obtain the desired depth. All surfaces were washed with a mild detergent, rinsed with distilled water, and dried prior to use in assays and field trials.

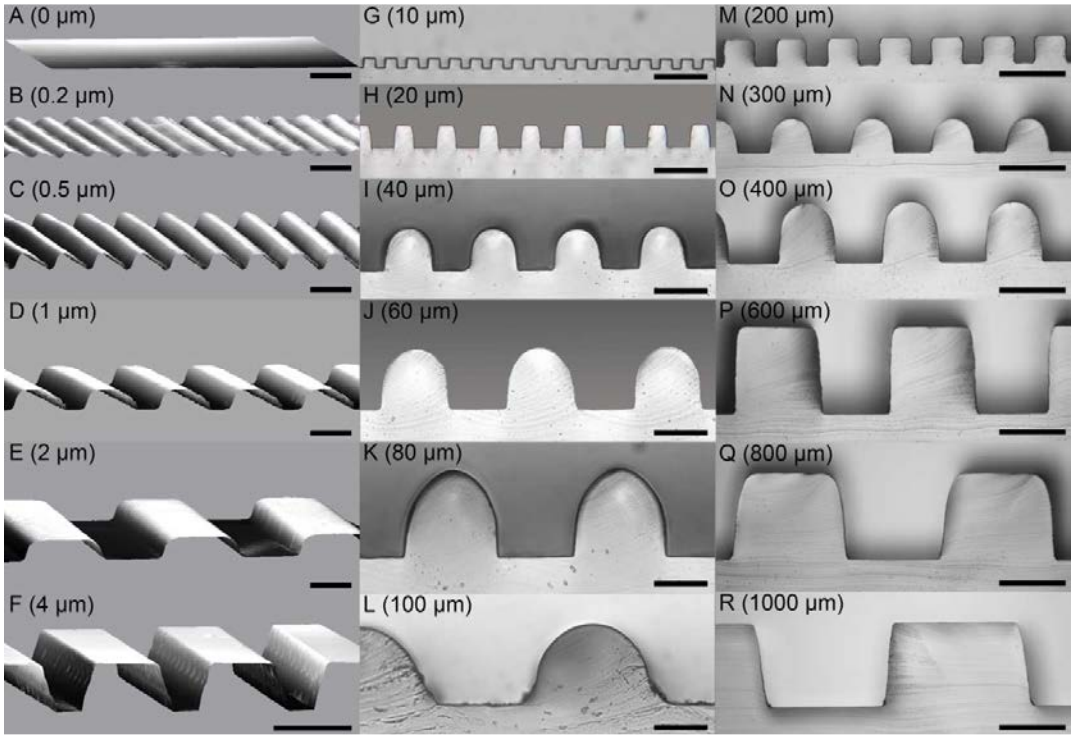

Figure 2.1. Cross sections of PDMS surfaces illustrating the topographical patterns of linear gratings using atomic force microscopy (**A–E**, scale bars = 1 µm; **F**, scale bar = 5 µm) and a compound microscope at 40x (**G–L**; scale bars = 50 µm) and 5x (**M–R**; scale bars = 500 µm) magnification. (**A**) non-textured PDMS (0 µm) and PDMS with textures of (**B**) 0.2 µm; (**C**) 0.5 µm; (**D**) 1 µm; (**E**) 2 µm; (**F**) 4 µm; (**G**) 10 µm; (**H**) 20 µm; (**I**) 40 µm; (**J**) 60 µm; (**K**) 80 µm; (**L**) 100 µm; (**M**) 200 µm; (**N**) 300 µm; (**O**) 400 µm; (**P**) 600 µm; (**Q**) 800 µm and; (**R**) 1,000 µm. N.B. See Table 2.1 for measurements; see Figure 2.2 for standard measurement locations.

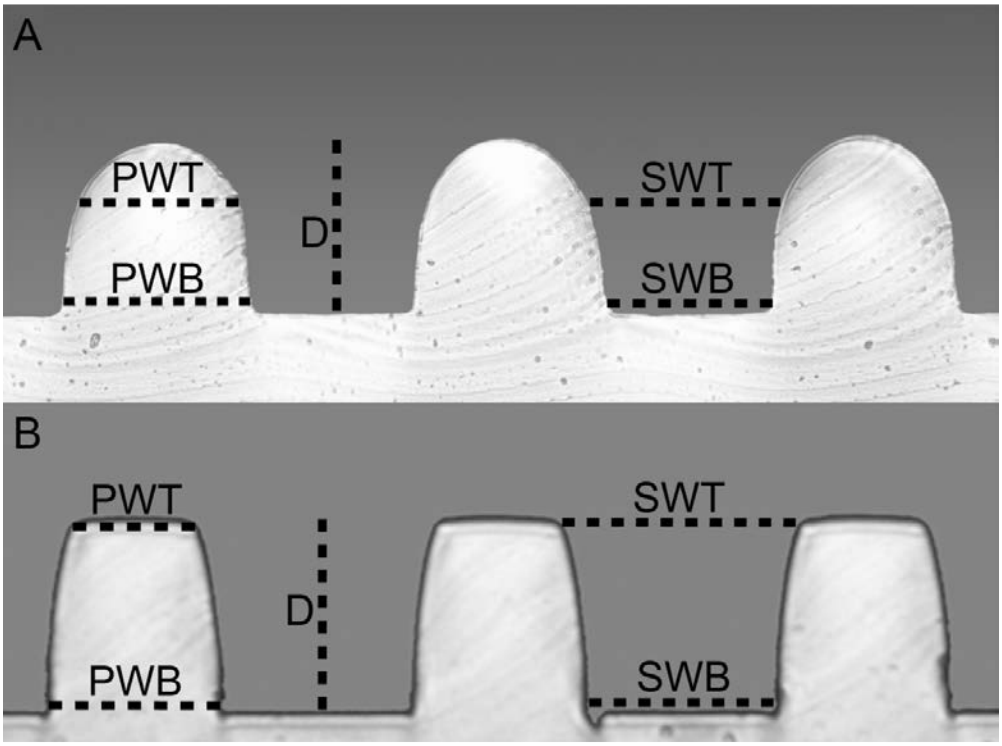

Figure 2.2. Standard measurement locations characterising textured PDMS surfaces used in laboratory assays and field trials against marine fouling organisms (see Table 2.1 for measurements of each surface). Measurement locations for surfaces with (**A**) round-wave linear grating profiles or (**B**) square-wave linear grating profiles. N.B. D, depth; SWT, space width of top before rounding out (for round-wave) and space width of top (square-wave); SWB, space width of base; PWT, peak width of top before rounding out (round-wave) and peak width of top (square-wave); PWB, peak width of base.

Table 2.1. Topographical measurements of textured PDMS surfaces with round- and square-wave linear grating profiles.

Texture (μm)	Shape	Aspect ratio	Depth (μm)	Space width (μm)		Peak width (μm)	
				Top	Base	Top	Base
0.2	Round	13.3:1	0.15	0.2	0.06	0.1	0.25
0.5	Round	1.4:1	0.5	0.7	0.25	0.3	0.8
1	Round	3:1	0.5	1.5	0.5	0.5	1.5
2	Square	4:1	0.5	2	1.5	1.5	2
4	Square	1.2:1	3	3.5	1.5	4	5.75
10	Square	1:1	10	10	9	10	11
20	Square	1.25:1	20	25	20	13	18
40	Round	1:1	40	40	35	38	43
60	Round	1:1	60	62	55	58	65
80	Round	0.9:1	85	77	73	80	85
100	Round	1.6:1	75	120	80	100	120
200	Square	0.9:1	200	180	150	200	220
300	Round	1.3:1	260	330	250	260	320
400	Round	0.9:1	450	420	350	370	430
600	Square	0.9:1	650	600	530	550	650
800	Square	1.4:1	650	900	700	630	850
1,000	Square	1.7:1	650	1,100	900	900	1,100

Notes: see Figure 2.1 for linear grating profile images; see Figure 2.2 for standard measurements locations.

2.2.2 Laboratory assays

The effects of textured and non-textured PDMS were tested against the settlement rates of organisms, representing the spectrum of size ranges within a fouling community, and consisting of the diatoms *Nitzschia closterium* ([Ehrenberg] W. Smith 1853) and *Amphora* sp., the filamentous alga *Ulva* sp., the barnacle *Amphibalanus reticulatus* (Utinomi 1967), the oyster *Saccostrea glomerata* (Gould 1850) and the bryozoan *Bugula neritina* (Linnaeus 1758). In addition to non-textured (0 μm) PDMS, the range of textured PDMS surfaces to be tested was determined from the smallest larval dimension of each organism (Table 2.2). This included 0.2–20 μm for *N. closterium* (cell width of 4 μm) and *Amphora* sp. (cell width of 7 μm), 0.2–60 μm for *Ulva* sp. (propagule diameter of 10 μm), 2–600 μm for *A. reticulatus* (larval width of 180 μm), 100–1,000 μm for *S. glomerata* (larval width of 200 μm) and 2–1,000 μm for *B. neritina* (larval diameter of 320 μm). All filtered seawater (FSW) used in culturing and laboratory assays was passed through 1, 0.35 and 0.2 μm filters, treated with

ultraviolet radiation, autoclaved at 121°C for 1 h, and stored for 7 days prior to use. In addition, at the beginning of each assay, all surfaces were inspected to ensure that there was no air trapped between the FSW and the PDMS surface.

Table 2.2. The antifouling effectiveness of a range of textured and non-textured PDMS surfaces was tested against common fouling organisms representing the spectrum of size ranges within a fouling community. These included the diatoms *N. closterium* and *Amphora* sp., the alga *Ulva* sp., the barnacle *A. reticulatus*, the oyster *S. glomerata* and the bryozoan *B. neritina.* The range of textured PDMS to be tested (depicted in grayscale) was determined from the smallest larval dimension of each organism.

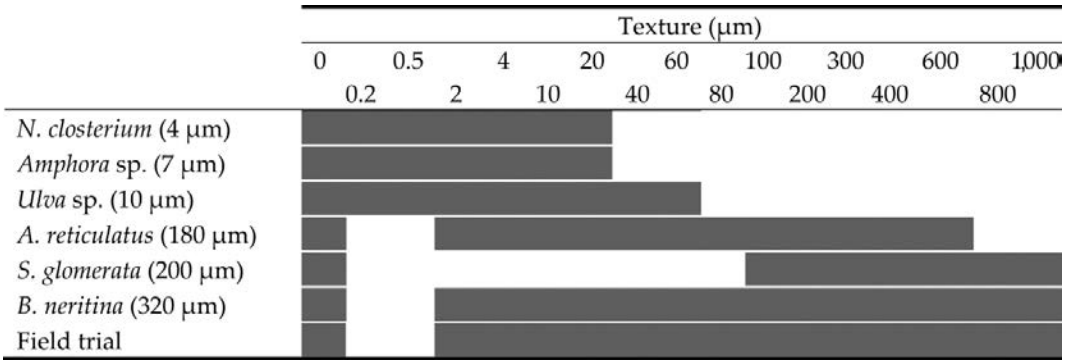

Note: numbers beside organisms represents smallest larval dimension.

2.2.2.1 N. closterium *and* Amphora *sp.*

N. closterium (CS-5) and *Amphora* sp. (CS-255) diatom cultures were accessed from the Commonwealth Scientific and Industrial Research Organisation culture collection and immediately used in drop assays. Test surfaces (0.2–20 μm and non-textured PDMS; n = 5) were cut to size (15 x 15 mm) and randomly placed into 6-well microplates (Iwaki 3810-006). Drops with volumes of 800 μL and concentrations equivalent to 250,000 cells mL^{-1} of *N. closterium* and *Amphora* sp. were placed onto each surface. Test surfaces were maintained in a temperature controlled room at 26°C under a 12 h light:12 h dark photoperiod. After 24 h, surfaces were dip rinsed three times in FSW to remove non-settled diatoms and the numbers of settled diatoms from ten randomly selected fields of view from each replicate were counted using a compound microscope (Leica DM LB; 200x magnification). Medians were obtained from each replicate to calculate means used for analyses.

2.2.2.2 Ulva *sp.*

Ulva sp. propagules were collected from algal scrubbers used to filter water associated with aquaria at the Marine and Aquaculture Research Facilities Unit (MARFU), James Cook University (JCU). The timing of spore activity was based on visible colonisation of the filamentous algae to algal scrubbers and determined the deployment of textured PDMS surfaces. Test surfaces (0.2–60 μm and non-textured PDMS; n = 8) were cut to size (15 x 15 mm) and randomly attached to polyvinyl chloride (PVC) backing plates (150 x 150 mm) using silicone (Selleys Glass Silicone sealant). The plates were secured in the algal scrubbers, left for 48 h, then dip rinsed three times in FSW to remove non-settled propagules. The surfaces were transferred to plastic trays with FSW and culture medium (Cell-hi F2P, Varicon Aqua Solutions Ltd.). The trays were covered with a clear sheet of Perspex to prevent evaporation and maintained in temperature controlled culture cabinets (Sanyo MLR-351) at 28°C under a 12 h light:12 h dark photoperiod. After 96 h, the numbers of settled *Ulva* sp. from five randomly selected fields of view from each replicate were counted using a compound microscope (Leica DM LB; 4.5x magnification). Medians were obtained from each replicate to calculate means used for analyses.

2.2.2.3 A. reticulatus

Brood stock of *A. reticulatus* was collected from the Townsville Yacht Club (TYC; Queensland, Australia) using PVC settlement plates (150 x 150 mm) suspended from boat moorings ranging in depth from 200 to 700 mm. Four sets of six PVC plates were strung onto polyethylene rope and the plates were separated from each other using 100 mm of plastic tubing. The plates were checked regularly and, when settled adults were observed, the brood stock was transported with natural seawater to MARFU, JCU where they were fed *Chaetoceros muelleri* (Lemmermann 1898; CS-176) and maintained in a temperature controlled room at 28°C under a 12 h light:12 h dark photoperiod. After 48 h, brood stock was dark adapted for 72 h. Thereafter, spawning was induced by replacing the holding water with water 2°C warmer, adding *C. muelleri* and a small LED light source. For the following 3 h, positively phototactic larvae were collected with a sterile syringe every 30 min and transferred to FSW.

A. reticulatus larvae were cultured in 3 L Erlenmeyer flasks with rubber stoppers penetrated by glass tubing delivering 0.20 μm filtered air (Midisart 2000 filters) at the same light and temperature conditions as the adult brood stock. Larvae were cultured at a density of 1 nauplii mL^{-1} in FSW containing 250,000 cells mL^{-1} *C. muelleri* (Thiyagarajan et al. 2002), 10 ppm Erythromycin (Sigma Aldrich E5389) and 10 ppm Streptomycin (Sigma Aldrich S6501). Water changes occurred daily including the addition of new diatoms and antibiotics. Larvae were maintained in culture for 6 days allowing all nauplii to reach the settling cyprid stage. After 6 days, cyprids were filtered and stored in FSW at 4°C in the dark for at least three days prior to use in drop assays. Test surfaces (2 – 600 μm and non-textured PDMS; n = 5) were cut to size (35 mm diameter) and randomly placed into 6-well microplates (Iwaki 3810-006). Approximately 20 cyprids were pipetted with 800 μL of FSW and placed onto each surface. Test surfaces were maintained in a temperature controlled room in the dark at 25°C. After 96 h, the number of settled *A. reticulatus* was recorded and percent settlement was quantified from the total.

2.2.2.4 S. glomerata

S. glomerata larvae that were competent to settle were obtained from the Port Stephens Fisheries Institute (New South Wales, Australia) and used immediately in volume assays. Test surfaces (100–1,000 μm and non-textured PDMS; n = 5) were cut to size (35 mm diameter) and randomly placed into 6-well microplates (Iwaki 3810-006). Approximately 20 larvae were pipetted with 3 mL of FSW and placed onto each surface. Test surfaces were maintained in a temperature controlled room in the dark at 25°C. After 72 h, the number of settled *S. glomerata* was recorded and percent settlement was quantified from the total.

2.2.2.5 B. neritina

B. neritina colonies were collected from the harbour infrastructure at the TYC and transported in a 30 L plastic drum with natural seawater to MARFU, JCU where they were placed into darkened plastic tubs with FSW and supplied with aeration. After 72 h, spawning was induced by exposing the colonies to light (Marshall and Keough

2003) and larvae were immediately used in drop assays. Test surfaces (2–1,000 μm and non-textured PDMS; n = 7) were cut to size (35 mm diameter) and randomly placed into 6-well microplates (Iwaki 3810-006). Approximately 20 larvae were pipetted with 800 μL of FSW and placed onto each surface. Test surfaces were maintained in a temperature controlled room in the dark at 25°C. After 24 h, the number of settled *B. neritina* was recorded and percent settlement was quantified from the total.

2.2.3 Field trials

The recruitment of fouling organisms to textured and non-textured PDMS surfaces was investigated in the field at the TYC. There is consistent, high fouling pressure at this dry tropical location, and the occurrence of specific species fluctuates depending on time of year. Since all surfaces were expected to become overgrown regardless of texture, the longer-term foul-release properties of the textures were investigated as a focus, in addition to recruitment onto textured surfaces. Therefore, surfaces were deployed in late December (Australian summer) for six months of exposure to fouling species including four hard foulers known to occur during this period. These are the tubeworm *Hydroides elegans* (Haswell 1883; larval width of 130 μm [Scardino et al. 2008]), the barnacle *A. reticulatus* (larval width of 180 μm), the oyster *Pinctada imbricata* (Gould 1850; larval width of 200 μm [Gervis and Sims 1992]) and the bryozoan *B. neritina* (larval diameter of 320 μm).

Test surfaces (2–1,000 μm and non-textured PDMS; n = 4) were cut into squares (60 x 60 mm) and randomly attached to PVC plates (150 x 150 mm) using silicone (Selleys Glass Silicone sealant) with four samples per plate and 15 mm between all samples. To aid adhesion, the PVC plates were roughened with abrasive paper (KMCA WA82 P120). Importantly, the linear grating profile of each texture was unidirectional within each plate to facilitate release trials (see materials and methods in '2.2.4 Release trials'). In total, three sets of five PVC plates were strung onto polyethylene rope and each plate was separated from the next using 100 mm of plastic tubing. The plates were suspended from boat moorings at the TYC, PDMS side down, 100 mm below the water surface against the pier. As a result, the shallowest plate was

100 mm below the surface and the deepest plate 500 mm. The plates were removed after six months at which point they were photographed using a digital camera. Results were quantified from images using ImageJ (v. 1.42q; National Institutes of Health, Bethesda, Maryland, USA) and the plates were kept for use in adhesion strength trials. Total fouling coverage (soft and hard fouling), total hard fouling coverage as well as the total numbers of specific hard fouler species were quantified from the images. Importantly, any fouling organisms which settled onto the PVC backing plate and encroached onto the PDMS surfaces were not included in the analyses.

2.2.4 Release trials

To test the release of fouling organisms from textured and non-textured PDMS surfaces after six months in the field, a flow channel was used. Upon conclusion of the field trial, the plates with test surfaces attached were placed into plastic tubs with natural seawater, and supplied with aeration for transport to the laboratory. Each plate with four samples was cut in half using a conventional handsaw so that two samples were placed into the flow channel side by side at any one time with grooves parallel to the flow of water. Since all test surfaces were spaced 15 mm apart, fouling was not disrupted when the plates were cut. Importantly, while preparing and testing all samples, air exposure did not exceed 30 s. The flow channel is described in detail in Carl et al. (2012a). In brief, FSW was pumped into an open channel and subsequently fell freely into a reservoir (1,000 L tank) where it could be recirculated back into the channel using a pump (Onga® Hi-flo 415). The flow rate of water was adjusted using stop valves between the pump and channel and water was dispersed through a custom fitting prior to entering the channel at a depth of less than 10 mm to establish a laminar-like flow over the test surfaces (Enríquez and Rodríguez-Román 2006). The samples were secured in the channel using customized fittings and a small PVC ramp was secured in front of the surfaces to ensure even flow over the samples. The adhesion strength of fouling taxa on textured PDMS surfaces was quantified before and after exposing test surfaces to flow rates of 1, 2 and 4.5 knots (equivalent to 0.5, 1.0 and 2.3 m s^{-1}, respectively), the maximum flow of the system. Each test surface was left

in the flow channel for 3 min. Test surfaces were photographed using a digital camera before and after exposure to each flow rate and results were quantified from images using ImageJ (v. 1.42q). The initial and remaining total fouling coverage (soft and hard fouling) and total hard fouling coverage were quantified from the images.

Following flow channel trials, release of remaining fouling taxa attached to PDMS surfaces was tested. To quantify release, each sample was exposed to a high-pressure water jet (Karcher® 3.450) using a method modified from (Scardino et al. 2009a). The pressure (kPa) acting on each sample was calculated using the force of the jet of water (calculated as weight in Newtons) multiplied by the area covered by the spray. The force, measured using a digital force gauge (Extech Instruments 475040, load capacity of 5 kg) fitted with a PVC plate to absorb the impact, measured 13.98 ± 0.04 N and was constant from different heights. The area covered by the spray was determined by measuring a series of holes left in foam and measured 184.24 ± 0.16 mm^2. Therefore, the jet of water produced a surface pressure of 75.9 kPa, which was passed over each surface for approximately 3 seconds from a height of 300 mm. Test surfaces were photographed using a digital camera before and after spraying and results were quantified from images using ImageJ (v. 1.42q; National Institutes of Health, Bethesda, Maryland, USA). The initial and remaining total fouling coverage (soft and hard fouling) and total hard fouling coverage were quantified from the images.

2.2.5 Statistical analysis

One-way permutational analysis of variance (PERMANOVA) analyses were used to test for significant differences in mean settlement of *N. closterium*, *Amphora* sp., *Ulva* sp., *A. reticulatus*, *S. glomerata* and *B. neritina* on textured and non-textured PDMS surfaces (fixed factor). PERMANOVA analyses was also used to test for significant differences in total fouling coverage (soft and hard fouling), total hard fouling coverage and total numbers of specific hard fouler species on textured and non-textured PDMS surfaces (fixed factor) at different submersion depths (covariate) after six months in the field. Pair wise *a posteriori* comparisons were used ($\alpha = 0.05$), where applicable. All PERMANOVA analyses were performed using PRIMER 6 (v. 6.1.13;

Ivybridge, United Kingdom) and PERMANOVA+ (v. 1.0.3 [Clarke and Gorley 2006]). For PERMANOVA, Bray-Curtis similarity matrices were produced using the untransformed raw data, *p*-values were calculated from 9,999 random permutations and dummy variables (0.0001) were used to account for zero values.

Pearson's product-moment correlations were used to test for correlations between the fouling recruitment after six months in the field (initial fouling) and remaining fouling after exposure to a high-pressure water jet as well as between textured surface aspect ratio and remaining fouling after exposure to a high-pressure water jet. This was done for total fouling coverage (soft and hard fouling) and total hard fouling coverage. Independent samples t-tests were used to test for differences in remaining fouling between round or square textures and this was done for total fouling coverage (soft and hard fouling) and total hard fouling coverage. All correlation analyses and t-tests were performed using the R language (v. 3.0.1 [R Core Team 2013]) and assumptions of normality were checked with Q-Q plots and Shapiro-Wilk normality tests. All data are presented as mean ± standard error (SE).

2.3 Results

2.3.1 Laboratory assays

2.3.1.1 N. closterium *and* Amphora *sp.*

There were fewer individuals of *N. closterium* and *Amphora* sp. on all textured surfaces regardless of periodicity, as compared to non-textured PDMS controls (Figures 2.3A and B). *N. closterium* was up to 18.0 times more abundant on non-textured PDMS controls while *Amphora* sp. was up to 7.4 times more abundant. The mean number of settled *N. closterium* per field of view on textured PDMS surfaces ranged from 14.3 ± 4.8 (0.2 μm) to 74.1 ± 12.1 (10 μm) with 258.0 ± 45.6 settling on non-textured PDMS. There was a significant effect of texture on attachment (PERMANOVA, pseudo-$F_{(7,32)} = 3.489$, $p < 0.001$; Figure 2.3A; Table 2.3) where non-textured (0 μm)

PDMS controls had significantly higher attachment rates than all other textured surfaces (pair-wise *a posteriori* comparison, $\alpha = 0.05$). The mean number of settled *Amphora* sp. per field of view on textured PDMS surfaces ranged from 21.9 ± 3.7 (0.2 μm) to 65.9 ± 8.9 (10 μm) with 161.2 ± 40.8 settling on non-textured PDMS. There was a significant effect of texture on attachment (pseudo-$F_{(7,32)} = 11.761$, $p < 0.001$; Figure 2.3B; Table 2.3) where non-textured (0 μm) PDMS surfaces had significantly higher attachment rates than 4, 10 and 20 μm PDMS surfaces which had significantly higher attachment rates than 0.5, 1 and 2 μm PDMS surfaces which had significantly higher attachment rates than 0.2 μm PDMS surfaces (pair-wise *a posteriori* comparison, $\alpha = 0.05$).

2.3.1.2 Ulva *sp.*

Ulva sp. was deterred by all textures smaller than the size of the propagule (diameter of 10 μm) with higher attachment on textures above this (Figure 2.3C). The mean number of settled *Ulva* sp. propagules on textured PDMS surfaces ranged from 31.9 ± 2.2 (0.2 μm) to 63.6 ± 2.3 (40 μm) with 31.0 ± 2.4 settling on non-textured PDMS. There was a significant effect of texture on attachment (pseudo-$F_{(9,70)} = 33.097$, $p < 0.001$; Figure 2.3C; Table 2.3) where non-textured (0 μm), 0.2, 0.5, 1, 2 and 4 μm PDMS surfaces had significantly lower attachment rates than 10, 20, 40 and 60 μm PDMS surfaces (pair-wise *a posteriori* comparison, $\alpha = 0.05$).

2.3.1.3 A. reticulatus

Overall, there was low settlement of *A. reticulatus* on all textured and non-textured PDMS (Figure 2.3D). The mean settlement of *A. reticulatus* on textured PDMS surfaces ranged from 0% (40, 60, 80 and 600 μm) to 8.7 ± 6.2% (2 μm) with 12.8 ± 4.6% (0 μm) settlement on non-textured PDMS. There was a significant effect of texture on the settlement of *A. reticulatus* cyprids (pseudo-$F_{(12,52)} = 3.089$, $p = 0.001$; Figure 2.3D; Table 2.3) where non-textured (0 μm), 2 and 4 μm PDMS surfaces had between 2 and 12 times more settlement than any other surfaces and significantly higher settlement rates than 40, 60, 80, 100 and 600 μm PDMS surfaces (pair-wise *a posteriori* comparison, $\alpha = 0.05$).

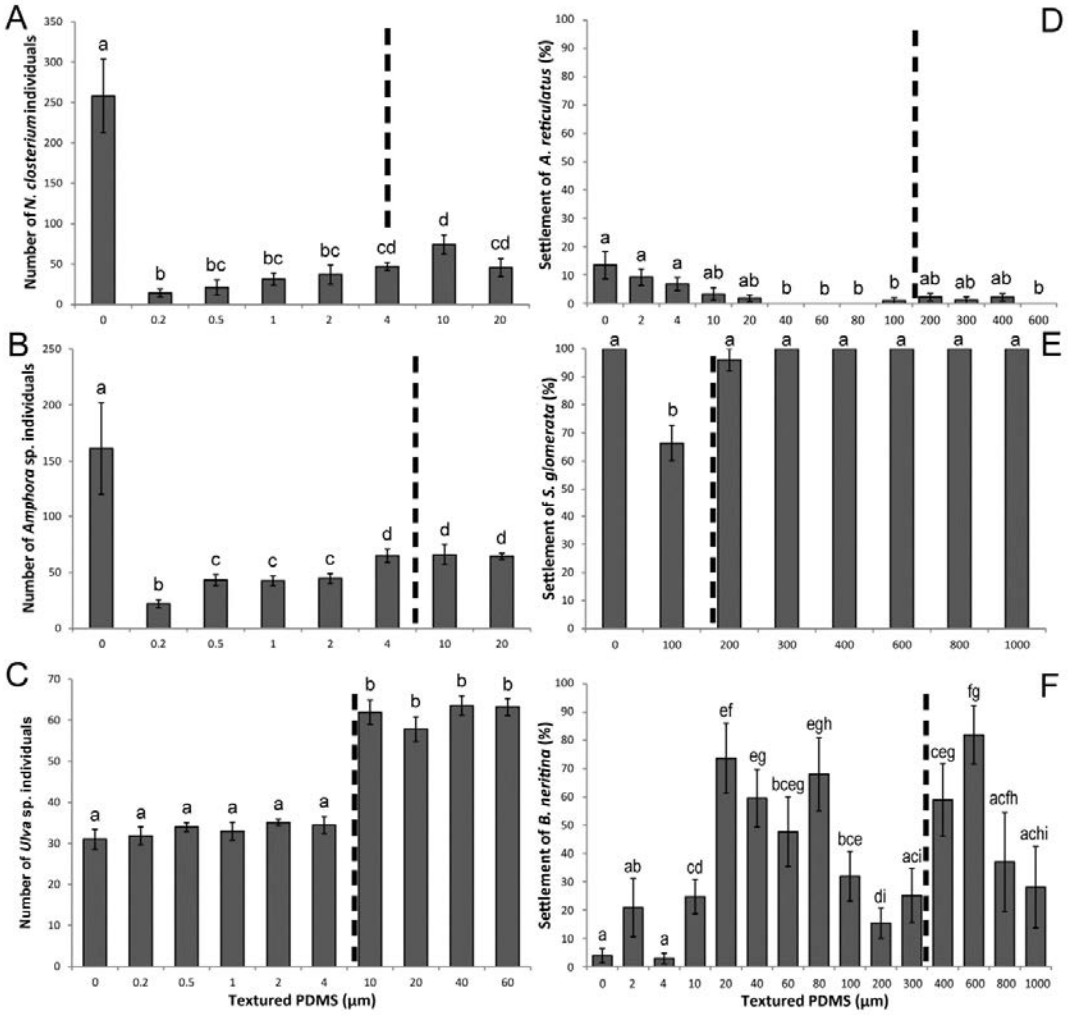

Figure 2.3. The effect of textured and non-textured PDMS surfaces on the settlement of various fouling organisms under laboratory conditions. Individual number of (**A**) *N. closterium*; (**B**) *Amphora* sp.; and (**C**) *Ulva* sp. and percent settlement of (**D**) *A. reticulatus*; (**E**) *S. glomerata*; and (**F**) *B. neritina*. N.B. Superscript letters above bars indicate significant groupings (pair-wise *a posteriori* comparison, $\alpha = 0.05$); dashed lines indicate approximate size of organism; all data displayed as mean ± SE.

2.3.1.4 S. glomerata

S. glomerata was deterred by textures closest to, but less than, the size of the larvae (width of 200 μm) with higher settlement on textures above this and overall, there was high settlement on all textured and non-textured PDMS surfaces (Figure 2.3E). The mean settlement of *S. glomerata* on textured PDMS surfaces ranged from 66.4 ± 6.3% (100 μm) to 100% (300, 400, 600, 800 and 1,000 μm) with 0% settlement on non-textured PDMS. There was a significant effect of texture on the settlement of

S. glomerata larvae (pseudo-$F_{(7,32)} = 15.733$, $p < 0.001$; Figure 2.3E; Table 2.3) where settlement on 100 μm PDMS surfaces was significantly lower than on all other PDMS surfaces (pair-wise *a posteriori* comparison, $\alpha = 0.05$).

Table 2.3. One-factor PERMANOVA analyses with significant effects of textured and non-textured PDMS surfaces on the settlement of fouling organisms (*N. closterium*, *Amphora* sp., *Ulva* sp., *A. reticulatus, S. glomerata* and *B. neritina*) in the laboratory.

Species	df	Mean square	pseudo-*F*	*p*-value
N. closterium	7, 32	4,287	3.489	0.0001*
Amphora sp.	7, 32	2,554	11.761	0.0001*
Ulva sp.	9, 70	1,916	33.097	0.0001*
A. reticulatus	12, 52	3,195	3.089	0.0011*
S. glomerata	7, 32	257	15.733	0.0001*
B. neritina	14, 83	6,274	3.571	0.0001*

Note: * denotes significant effect; $\alpha = 0.05$.

2.3.1.5 B. neritina

B. neritina was deterred by textures closest to, but less than, the size of the larvae (320 μm) with higher settlement on textures above this (Figure 2.3F). In addition, there was high settlement on textured surfaces much smaller than larval size (20–80 μm). The mean settlement of *B. neritina* on textured PDMS surfaces ranged from 2.8 ± 1.9% (4 μm) to 82.0 ± 10.4% (600 μm) with 3.8 ± 2.5% on non-textured PDMS. There was a significant effect of texture on the settlement rates of *B. neritina* larvae (pseudo-$F_{(14, 84)} = 3.724$, $p < 0.001$; Figure 2.3F; Table 2.3) where non-textured (0 μm) and 4 μm PDMS surfaces had significantly lower settlement rates than 10, 20, 40, 60, 80, 100, 200, 400 and 600 μm PDMS surfaces (pair-wise *a posteriori* comparison, $\alpha = 0.05$).

2.3.2 Field trials

There was no effect of texture on total fouling coverage (soft and hard fouling), hard fouling coverage or the number of specific hard fouler type (*H. elegans*, *A. reticulatus*, *P. imbricata* and *B. neritina*) on textured PDMS surfaces after six months in the field (Figures 2.4A and 2.5A–D). In contrast, there was an effect of submersion depth where more fouling was observed on deeper plates (Figures 2.4B and 2.5E–H).

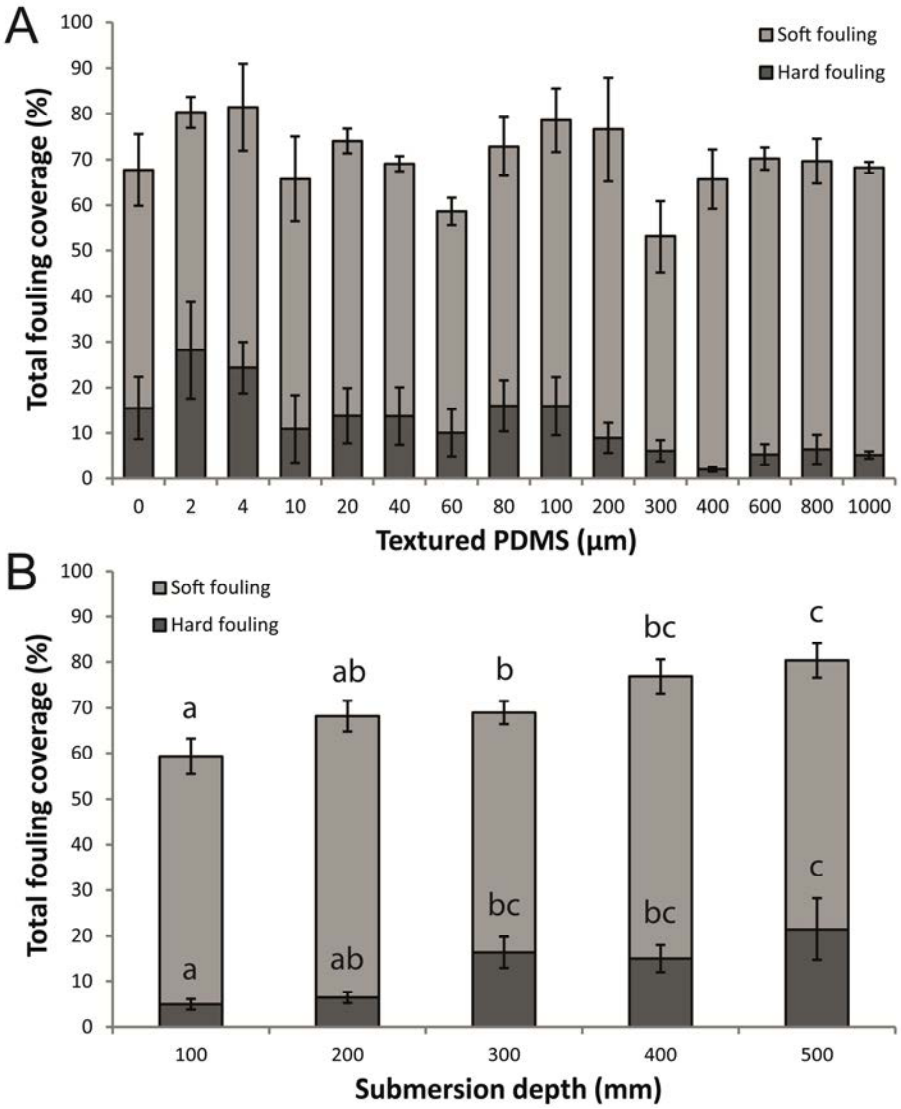

Figure 2.4. Total fouling coverage (soft and hard fouling) on (**A**) textured and non-textured PDMS surfaces and overall at (**B**) different submersion depths after six months in the field. N.B. Superscript letters above bars indicate significant groupings (pair-wise *a posteriori* comparison, $\alpha = 0.05$); all data displayed as mean ± SE.

The mean total fouling coverage (soft and hard fouling) on textured PDMS surfaces after six months in the field ranged from 53.1 ± 7.8% (300 µm) to 81.5 ± 9.5% (4 µm) with 67.7 ± 7.8% coverage on non-textured PDMS. There was no effect of texture (PERMANOVA, pseudo-$F_{(14,40)} = 0.972$, $p = 0.499$; Figure 2.4A; Table 2.4) but a significant effect of submersion depth (covariate; pseudo-$F_{(1,40)} = 17.714$, $p < 0.001$; Figure 2.4B; Table 2.4) with total fouling coverage increasing with plate submergence depth. There was significantly less total fouling at 100 mm submergence compared to

300, 400 and 500 mm while there was significantly more total fouling at 500 mm submergence compared to 100, 200 and 300 mm (pair-wise *a posteriori* comparison, $\alpha = 0.05$).

The mean total hard fouling coverage on textured PDMS surfaces after six months in the field ranged from 2.0 ± 0.5% (400 μm) to 28.2 ± 10.6% (2 μm) with 15.5 ± 6.8% coverage on non-textured PDMS. There was no effect of texture (pseudo-$F_{(14,40)} = 1.429$, $p = 0.108$; Figure 2.4A; Table 2.4) but a significant effect of submersion depth (covariate; pseudo-$F_{(1,40)} = 9.091$, $p = 0.001$; Figure 2.4B; Table 2.4) with total fouling coverage increasing with plate submergence depth. There was significantly less hard fouling at 100 mm submergence compared to 300, 400 and 500 mm while there was significantly more hard fouling at 500 mm submergence compared to 100 and 200 mm (pair-wise *a posteriori* comparison, $\alpha = 0.05$).

The mean number of specific hard fouler type on textured PDMS surfaces after six months in the field ranged from 0 (*A. reticulatus*, 400 μm; *P. imbricata*, 200, 400 and 1,000 μm) to 20.8 ± 10.8 (*H. elegans*, 100 μm) with 0.5 ± 0.5 (*P. imbricata*) to 12.0 ± 2.3 (*H. elegans*) on non-textured PDMS. There was no effect of texture on the recruitment of *H. elegans* (pseudo-$F_{(14,40)} = 1.098$, $p = 0.352$; Figure 2.5A; Table 2.4), *A. reticulatus* (pseudo-$F_{(14,40)} = 1.354$, $p = 0.164$; Figure 2.5B; Table 2.4), *P. imbricata* (pseudo-$F_{(14,40)} = 1.053$, $p = 0.422$; Figure 2.5C; Table 2.4) or *B. neritina* (pseudo-$F_{(14,40)} = 1.068$, $p = 0.406$; Figure 2.5D; Table 2.4). Although no significant statistical effects were observed, there were general trends in the recruitment patterns. Both *A. reticulatus* and *P. imbricata* had decreasing recruitment with larger sizes of textured PDMS. In contrast, although both *B. neritina* and *H. elegans* demonstrated varied recruitment on all surfaces, the lowest recruitment was on 300 and 400 μm surfaces for both.

In addition to texture, plate submergence depth was analysed as a covariate. There was no effect of depth on the numbers of *A. reticulatus* (covariate; pseudo-$F_{(1,40)} = 1.046$, $p = 0.344$; Figure 2.5F; Table 2.4), although higher numbers were found at 500 mm compared to all other depths. There was however a significant effect of depth on the numbers of *H. elegans* (pseudo-$F_{(1,40)} = 8.269$, $p < 0.001$; Figure 2.5E; Table 2.4), *P.*

imbricata (pseudo-$F_{(1,40)} = 4.037$, $p = 0.046$; Figure 2.5G; Table 2.4) and *B. neritina* (pseudo-$F_{(1,40)} = 7.809$, $p = 0.004$; Figure 2.5H; Table 2.4). There were higher numbers of each hard fouler type as plates got deeper and more *B. neritina* were found at 500 mm, more *H. elegans* were found at 300, 400 and 500 mm and more *P. imbricata* were found at 300 and 500 mm (pair-wise *a posteriori* comparison, $\alpha = 0.05$).

Table 2.4. One-factor PERMANOVA analyses with significant effects of textured and non-textured PDMS surfaces as well as submersion depth (covariate) on total fouling coverage, total hard fouling coverage and recruitment of hard foulers (*H. elegans, A. reticulatus*, *P. imbricata* and *B. neritina*) after six months in the field.

Factor		df	Mean square	pseudo-*F*	*p*-value
Texture	Total fouling coverage	14, 40	76.96	0.973	0.499
	Total hard fouling coverage	14, 40	1,820	1.429	0.108
	H. elegans	14, 40	1,232	1.098	0.352
	A. reticulatus	14, 40	3,529	1.354	0.164
	P. imbricata	14, 40	2,345	1.053	0.422
	B. neritina	14, 40	2,550	1.068	0.406
Depth	Total fouling coverage	1, 40	1,401	17.714	0.0001*
	Total hard fouling coverage	1, 40	11,587	9.091	0.001*
	H. elegans	1, 40	9,284	8.269	0.0005*
	A. reticulatus	1, 40	2,727	1.046	0.344
	P. imbricata	1, 40	8,994	4.037	0.046*
	B. neritina	1, 40	18,646	7.809	0.004*

Note: * denotes significant effect.

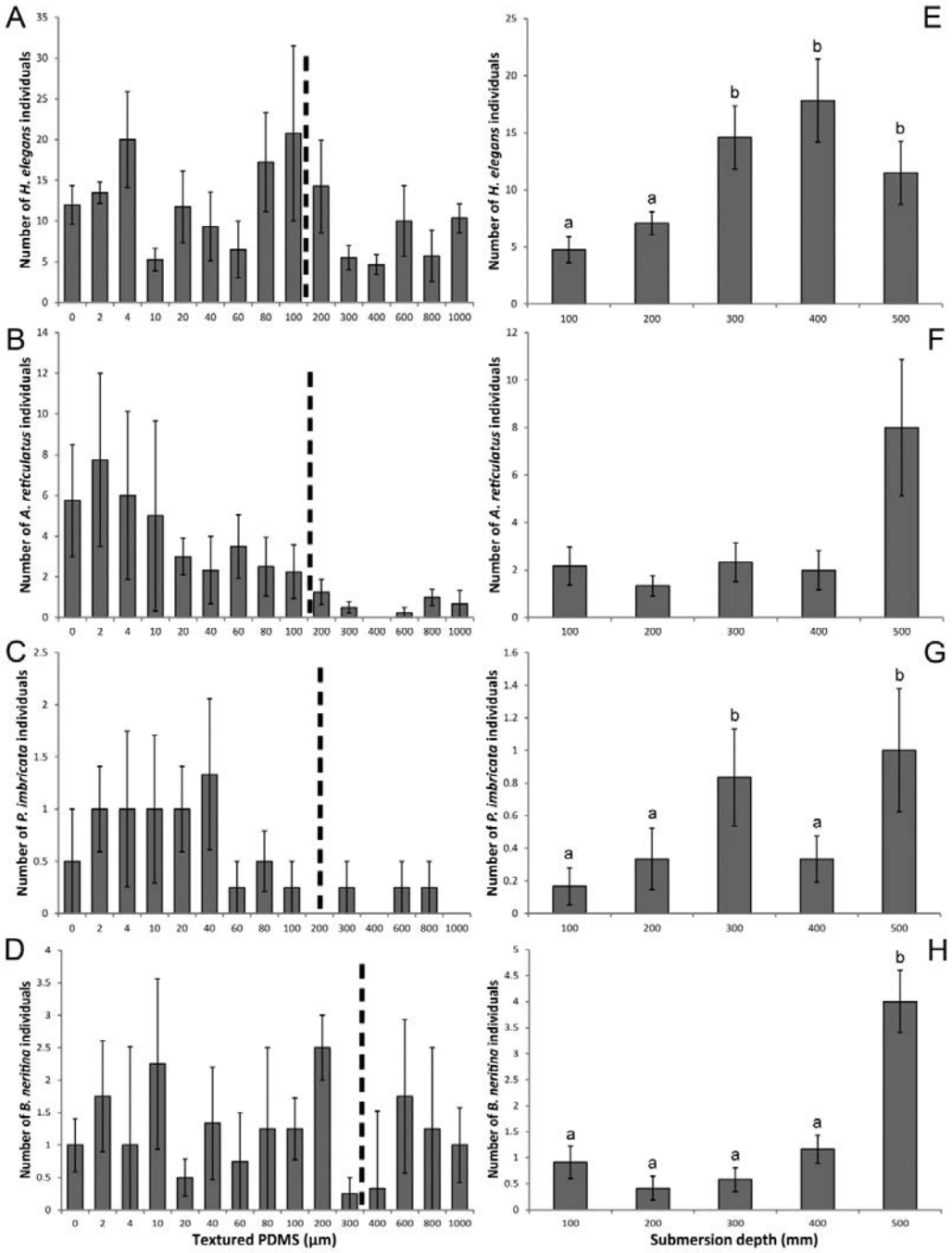

Figure 2.5. The effect of textured and non-textured PDMS surfaces on the recruitment of hard foulers at different submersion depths after six months in the field. Total number of (**A**) *H. elegans*; (**B**) *A. reticulatus*; (**C**) *P. imbricata*; and (**D**) *B. neritina* recruited to textured and non-textured PDMS surfaces. Total number of (**E**) *H. elegans*; (**F**) *A. reticulatus*; (**G**) *P. imbricata*; and (H) *B. neritina* at different submersion depths. N.B. Superscript letters above bars indicate significant groupings (pair-wise *a posteriori* comparison, $\alpha = 0.05$); dashed lines indicate approximate size of organism; all data displayed as mean ± SE.

2.3.3 Release trials

Overall, fouling taxa were essentially unaffected by the flow of water in the flow channel. However, there was a positive correlation between initial hard fouling coverage and the hard fouling coverage remaining after exposure to a high-pressure water jet (Figure 2.6) but no effect of round or square textures or any effect of aspect ratio on remaining fouling.

Fouling taxa were largely unaffected by the flow of 4.5 knots, which removed only trumpet ciliates, representing a small fraction of the total fouling population (< 1%). All other soft and hard fouling was unaffected and consequently, no flow channel results have been presented. In contrast, after exposure to a water jet from a pressure washer, textured PDMS surfaces which had the highest initial fouling coverage also had the highest amount of fouling remaining. There was no significant correlation between initial total fouling coverage (soft and hard fouling) and remaining total fouling coverage (Pearson's product-moment correlation; $r = 0.369$, $t_{(13)} = 1.432$, $p = 0.176$; Figure 2.6A), however, there was a positive trend. More importantly, after spraying, only hard foulers remained on the textured surfaces. For hard fouling, there was a significant positive correlation between initial total hard fouling coverage and remaining total hard fouling coverage ($r = 0.532$, $t_{(13)} = 2.263$, $p = 0.041$; Figure 2.6B) after exposure to a pressure washer. Surfaces with 2 and 4 μm periodicities had high initial settlement and the highest remaining hard fouling coverage while surfaces with 600 and 800 μm periodicities had low initial settlement and the lowest remaining hard fouling coverage. In addition, there was no significant effect of aspect ratio on total fouling coverage remaining (Pearson's product-moment correlation; $r = 0.524$, $t_{(12)} = 2.132$, $p = 0.054$) and total hard fouling coverage remaining ($r = 0.229$, $t_{(12)} = 0.815$, $p = 0.431$) on textured PDMS surfaces after being sprayed with the water jet. There was also no significant difference between total fouling coverage remaining (independent samples t-test, $t_{(50)} = -0.176$, $p = 0.861$) and total hard fouling coverage remaining (t-test, $t_{(50)} = 0.119$, $p = 0.906$) on round- or square-wave textured PDMS profiles after being sprayed with the water jet.

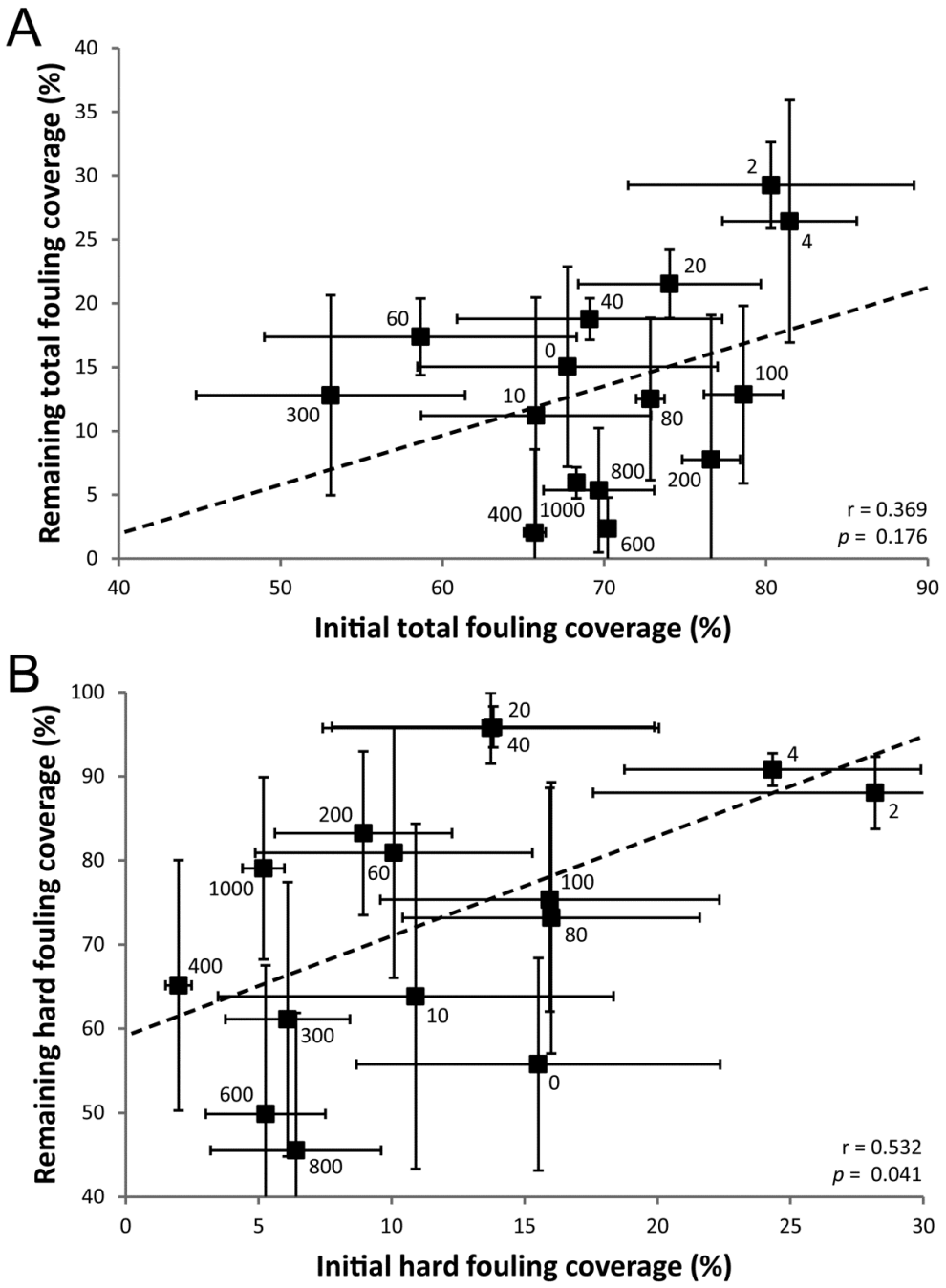

Figure 2.6. Correlation between initial fouling after six months in the field and remaining fouling after being sprayed with a high-pressure water jet (75.9 kPa). (**A**) total fouling coverage (soft and hard fouling) and (**B**) total hard fouling coverage. N.B. Data points labelled with PDMS texture; all data displayed as mean ± SE.

2.4 Discussion

The findings presented here support attachment point theory, corroborating previous findings (Callow et al. 2002; Scardino et al. 2006; Scardino et al. 2008) where, under laboratory conditions, *Ulva* sp. was significantly deterred by textures smaller than its propagule size and *S. glomerata* and *B. neritina* were significantly deterred by textures closest to, but smaller than their respective larval sizes. In addition, this Chapter demonstrates the importance of longer term field trials where, as expected, textured surfaces lost their deterrent effect and showed high rates of settlement regardless of texture after six months in the field. More importantly however, there was a positive correlation between recruitment of hard fouling and their attachment strength regardless of species composition.

Under laboratory conditions, all six tested fouling species showed preferential settlement to surfaces which varied depending on specific texture sizes. The pennate diatom *N. closterium* is characterised by a slender needle-like morphology with an approximate width of 4 μm. In contrast, *Amphora* sp. is ovular with flat ends and has an approximate width of 7 μm. Despite these differences in morphology, there fewer individual diatoms attached to all surface topographies regardless of texture size as compared to non-textured PDMS. The diatoms were between 2.3 (*Amphora* sp., 4 μm texture) and 18.0 (*N. closterium*, 0.2 μm texture) times more abundant on non-textured PDMS surfaces indicating that surface texture itself decreases attachment in these species. This is in agreement with a previous study examining benthic diatoms *in situ*, where there was higher recruitment to smooth surfaces as compared to treatments with fine and coarse roughness (Sweat and Johnson 2013). When examining textured surfaces alone, *Amphora* sp. and *N. closterium* settlement was lower on textures as periodicity decreased. These results support previous studies examining textured surfaces with similar wave-profiles, where *Amphora* sp. and *Nitzschia jeffreyi* (Hallegraeff et Burford; cell width of 4 μm) were deterred by textures smaller and equal to cell size, respectively (Scardino et al. 2006; Scardino et al. 2008).

In contrast to the diatoms which were deterred by all textured surfaces, *Ulva* sp., *S. glomerata* and *B. neritina* were deterred by textures closest to, but less than, propagule/larval size (i.e. 0–4 μm for *Ulva* sp., 100 μm for *S. glomerata* and 100–300 μm for *B. neritina*) and had higher settlement on textures above propagule/larval size (i.e. 10–60 μm for *Ulva* sp., 300 μm for *S. glomerata* and 400–600 μm for *B. neritina*). Upon visible examination of the surfaces, propagules/larvae were attached within surface gratings larger than the propagule/larva (i.e. not across or on top of gratings) and more uniformly to smaller surface gratings (i.e. across and on top of gratings). This finding suggests that the propagules/larvae may gain advantageous attachment within larger surface textures where they can fit easily and have protection from predators and resistance to hydrodynamic forces (Callow et al. 2002; Scardino et al. 2008). For *Ulva* sp., these results are in agreement with previous studies where the settlement of *U. linza* (Linnaeus 1753) spores (diameter of 5 μm) was higher between intersections of features and within surface depressions larger than spore size (Long et al. 2010; Cooper et al. 2011) and the settlement of *U. rigida* (Agardh 1823) spores (diameter of 7 μm), although not significant, increased in relation to surface groove widths that were larger than spore size (Scardino et al. 2008). For *S. glomerata*, complete settlement on all surfaces, except for 100 and 200 μm, demonstrated a strong effect of the hydrophobic PDMS material, which itself was a strong attractant. Furthermore, for *B. neritina* there was high settlement on textured surfaces much smaller than their larval size (20–80 μm) and the most parsimonious mechanism for this outcome is a high number of attachment points accessible to larvae on these textures. In contrast, lower settlement on the smallest (non-textured PDMS, 2, 4 and 10 μm) and largest (800 and 1,000 μm) textures is most likely due to fewer attachment points associated with those surfaces. Textured polycarbonate surfaces have also been shown to deter *B. neritina* with significantly lower settlement on surfaces smaller than larval size (256 μm grooves) than on surfaces larger than larval size (512 μm grooves; [Scardino et al. 2008]). In contrast, Vucko et al. (2013b; Chapter 3) used similar PDMS surfaces with a periodicity of 0, 20, 200, 300 and 600 μm, but found no differences in the settlement and recruitment of *B. neritina* in the laboratory or in the field, respectively. It is unclear

why texture had no effect on settlement, especially in laboratory assays where results should have been comparable to the ones demonstrated here.

In general, settlement of *A. reticulatus* was extremely low on all surfaces. Given that the larvae were able to swim freely throughout the assay, and were not adsorbed involuntarily to the surface, or died prior to completion of the assay, this demonstrated a strong deterrent effect of the hydrophobic PDMS itself. The effects of wettability have been well documented with marine organisms being deterred by hydrophilic surfaces (Callow et al. 2000; Finlay et al. 2002; Dahlström et al. 2004; Huggett et al. 2009), hydrophobic surfaces (Scardino et al. 2009b; Carl et al. 2012a) as well as combination of the two in the form of amphiphilic surfaces (Cho et al. 2011; Bauer et al. 2013; Di Fino et al. 2014). Therefore, testing the effects of texture on *A. reticulatus* may be best demonstrated using hydrophilic materials. In addition, by using a combination of surface texture and material type, there is potential to produce unique surfaces for single species applications in antifouling where deterrence is required, or in aquaculture where enhancement is required.

Although there were clear effects of texture on individual fouling species in the laboratory, as expected, there was no effect of texture on the recruitment of fouling (both soft and hard) when exposed to field conditions for six months. In fact, recruitment of fouling in the field was highest on the 4 μm textured surfaces, directly contradicting results from laboratory assays, where some of the lowest settlement was observed on this texture. In addition, PDMS itself was clearly a deterrent to *A. reticulatus* larvae under laboratory conditions regardless of texture, which was contrary to field results where *A. reticulatus* settled readily onto many textured PDMS surfaces. This was most likely due to biofilm build-up and smaller fouling organisms settling onto, and masking the effect of texture and the hydrophobic properties of the material. Similarly, although *H. elegans* prefer surfaces with low to medium hydrophilicity, the accumulation of a biofilm reduces these deterrent effects producing equal settlement on all surfaces regardless of initial hydrophilicity (Huggett et al. 2009). This demonstrates the importance of field trials, in addition to laboratory assays, when examining the antifouling properties of surfaces that have been

physically modified. Laboratory assays are an essential initial step to determine the deterrent capabilities of a surface. However, they do not account for the build-up of bacteria, diatoms, algae and other foulers as well as the complex interactions between environment, fouling and material properties over longer periods of time during the formation of a complex, multi-species, natural fouling community (Molino and Wetherbee 2008; Molino et al. 2009a; Molino et al. 2009b; Bers et al. 2010; Zargiel et al. 2011; Martinelli et al. 2012).

Although texture had no effect on soft or hard fouling in field trials, when specific hard fouler species were examined more closely, there were some patterns. *A. reticulatus*, *P. imbricata* and *B. neritina* had low recruitment on textured surfaces closest to, but less than larval size (180, 200 and 320 μm, respectively) and the highest recruitment on surfaces much lower than larval size. However, for these three species there was also low recruitment on textures closest to, but larger than larval size. In contrast, *H. elegans* had the highest recruitment on textures (100 μm) closest to, but less than, larval size (130 μm), contradicting previous findings using textured surfaces under laboratory conditions, where *H. elegans* were significantly deterred by textures closest to, but less than, larval size (Scardino et al. 2008). It is likely that *H. elegans* larvae were able to fit within the 100 μm texture since this periodicity had a round wave profile and a space width between 80 and 120 μm (Table 2.1). In addition, *H. elegans* is known to settle preferentially based on the presence of a biofilm (Unabia and Hadfield 1999) rather than initial surface properties (Huggett et al. 2009). For *B. neritina*, laboratory assays demonstrated the effectiveness of the 200 μm texture in deterring settlement while in the field, the 200 μm texture had the highest recruitment of all surfaces. The varied and unpredictable recruitment of these species was most likely affected by the complex nature of the fouling community as a whole, emphasised by the high fouling pressure of the tropical location, creating desirable/undesirable settlement locations and constantly changing the dynamics of the textured surfaces.

In general, fouling was more abundant with increasing submersion depth of test surfaces in the field. This could be due, in part, to settling larvae seeking out sheltered

locations and avoiding damaging ultraviolet light by moving deeper in the water column (Gleason et al. 2006; Vucko et al. 2013a; Chapter 5), or perhaps deeper surfaces, not directly adjacent the pier, offered the most water flow and therefore an increase in food availability.

After the completion of field trials, the release of fouling from textured surfaces was tested. When surfaces were exposed to flow rates of 1, 2 and 4.5 knots, there was no effect of flow on the release of fouling, regardless of texture or fouling type (soft or hard). In contrast, when the same flow channel setup and similar flow rates were tested against the short term fouling of *Mytilus galloprovincialis* (Lamarck 1819) on similar textured surfaces, there was a positive correlation between settlement preferences and the likelihood of pediveligers remaining (Carl et al. 2012a). In this Chapter, the exposure time of surfaces in the field may have led to conditioning, thereby contributing to an increase in the surface available for attachment as well as stronger attachment of the natural fouling community. Subsequently, when surfaces were exposed to a water jet, those with the highest initial fouling coverage also had, proportionally, the most fouling remaining after release trials. These results were driven by the recruitment of hard fouling as all soft fouling was removed after water jet exposure. Hard foulers were attached most strongly to textures (2 and 4 μm) where they had initially attached in the highest numbers and most weakly to textures (600 and 800 μm) where they had initially attached in the lowest numbers. Therefore, hard fouling organisms were more likely to recruit to surfaces upon which they were most likely to remain attached, supporting previous findings using textured polycarbonate surfaces, where *Balanus amphitrite* (Darwin 1854) settlement was inversely correlated with hydrodynamic removal (Aldred et al. 2010). It is unlikely that higher, or lower, recruitment was due to a higher, or lower, number of available attachment points on the surface, based on the larval size of these organisms (130–320 μm) and the fact that the 2 and 4 μm textures were most likely overgrown, masking the actual topography of the surface. Nevertheless, for many of these textures, it is conceivable that aspect ratio or texture shape (round or square) could have had an effect on the release of fouling due to differences in surface area. However, for both aspect ratio and round or

square textures, no differences were found, and interestingly, textures with both strongly (2 and 4 μm) and weakly (600 and 800 μm) adhered fouling organisms had square-wave profiles. It is unknown what other factors may have played a role in the higher recruitment to certain surfaces and why the attachment strength of hard fouling was enhanced.

In conclusion, as demonstrated in this Chapter, surface texture provides a strong deterrent to the settlement of individual fouling species in laboratory assays. This deterrence was based on larval dimensions, and preference of settlement sites is related to the number of attachment points. However, settlement of specific species under laboratory conditions does not equate to overall recruitment in the field where the deterrent effect of texture is lost due to the multitude of differently-sized species of a natural fouling community. Although short-term laboratory assays are required to obtain the fundamental data needed to improve our understanding of the effects of textured surfaces on fouling organisms, field trials are an essential part of the process and must be employed. Most importantly, the foul-release capabilities of textures were still present even after the apparent loss of any deterrent effect in the field.

Chapter 3

Combining a photocatalyst with microtopography to develop effective antifouling materials*

3.1 Introduction

Biologically inspired antifouling solutions rely on surface effects as an alternative to traditional biocidal technologies. Surface-based technologies such as textured, amphiphilic, superhydrophobic and ambiguous materials can lose their deterrent effect once conditioned and overgrown (Molino and Wetherbee 2008; Molino et al. 2009a; Molino et al. 2009b; Bers et al. 2010; Zargiel et al. 2011; Martinelli et al. 2012). Specifically, surfaces with topography targeted at a particular size of fouling organism based on 'attachment point theory' (Scardino et al. 2006; Scardino et al. 2008) can be fouled by organisms that are either too small or too large to be affected. Given that biofouling has negative impacts on all aspects of marine industry including shipping (Edyvean 2010; Schultz et al. 2011), aquaculture (Fitridge et al. 2012), power stations and desalination plants (Henderson 2010), and geophysical exploration (Vignaux 2010; Harrick and Stenzel 2011), it is important to optimise the efficacy of surface-based technologies to control a broad range of fouling organisms.

A potential broad-spectrum alternative to complement and enhance surface-based technologies is the use of photocatalysis, a chemical oxidation process activated by light which generates highly reactive oxidising agents *in situ*, including the highly potent hydroxyl radical (Fujishima et al. 2008). Hydroxyl radicals react with most organic molecules and biological substrates at rates close to diffusion limited (10^{-6}–10^{-11} d m^{-3} mol^{-1} s^{-1}) (Bhatkhande et al. 2002) and have an oxidising power of

*Chapter 3 adapted from Vucko MJ, Poole AJ, Sexton BA, Glenn FL, Carl C and de Nys R (2013). Combining a photocatalyst with microtopography to develop effective antifouling materials. Biofouling 29: 751-762.

2.8 eV; greater than ozone (2.08 eV) and second only to fluorine (3.06 eV) (dos Santos et al. 2007). Photocatalytic technology is used in antifouling membranes (Choi et al. 2007; Madaeni and Ghaemi 2007), heat exchange surfaces (Gopal et al. 2007), self-sterilising surfaces, self-cleaning surfaces (Fujishima and Zhang 2006; Fujishima et al. 2008), and air and water remediation often with mineralisation of toxic and recalcitrant organic compounds (Bhatkhande et al. 2002; Gogate and Pandit 2004; Choi et al. 2007; Demeestere et al. 2007). Biologically, photocatalysts are lethal to bacteria, fungi, viruses, prions, algae, protozoans, spores, oocysts and cancer cells due to non-specific decomposition and mineralisation (Watts et al. 1995; Lonnen et al. 2005; Mendez-Hermida et al. 2007; Xu et al. 2007; Sokmen et al. 2008; Paspaltsis et al. 2009; Zhao et al. 2009). In the marine environment, photocatalysts can cause mortality in macrofouler larvae and a decrease in adhesion strength (Carl et al. 2012b). Although photocatalysts have the clear potential to degrade conditioning molecules, settlement cues and extracellular polysaccharide glues, they are not currently used in marine antifouling and offer a promising avenue as a broad spectrum antifouling technology that can prevent settlement of a range of marine fouling organisms.

In general, photocatalysts are semi-conductor metal oxides such as TiO_2, ZnO, WO_3, CdS, ZnS, $SrTiO_3$ and SnO_2 (Bhatkhande et al. 2002). Of these, titanium dioxide (TiO_2) is regarded as an ideal photocatalyst due to its low cost, high energy, abundance, corrosion resistance, and chemical safety (Aprile et al. 2008), with the caveat that human safety concerns have been raised about the nanoparticulate form (Long et al. 2007).

When TiO_2 is activated by light of sufficient energy (3.2 eV; $300 < \lambda < 388$ nm), which in environmental applications is sunlight, a photo-excited electron in the valence band is promoted to the conduction band (Wang et al. 2007; Gaya and Abdullah 2008) resulting in the formation of a positive hole (h^+) in the valence band and an electron (e^-) in the conduction band creating a hole-electron pair (Fujishima et al. 2008). The conduction band electron can reduce molecular oxygen to form superoxide radicals, which can further react as another route to form hydroxyl radicals or they can oxidise target compounds directly (Demeestere et al. 2007; Gaya and Abdullah 2008). In the

absence of suitable electron and hole scavengers, the stored energy is dissipated within a few nanoseconds by recombination (Bhatkhande et al. 2002). The high reactivity of the radicals formed makes them safe for use because they are not persistent in the environment, and are unlikely to react with non-target organisms as the photo-killing zone is restricted to the near-surface of the material.

The overall aim of this Chapter was to investigate the antifouling efficacy of a range of textured and non-textured polydimethylsiloxane (PDMS) surfaces embedded with the TiO_2 photocatalyst using the common fouling bryozoan, *Bugula neritina* (Linnaeus 1758) as a test organism. In tropical environments of Australia, *B. neritina* is common and abundant during the winter months (May–August) but less common during the summer months (November–February) when ultraviolet (UV) radiation intensities are higher. Therefore, laboratory assays and field trials were conducted. Laboratory assays were used to firstly determine which surface treatments, if any, deterred settlement differently based on UV intensity using two light regimes representing Australian tropical winter and summer UV light intensities. Secondly, these laboratory assays determined if there was an interaction between texture and TiO_2 on the settlement of *B. neritina* larvae. In addition, surfaces were deployed in the field when *B. neritina* was most prevalent to quantify the effects of texture and TiO_2 on fouling by *B. neritina in situ* and against a natural multi-species fouling community under tidal flow conditions.

3.2 Materials and methods

3.2.1 Production of TiO_2–filled textured PDMS surfaces

To test the efficacy of TiO_2-filled PDMS surfaces against larvae of *B. neritina*, PDMS (Sylgard 184, Dow Corning, USA; 10:1 ratio of base elastomer to curing agent) matrices were filled with TiO_2 (Degussa P25; mixture of anatase [79.5%] and rutile [20.5%]) at concentrations of 0 (control), 3.75, 7.5, 11.25, and 15 weight percent (wt%) as described in detail in Carl et al. (2012b). In brief, the appropriate amount of TiO_2 nanofiller was

added to the base elastomer and mixed by vigorous stirring. The curing agent was then added to the mixture which was vigorously stirred again, degassed in a vacuum desiccator to remove any bubbles and immediately cast over a template. The effect of texture was also tested by casting the control and TiO_2-filled PDMS matrices. Non-textured (0 μm) and textured surfaces of 20, 200, 300 and 600 μm periodicity were produced by casting onto corresponding templates as described in detail in Carl et al. (2012a). In brief, textured templates were fabricated using a photolithography technique to produce grating master templates with a square-wave linear grating profile and mark-space ratio of 1.0 (groove width = land area width; Figure 3.1). Grating masters of 20, 200, 300 and 600 μm were first sprayed with a release agent and baked for 30 min at 75°C. A stainless steel mold was secured around the template using adhesive tape to form a well. The control and TiO_2-filled PDMS matrices were poured into the well and the assembly was heated for 30 min at 75°C to cure the polymer. The samples generated had an approximate thickness of 8 mm.

Importantly, the TiO_2 nanofiller, which had an average primary particle size of 21 nm, had no effect on the topography (at the micron scale) of the TiO_2-filled PDMS matrix, as compared to non-textured PDMS without TiO_2 (Carl et al. 2012b). In addition, analysis of the 20 μm textured surface, which had been coated with a conductive carbon film ~20 nm thick, using backscattered scanning electron microscopy (SEM; FEI Quanta 400F), demonstrated the sharpness and evenness of the linear grating profile (Figure 3.1). This was also true for the 200 and 600 μm surfaces, while the 300 μm linear grating profile was slightly rounded. All surfaces were washed with a mild detergent, rinsed with distilled water, and dried prior to use in assays.

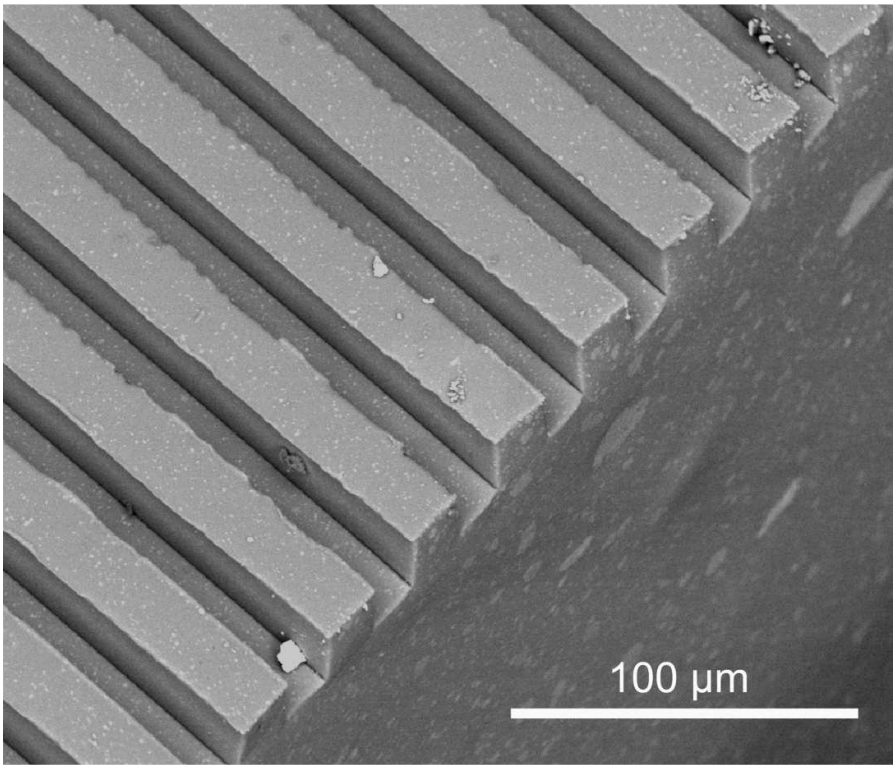

Figure 3.1. Backscattered SEM image of TiO_2-embedded (7.5 wt%) textured PDMS (20 µm) showing the linear grating with a square-wave profile and mark-space ratio of 1.0 (groove width = land area width). Scale bar = 100 µm.

3.2.2 Culture methods of B. neritina

B. neritina colonies were collected from the harbour infrastructure at the Townsville Yacht Club (TYC), Townsville, Australia. Colonies were placed into darkened plastic tubs with filtered seawater (FSW) and supplied with aeration for 72 hours. All FSW used in culturing and laboratory assays was passed through 0.35 and 0.2 µm filters, UV treated, autoclaved at 121°C for 1 hour, and stored for 7 days. After 72 hours the colonies were exposed to light to induce spawning (Marshall and Keough 2003).

3.2.3 Laboratory drop assays

The effects of TiO_2-filled textured PDMS on *B. neritina* larval settlement under winter and summer UV light intensities were quantified. To prevent evaporation while allowing penetration of UV light, 6-well microplates (Iwaki 3810-006) were used for drop assays. Surfaces were cut to size (34 mm diameter) to fit into the wells. There

were 24 replicates of each texture (no texture [0 μm], 20, 200, 300 and 600 μm) embedded with each TiO_2 loading (0, 3.75, 7.5, 11.25 and 15 wt%). Approximately 30 *B. neritina* larvae were pipetted with 800 μL of FSW and the larvae-filled drop was then placed onto the middle of each test surface (Figure 3.2A). The 800 μL drop size was small enough to prevent contact with the side wall of the well.

For the winter UV regime, a total of 12 replicates of each surface were used, of which six replicates were left in a dark room at room temperature (26°C) and six were immediately placed under a UV light bank. The intensity of the light bank was 24 W m^{-2}; comparable to the average 11:00 am winter UV intensity in Townsville, north-eastern Australia. For the summer UV regime, the remaining 12 replicates of each surface were used, of which six were left in a dark room at room temperature (26°C) and six were immediately placed under the UV light bank. The intensity of the light bank was 35 W m^{-2}; comparable to the average 11:00 am summer UV intensity in Townsville. All replicates within each assay type were randomly assigned a position within the 6-well microplates.

A photoperiod of 12 h light:12 h dark was used for both tested UV intensities. The 6-well microplates were submerged in a circulating water bath while a fan circulated air between the lights and water bath where the temperature was approximately 26°C. Light intensities were measured with a light meter (Solar Light Company PMA2100) at a wavelength of 320–400 nm (UVA). The light bank consisted of 12 Cosmedico 15508 180W RA plus Cosmolux lights (280–400 nm) and 11 Phillips Master TL5 HO 49W/865 lights (400–700 nm). The drop assays not exposed to UV were left in the dark to ensure the complete elimination of any light that could cause the TiO_2 surfaces to photoactivate. Furthermore, conducting assays in the dark is a standard method for carrying out settlement assays with *B. neritina* (Scardino et al. 2009b; Zhang et al. 2012). After 24 hours, larval settlement was quantified for all treatments.

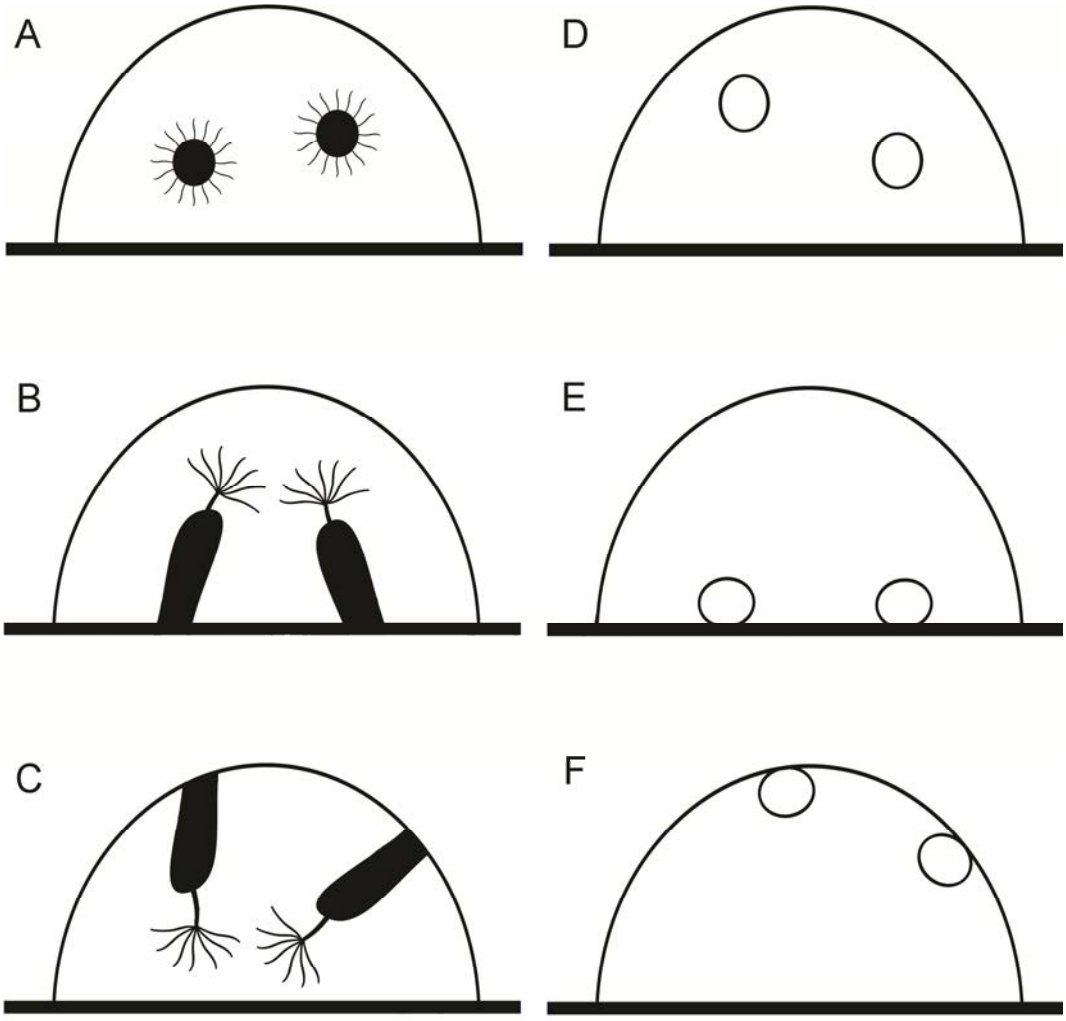

Figure 3.2. Drop assay settlement outcomes for *B. neritina* larvae. (**A**) Larvae swimming prior to settlement; (**B**) larvae settled and metamorphosed onto the surface (bottom settlement); (**C**) larvae settled and metamorphosed onto the droplet itself away from the surface (air/water interface settlement); (**D**) larvae died before having a chance to settle (dead, floating larvae); (**E**) larvae settled onto surfaces and died immediately after settlement; (**F**) larvae settled onto the air/water interface and died immediately after settlement.

3.2.4 Field trials

The effects of TiO_2-filled textured PDMS on *B. neritina* recruitment under field conditions were quantified. The surfaces were deployed in June (Australian winter), when *B. neritina* was most prevalent, to increase the likelihood of recruitment. Surfaces were cut into squares (60 x 60 mm) and randomly attached to polyvinyl chloride (PVC) plates (1350 x 225 mm, $n = 2$; 1200 x 225 mm, $n = 2$) using silicone (Selleys Glass

Silicone sealant) after the plates were roughened with abrasive paper (KMCA WA82 P120) to aid adhesion. Eight replicates of each texture (no texture [0 μm], 20, 200, 300 and 600 μm) with each TiO_2 loading (0, 3.75, 7.5, 11.25 and 15 wt%) were used. The plates were attached to PVC tube frames using cable ties and the frames were tied to boat moorings with polyethylene rope and lowered vertically, immediately below the water surface at the TYC. The frames were left for 28 days at which point the number of adult *B. neritina* individuals were counted. In addition to *B. neritina*, *Hydroides elegans* (Haswell 1883) was also present in abundant numbers at the TYC and therefore, the number of adult *H. elegans* individuals were counted.

3.2.5 Statistical analysis

For drop assays without UV (in the dark), all *B. neritina* larvae survived and metamorphosed into adults. There were two experimental outcomes with larvae settling onto either the surface (bottom settlement; Figure 3.2B) or onto the droplet itself away from the surface (air/water interface settlement; Figure 3.2C). For drop assays with UV, there were five experimental outcomes with larvae settling onto the surface and metamorphosing (Figure 3.2B), settling onto the air/water interface and metamorphosing (Figure 3.2C), dying before having a chance to settle (dead, floating larvae; Figure 3.2D), settling onto surfaces and dying immediately after settlement (Figure 3.2E), or settling onto the air/water interface and dying immediately after settlement (Figure 3.2F). Death after settlement, prior to metamorphosis, was determined as the outcome when the larvae failed to elongate past the point of being spherical, changed colour from black to dark orange and could not be moved from the surface with gentle agitation, unlike larvae which died prior to settlement. Although, theoretically, there were five possible outcomes for both treatments (without UV and with UV), only two of the possible five outcomes occurred in treatments without UV, therefore the two treatments were analysed separately. Since air/water interface settlement was a by-product of larvae not settling on the surface or dying immediately, these data were not presented graphically or analysed statistically.

Two-factor permutational multivariate analysis of variances (PERMANOVA) analyses were used to test for significant differences in bottom settlement rates of larvae not exposed to UV as well as bottom settlement rates and numbers of dead, floating larvae exposed to UV on textured PDMS surfaces with different TiO_2 loadings under summer and winter light regimes. Pair-wise *a posteriori* comparisons were used ($\alpha = 0.05$), where applicable. PERMANOVA was also used to test for significant differences in recruitment rates of *B. neritina* and *H. elegans* on textured PDMS surfaces with different TiO_2 loadings exposed to field conditions. All statistical analyses were performed using PRIMER 6 (v. 6.1.13; Ivybridge, United Kingdom) and PERMANOVA+ (v. 1.0.3 [Clarke and Gorley 2006]). For PERMANOVA, the untransformed raw data were used to produce Bray-Curtis similarity matrices. Dummy variables of 0.0001 were used to account for zero values and *p*-values were calculated from 9,999 random permutations. All data are presented as mean ± standard error.

3.3 Results

3.3.1 Laboratory drop assays

Under laboratory conditions, the presence of TiO_2 in conjunction with UV light completely inhibited larval metamorphosis of those larvae that were able to settle across both UV treatments, even at the lowest weight percent loading (3.75 wt%) and the lowest intensity of UV light (24 W m^{-2}). In contrast, there was no detrimental effect on larvae when exposed to non-activated TiO_2 (without UV). The presence of texture, while not as critical to larval settlement behaviour, deterred larval settlement, with the lowest observed numbers on 20 μm surfaces. This is contrary to results from Chapter 2 where the lowest settlement was observed on non-textured and 4 μm textured PDMS surfaces and the highest settlement was on the 20 μm texture (see discussion in Chapter 2 section 2.4 and Chapter 3 section 3.4).

3.3.1.1 Winter

Mean bottom settlement of *B. neritina*, not exposed to UV, ranged from 25.6% (no texture, 11.25 wt%) to 79.2% (no texture, 15 wt%). There was no effect of surface texture (PERMANOVA, pseudo-$F_{(4,120)}$ = 1.714, p = 0.066), TiO_2 loading (pseudo-$F_{(4,120)}$ = 0.787, p = 0.642) or an interaction (pseudo-$F_{(16,120)}$ = 1.159, p = 0.233) between the two on the settlement of *B. neritina* (Figure 3.3A; Table 3.1).

Mean bottom settlement of *B. neritina*, exposed to winter UV, ranged from 15.5% (20 μm, 15 wt%) to 89.5% (300 μm, 7.5 wt%). There was a significant effect of surface texture (pseudo-$F_{(4,117)}$ = 9.243, p < 0.001) but no effect of TiO_2 loading (pseudo-$F_{(4,117)}$ = 1.832, p = 0.054) or an interaction (pseudo-$F_{(16,117)}$ = 1.291, p = 0.123; Figure 3.3B; Table 3.1). Bottom settlement was lowest on 20 μm surfaces (pair-wise *a posteriori* comparison, α = 0.05).

Mean numbers of dead, floating *B. neritina* larvae, exposed to winter UV, ranged from 0.43% (200 μm, 0 wt%) to 81.3% (20 μm, 15 wt%). There was a significant interaction (pseudo-$F_{(16,117)}$ = 1.692, p = 0.013) between surface texture and TiO_2 loading (Figure 3.3C; Table 3.1). This interaction was mainly due to the general trend of increasing numbers of dead, floating larvae on 20 μm surfaces from 0 to 15 wt% TiO_2 while 20 μm surfaces had the highest numbers of dead larvae overall.

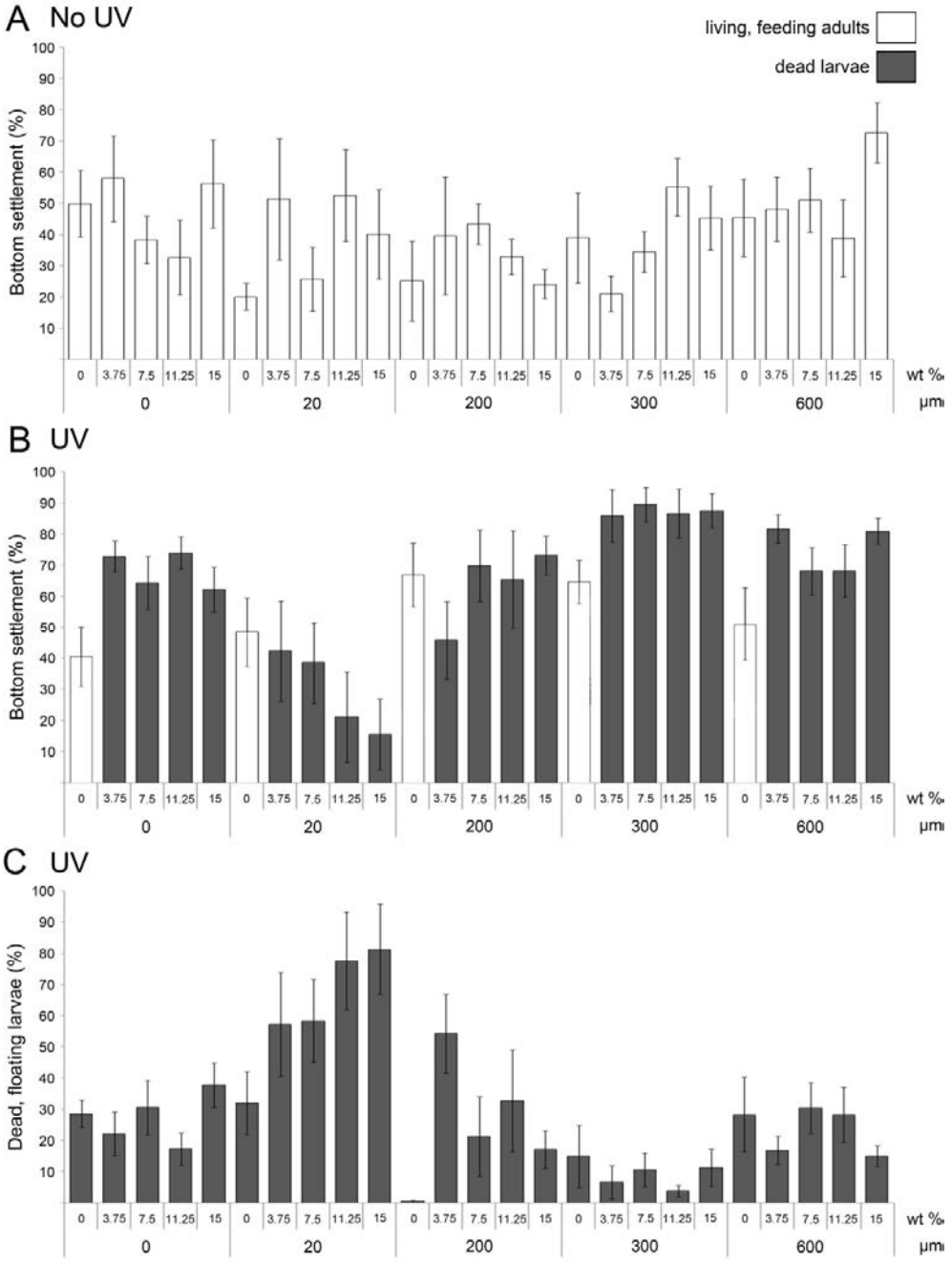

Figure 3.3. Mean settlement (± S.E.) of *B. neritina* in response to different TiO_2 loadings (0, 3.75, 7.5, 11.25 and 15 wt%) on textured (20, 200, 300 and 600 µm) and non-textured (0 µm) PDMS under the winter UV light regime. (**A**) Bottom settlement of larvae not exposed to UV (in the dark); (**B**) bottom settlement of larvae exposed to winter UV intensities; (**C**) numbers of dead, floating larvae exposed to winter UV intensities. N.B. Bottom settlement onto TiO_2-embedded surfaces exposed to UV are indicative of initial settlement only as all larvae died shortly after settling and were not able to metamorphose.

In general, *B. neritina* larvae settled onto photocatalytically activated TiO_2 surfaces, but died immediately after settlement and were unable to metamorphose. In contrast, larvae that settled onto surfaces with 0 wt% TiO_2, exposed to UV, metamorphosed into living, feeding adults.

3.3.1.2 Summer

Mean bottom settlement of *B. neritina*, not exposed to UV, ranged from 20.1% (20 μm, 0 wt%; 300 μm, 3.75 wt%) to 72.7% (600 μm, 15 wt%). There was no effect of surface texture (PERMANOVA, pseudo-$F_{(4,113)}$ = 1.244, p = 0.253), TiO_2 loading (pseudo-$F_{(4,113)}$ = 1.083, p = 0.363) or an interaction (pseudo-$F_{(16,113)}$ = 1.225, p = 0.178) between the two on the settlement of *B. neritina* (Figure 3.4A; Table 3.1).

Table 3.1. Two-factor PERMANOVA analysis with significant effects of surface texture (Text; 0, 20, 200, 300 and 600 μm) and TiO_2 loading (TiO_2; 0, 3.75, 7.5, 11.25 and 15 wt%) on the settlement of *B. neritina* on PDMS surfaces after 24 hours under winter and summer light regimes exposed and not exposed to UV.

		Factor	df	MS	pseudo-*F*	*p*-value
Winter	Bottom settlement without UV	Text	4	1,731	1.714	0.0660
		TiO_2	4	794	0.787	0.6420
		Text x TiO_2	16	1,170	1.159	0.2330
	Bottom settlement with UV	Text	4	7,062	9.243	0.0001
		TiO_2	4	1,400	1.832	0.0001
		Text x TiO_2	16	987	1.291	0.0001*
	Dead, floating larvae with UV	Text	4	17,501	9.584	0.0001
		TiO_2	4	3,245	1.777	0.0678
		Text x TiO_2	16	3,089	1.692	0.0125*
Summer	Bottom settlement without UV	Text	4	1,659	1.244	0.2530
		TiO_2	4	1,445	1.083	0.3630
		Text x TiO_2	16	1,634	1225	0.1780
	Bottom settlement with UV	Text	4	6,001	10.949	0.0001
		TiO_2	4	3,814	6.959	0.0001
		Text x TiO_2	16	2,181	3.979	0.0001*
	Dead, floating larvae with UV	Text	4	13,025	10.366	0.0001
		TiO_2	4	30,158	24.002	0.0001
		Text x TiO_2	16	3,364	2.677	0.0002*

Note: * denotes significant effect; α = 0.05.

Mean bottom settlement of *B. neritina*, exposed to summer UV, ranged from 4.6% (20 μm, 3.75 wt%) to 100% (200 μm, 0 wt%). There was a significant interaction (pseudo-$F_{(16,121)} = 3.979$, $p < 0.001$) between surface texture and TiO_2 loading (Figure 3.4B; Table 3.1). This interaction was mainly due to reduced bottom settlement on non-textured and 20 μm surfaces containing TiO_2 (3.75, 7.5, 11.25 and 15 wt%) and increased bottom settlement on 300 μm surfaces with 0 wt% TiO_2. Settlement on 200 and 600 μm surfaces was higher than both non-textured and 20 μm surfaces but lower than 300 μm surfaces.

Mean numbers of dead, floating *B. neritina* larvae, exposed to summer UV, ranged from 0% (200 μm, 0 wt%; 300 μm, 0 and 3.75 wt%) to 95.4% (20 μm, 3.75 wt%). There was a significant interaction (pseudo-$F_{(16,121)} = 2.677$, $p < 0.001$) between surface texture and TiO_2 loading (Figure 3.4C; Table 3.1). This interaction was mainly due to lower numbers of dead, floating larvae on 300 μm surfaces and highly variable dead, floating larvae on the different TiO_2 loadings.

Larvae of *B. neritina* were able to settle on photocatalytically activated TiO_2 surfaces, but died immediately after settlement. There was a high proportion of bottom settlement in *B. neritina* larvae when exposed to UV regardless of the presence of photoactivated TiO_2 or deterrent textured surfaces. *B. neritina* responded to UV light by moving away and closer to the surface, unlike the treatment without UV where larvae readily settled onto either the bottom or the air/water interface. Notably, following settlement, the presence of summer UV completely inhibited larval growth and metamorphosis on all surface textures and loadings including those without TiO_2.

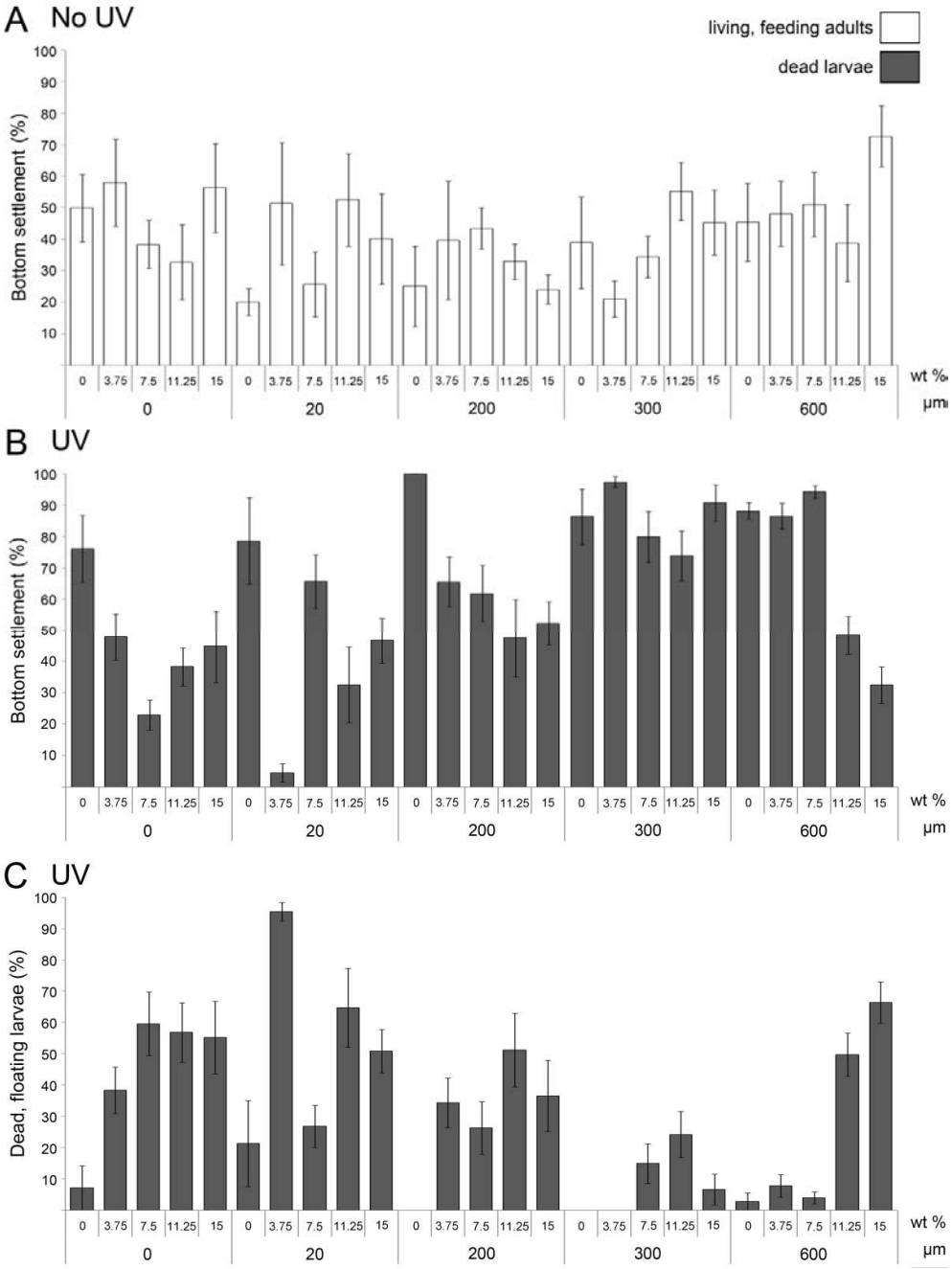

Figure 3.4. Mean settlement (± S.E.) of *B. neritina* in response to different TiO_2 loadings (0, 3.75, 7.5, 11.25 and 15 wt%) on textured (20, 200, 300 and 600 µm) and non-textured (0 µm) PDMS under the summer UV light regime. (**A**) Bottom settlement of larvae not exposed to UV (in the dark); (**B**) bottom settlement of larvae exposed to summer UV intensities; (**C**) numbers of dead, floating larvae exposed to summer UV intensities. N.B. Bottom settlement on surfaces exposed to UV are indicative of initial settlement only as all larvae died shortly after settling and were not able to metamorphose.

3.3.2 Field trials

Under field conditions, the recruitment of *B. neritina* and *H. elegans* was significantly lower on surfaces containing TiO_2 (3.75, 7.5, 11.25 and 15 wt%) than on textured and non-textured PDMS controls without TiO_2 (pair-wise *a posteriori* comparison, $\alpha = 0.05$).

Mean recruitment of *B. neritina* ranged from 1.6 individuals (20 μm, 15 wt%) to 47.8 individuals (no texture, 0 wt%). There was a significant effect of surface texture (PERMANOVA, pseudo-$F_{(4,179)} = 2.503$, $p = 0.005$) and TiO_2 loading (pseudo-$F_{(4,179)} = 11.473$, $p < 0.001$) but no interaction (pseudo-$F_{(16,179)} = 0.671$, $p = 0.958$) on the recruitment of *B. neritina* onto textured PDMS surfaces with different TiO_2 loadings exposed to UV in the field (Figure 3.5A; Table 3.2).

Mean recruitment of *H. elegans* ranged from no individuals to 3.1 individuals (600 μm texture, 0 wt%). There was a significant effect of surface texture (pseudo-$F_{(4,179)} = 2.324$, $p = 0.0497$) and TiO_2 loading (pseudo-$F_{(4,179)} = 44.144$, $p < 0.001$) but no interaction (pseudo-$F_{(16,179)} = 1.033$, $p = 0.421$) on the recruitment of *H. elegans* onto textured PDMS surfaces with different TiO_2 loadings exposed to UV in the field (Figure 3.5B; Table 3.2).

Table 3.2. Two-factor PERMANOVA analysis with significant effects of surface texture (Text; 0, 20, 200, 300 and 600 μm) and TiO_2 loading (TiO_2; 0, 3.75, 7.5, 11.25 and 15 wt%) on the settlement of *B. neritina* and *H. elegans* on PDMS surfaces after 28 days under field conditions.

	Factor	df	MS	pseudo-*F*	*p*-value
B. neritina	Text	4	5,312	2.503	0.0053*
	TiO_2	4	24,353	11.473	0.0001*
	Text x TiO_2	16	1,425	0.671	0.9580
H. elegans	Text	4	1,936	2.324	0.0497*
	TiO_2	4	36,769	44.144	0.0001*
	Text x TiO_2	16	860	1.033	0.4210

Note: * denotes significant effect; $\alpha = 0.05$.

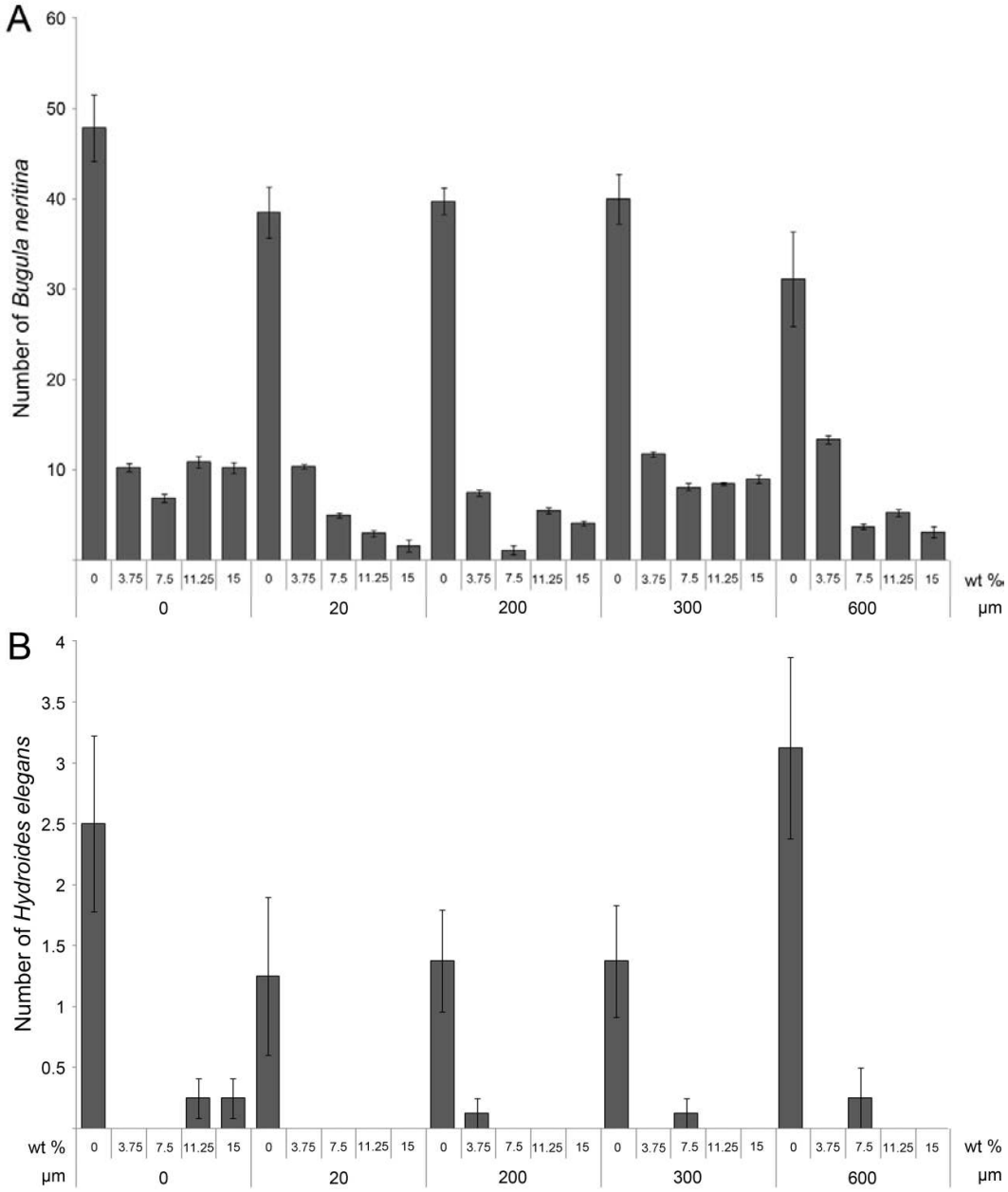

Figure 3.5. Mean recruitment (± S.E.) of (**A**) *B. neritina* and (**B**) *H. elegans* in response to different TiO_2 loadings (0, 3.75, 7.5, 11.25 and 15 wt%) on textured (20, 200, 300 and 600 μm) and non-textured (0 μm) PDMS after 28 days in the field.

3.4 Discussion

TiO_2, photocatalytically activated by UV light, was highly effective against *B. neritina* larvae in laboratory assays with no detrimental effect on larvae when exposed to non-activated TiO_2. All loadings (3.75, 7.5, 11.25 and 15 wt%) of embedded TiO_2 were equally effective against this species, and for laboratory assays, TiO_2 in conjunction with UV light demonstrated complete inhibition of larval growth and maturation. Similarly, there was a strong deterrence of recruitment of *B. neritina* and *H. elegans* after 28 days in field trials. These results, even at the lowest loading, show that 3.75 wt% TiO_2 is sufficient for use as a minimum inhibitory concentration under laboratory conditions and field conditions in the tropics.

There was a significant effect of UV on the settlement of *B. neritina* in laboratory assays for both winter and summer UV light regimes. When larvae were exposed to winter UV conditions (24 W m^{-2}), there was a higher proportion of bottom settlement on all TiO_2 loadings and textures compared to conditions without UV regardless of the presence of photoactivated TiO_2 or deterrent textured surfaces. This could be a mechanism to avoid UV damage by moving away (i.e. moving deeper, towards the material surface) and settling even though this species is positively phototactic, unlike in the treatment without UV where larvae readily settled onto the air/water interface. This is consistent with field observations where the largest colonies of settled, mature *B. neritina* occur where UV is less intense, deeper below the surface (Conde et al. 2000). Upon settling onto photoactivated TiO_2 surfaces the larvae were killed and unable to metamorphose, whereas larvae settling under UV on blank PDMS surfaces (0 wt% TiO_2), and larvae settling onto all PDMS surfaces with or without TiO_2 when not photoactivated (without UV) also survived and metamorphosed. This clearly demonstrates that the lethal effect on the larvae was a result of photocatalysis. In contrast, all larvae exposed to summer UV conditions (35 W m^{-2}) in the laboratory were killed by the intense UV, independent of substrate, demonstrating that this high level of UV is, in itself, lethal.

There was also a significant effect of UV on the recruitment of *B. neritina* and *H. elegans* under field conditions. *B. neritina* and *H. elegans* larvae were able to settle and metamorphose on photocatalytically activated TiO_2 surfaces but in significantly lower numbers than on surfaces without TiO_2. This ability of the larvae to settle onto naturally activated TiO_2 at all, may have been due to lower UV intensities under the water due to dissolved and particulate organic matter (Conde et al. 2000). At this field location, the highest UV measured under the water during the trial was 8 W m^{-2}, which is much lower than the laboratory conditions and most likely due to particulate matter in the marina at that time. It is likely that these photocatalytic surfaces would perform more efficiently if used in open, clearer waters (Jerlov 1950; Smith et al. 1992). However, despite the lower UV, larval settlement was deterred at the lowest tested TiO_2 concentration (3.75 wt%), which is consistent with laboratory assay results. This confirms that, for these species of fouling organism, TiO_2 loadings as low as 3.75 wt% can be used to prevent larval settlement and therefore adult recruitment.

The use of photoactivated TiO_2 as a deterrent to marine fouling was not only effective against *B. neritina* and *H. elegans* here, but has also been shown to be effective against the mussel *Mytilus galloprovincialis* (Carl et al. 2012b), further supporting the utility of this technology in the development of antifouling materials for use in the photic zone.

Texture also had a significant effect on *B. neritina* larval settlement in laboratory assays under winter UV conditions and on the recruitment of *B. neritina* in field trials. Since *B. neritina* have a larval body size of approximately 350 μm, the 300 μm texture was expected to deter settlement and recruitment based on 'attachment point theory' (Scardino et al. 2008). This was not the case, and although this was possibly due to the gregarious nature of settling *B. neritina* larvae or the confounding ability to settle on either the material surface or the air/water interface, it is more likely due to the pliable nature of PDMS. This pliable nature, in conjunction with the slightly rounded edge of the square-wave linear grating profile, would have allowed larvae to fit within the 300 μm grooves causing the higher larval settlement and therefore adult recruitment. On 200 μm surfaces, the smaller grating size in conjunction with the sharpness and evenness of the square-wave linear grating profile would make it difficult for larvae to

fit. In contrast, the 20 μm surface texture had the lowest overall settlement in the laboratory and lowest overall recruitment in the field. For the laboratory assays, it is presumed that larvae, deterred by both textured surfaces and UV light, were forced to continue swimming, and the higher concentrations of TiO_2 were able to kill the larvae before they had a chance to settle. Interestingly, it should be noted that the deterrent effect of the 20 μm surfaces in the field was not apparent on treatments without TiO_2. This was most likely due to the conditioning of the surface which can become overgrown, thereby reducing the effectiveness of the texture (Bers et al. 2010). Therefore, for *B. neritina*, settlement deterrence is optimised with the use of 20 μm grooved surfaces in conjunction with 3.75 wt% TiO_2. In addition, although texture had a significant effect on the recruitment of *H. elegans*, the results should be treated with caution since the low overall recruitment to surfaces was coupled with high variability among treatments.

Using the 20 μm texture has also been shown to be effective against cyprids of the barnacle *Balanus amphitrite* (Darwin 1854) where PDMS with a similar square-wave profile also deterred larval settlement but without the use of TiO_2 (Schumacher et al. 2007b). Considering the difference in morphology between the two species, where *B. amphitrite* cyprids use an antennular attachment disc to search for a suitable settlement site (Phang et al. 2008) and *B. neritina* use large flagella (Mawatari 1951), it is likely that body size, which is similar between the two, plays an important role in settlement behaviour.

From a materials perspective, it is important to establish effects of TiO_2 on PDMS. Using PDMS for this application is ideal since it is transparent allowing photoactivation of TiO_2 and, although hydroxyl radicals are highly reactive, they do not break silicone bonds (Iketani et al. 2003). In addition, adding high levels of TiO_2 (15 wt%) to PDMS only marginally alters the physical properties that affect fouling resistance (hardness, water contact angle after UV exposure, roughness [Carl et al. 2012b]). Since PDMS is a widely used foul-release coating (Townsin and Anderson 2009), the combination with TiO_2 represents a potentially effective broad spectrum, environmentally benign, antifouling option.

While photoactivated TiO_2 appears promising, since the activation of photocatalytic TiO_2 in environmental applications is by sunlight, surfaces are only effective when exposed to UV. This raises questions about the potential efficacy against fouling organisms that settle and metamorphose at night and, for marine underwater applications, about UV attenuation in the water column, which is likely to reduce effectiveness. UV penetration is limited in inland and some in-shore coastal waters due to chromophoric dissolved organic matter and particulate organic and inorganic matter (Conde et al. 2000; De Lange 2000; Hader and Sinha 2005). In contrast, clear ocean water UV penetration is reported to reach depths of 10–20 m (Jerlov 1950; Smith et al. 1992), sufficient for many antifouling applications.

In conclusion, the TiO_2 photocatalyst was effective in deterring settlement and recruitment of *B. neritina* and recruitment of *H. elegans*, even at the lowest concentration, with the lowest *B. neritina* attachment occurring on 20 μm textured surfaces in both laboratory and field experiments. Combining these two technologies supports the development of an effective broad spectrum antifouling material, where texture prevents colonisation of key macrofouler larvae while the photocatalyst has the potential to minimise biofilms, kill microfoulers, degrade chemical settling cues, weaken the macrofouler cement and further prevent larval settlement and adult recruitment in the photic zone, where fouling is greatest and most diverse.

Chapter 4

Cold spray metal embedment:

an innovative antifouling technology*

4.1 Introduction

Fouling impedes the functional capacity of man-made underwater marine structures including vessels, finfish cages and oceanographic equipment. It decreases the efficiency of vessel movement through water causing range and manoeuvrability reduction, increased fuel consumption and lateness penalties (Brady and Singer 2000; Townsin 2003; Schultz et al. 2011). It affects finfish aquaculture cages by restricting water exchange thereby reducing water quality and increasing disease as well as causing deformations and structural fatigue of the cage itself (de Nys and Guenther 2009). It also affects the function of oceanographic equipment used in the geophysical exploration industry (Goode et al. 1982).

A variety of processes facilitate successful recruitment of marine invertebrate larvae including physical, chemical and biological surface-associated cues (Pawlik 1992; Huang and Hadfield 2003; Dahlström et al. 2004; Scardino and de Nys 2011), surface texture (Aldred and Clare 2008; Scardino et al. 2008), wettability (Bennett et al. 2010), elastic modulus (Chaudhury et al. 2005), the presence of conspecifics (Elbourne et al. 2008) and environmental conditions including salinity, flow, temperature and ultraviolet irradiation (Prendergast 2010). Because so many factors contribute to the successful recruitment of foulers, technologies to prevent fouling have focused on broad spectrum metal and organic biocides released from coatings to inhibit larval settlement (Finnie and Williams 2010).

*Chapter 4 adapted from Vucko MJ, King PC, Poole AJ, Carl C, Jahedi MZ and de Nys R (2012). Cold spray metal embedment: an innovative antifouling technology. Biofouling 28: 239-248.

Copper and copper-based coatings are the largest volume functional broad spectrum antifouling technology (Brooks and Waldock 2009; Finnie and Williams 2010). The toxicity of copper in marine invertebrates occurs directly through the absorption of waterborne free Cu^{+} and Cu^{2+} ions, arguably the most toxic form of the metal (Pinho et al. 2007; Thomas and Brooks 2010). The mechanism of toxicity of copper is associated with the inhibition of Na^{+}- and K^{+}-ATPase activity, causing intracellular ion imbalances and the inhibition of carbonic anhydrase enzyme activity, impairing gas exchange and acid-base regulation (Grosell et al. 2007; Lopes et al. 2011). Copper is effective within surface boundary layers while being less toxic when released into the environment as a result of complexation with dissolved organic carbon in the water column and a low bioavailability within sediments (Lu and Allen 2001; Brooks et al. 2008; Brooks and Waldock 2009; Thomas and Brooks 2010). However, copper-based coatings and coatings in general have, in many cases poor adhesion to thermoplastic polymers (polymers) which are widely used in aquaculture (high-density polyethylene [HDPE] and nylon) and marine industries (polyurethane) including geophysical exploration (Luscombe et al. 1999; Braithwaite and McEvoy 2005; Fredriksson et al. 2007; Moe et al. 2009). For example, aquaculture nets utilise specialised flexible copper coatings based on wax emulsions, rather than standard boat paints which are designed for solid inflexible surfaces. Consequently, these coatings have a typical life span of six to nine months before failure which is sufficient for high latitude (temperate) aquaculture industries (reviewed in Braithwaite and McEvoy 2005; Braithwaite et al. 2007; Svane et al. 2006; reviewed in de Nys and Guenther 2009; Guenther et al. 2010). However, there are no functional coatings available for use on flexible polyurethane streamers used in geophysical exploration due to polymer properties and operational requirements where streamers are handled mechanically on-board specialised exploration vessels. In the present Chapter, copper particles embedded into polymers using cold spray are tested to determine whether they are an effective deterrent against fouling organisms.

Cold spray is a metal spray process whereby solid metal particles (typically < 50 μm) are accelerated to supersonic velocities in an inert gas flow and deposited onto a

substrate surface, forming a coating (Stoltenhoff et al. 2002; Papyrin et al. 2007). Gas is accelerated using high pressure (1.5–3.5 MPa) and heat (less than the melting point of the metal being used) and once stabilised, particles are injected into the gas flow and pass through a converging-diverging nozzle and onto the surface (Gärtner et al. 2006). Many factors can be manipulated during the cold spray process (nozzle type, nozzle dimensions, gas type, gas temperature, powder size, powder flow rate, powder insertion location and dimensions), and the appropriate balance depends heavily on the type of metal powder being used and the substrate being sprayed (Pattison et al. 2007; Lupoi and O'Neill 2011). This balance must then be maintained throughout the cold spray process and will allow particles to surpass a critical velocity where, instead of rebounding (low velocity) or abrading (moderate velocity) the intended substrate, particles embed or adhere to the surface. Heating of the gas not only increases velocity but also enhances particle plasticity enabling effective deposition and heat transfer to the surface which may improve embedment into the substrate. Applications of cold spray are very broad and include the formation of wear- and corrosion-resistant coatings, improvement of electrical and heat conductivity (Gärtner et al. 2006), freeform shape production without the use of moulds, and structure reinforcement (Pattison et al. 2007). Cold spray is ideal in these situations due to the dense nature of the deposits and the absence of defects such as material stress and warping, substandard mechanical properties and changes in microstructure caused by excessive heating or melting of the particles seen with competing thermal spray techniques (Amon et al. 1993; Gärtner et al. 2006; Pattison et al. 2007). The use of cold spray technology as a method to control biofouling by embedding metal particles into polymers is an innovative approach with the promise of delivering new antifouling materials.

In this Chapter, firstly, the ability of cold spray technology to produce Cu-embedded polymers for marine antifouling applications using a thin layer of embedded metal particles without building up large deposits or coatings was developed and quantified. Polymer surfaces should be robust to the technique of cold spray as they are resistant to corrosion and have good mouldability. Secondly, these polymers were

trialled over 250 days to quantify their efficacy as antifouling materials under intense fouling conditions, and analytical techniques were used to identify individual particle characteristics and basic elements dominating the metal patina at the point of material failure (fouling).

4.2 Materials and methods

4.2.1 Polymer surface preparation

Polymers, polymers metallised using cold spray, copper plate, and a positive control surface (Perspex) were tested for their effect on the settlement of organisms in the field. The polymers used were HDPE (Simona) and nylon 6 (nylon; Quadrant EPP Ltd.). The test surfaces were washed with a detergent solution Decon 90 (Decon Laboratories Ltd.), rinsed with distilled water and air dried before being used.

Polymer sheets (140 x 170 mm) were metallised by cold spray using a Kinetiks 4000 cold spray system (Cold Gas Technology GmbH, Ampfing, Germany) at the Commonwealth Scientific and Industrial Research Organisation, Clayton. AEE-112 copper powder (Atlantic Equipment Engineers, Bergenfield, NJ) was chosen as the feedstock material and the specified Cu purity was 99.9% on a metals-basis. The as-supplied powder was -325 mesh, having been passed through a 45 μm sieve. Particle analysis using a Mastersizer Laser Analyser (Malvern Instruments Ltd., Malvern, Worcestershire, UK) showed that the average particle size (d_{50}) was 26.9 μm, while d_{10} and d_{90} were 12.8 and 49.7 μm, respectively. Nitrogen was used as the carrier gas and was kept at a constant temperature of 100°C and pressure of 2.0 MPa throughout spraying. This temperature and pressure facilitated a gas velocity that was high enough to accelerate and embed copper particles into the polymers. The nozzle was held 30 mm from the polymer surface and moved laterally by a robot arm (ABB IRB 2600) in a raster program with an inter-pass distance of 2 mm. A traverse speed of 0.1 m s^{-1} was used to cold spray the HDPE and nylon plates which resulted in copper densities of 125 ± 12 g m^{-2} and 115 ± 10 g m^{-2}, respectively. These densities are

comparable to a single coat of antifouling paint (Wattyl® SEAPRO® CU120 Antifouling; 100 μm dry coating thickness at 50% copper content by volume) which has a copper loading, present as cuprous oxide, of approximately 110 g m^{-2}. Once the polymers were cold sprayed, 34 mm plugs were cut from each sheet using a circular punch.

4.2.2 Polymer surface characterisation

Cold spray polymer surfaces were examined using backscattered scanning electron microscopy (SEM; JEOL JSM-5410LV; sputter coated with platinum) and in all cases, high impact velocities caused copper particles to embed into the surface, subsequently forming a discontinuous coating where embedment of particles depends on polymer type (Figures 4.1A and B). Depth of embedment was relatively shallow (< 100 μm; see results Polymer Surface Characterisation; Figures 4.1C and D), therefore it is unlikely that metal particle embedment will have any effect on bulk polymer properties such as flexibility. To determine whether the polymer characteristics facilitate a high degree of copper retention, elastic modulus and hardness of HDPE and nylon was measured. Elastic modulus relates to the temporary deformation resistance of materials and is a measure of the ability of a material to store energy. Elastic modulus was measured at room temperature on polymers (60 x 13 mm; $n = 3$) clamped (dual cantilever clamp; 5 lbs of pressure) in a Dynamic Mechanical Analyser (TA Instruments DMA Q800) in Multifrequency Strain mode and 20 μm amplitude operating conditions. Measurements were collected at a single frequency of 1 Hz and elastic modulus was obtained after 2 min from a preinstalled software program. Hardness relates to the resistance of a material to permanent indentation. Shore D2 hardness was measured with a Shore® Durometer (Shore Instrument and Mfg. Co. Inc., NY, USA) in accordance with the ASTM D2240-05 standard (ASTM 2010). Hardness readings were taken after the indentor had stopped for 1 s subsequent to initial indentor travel. Nylon plugs (2 mm thickness) were stacked so the total thickness was at least 6 mm.

The surface area covered by copper particles was calculated from digital microscopy (SZ61; Olympus, Eagle Farm, Queensland, Australia) images (DP25; Olympus, Eagle

Farm, Queensland, Australia) of each plug ($n = 20$), by inverting the colours and obtaining a black (copper particles) and white (polymer surface) pixel threshold (Photoshop v. 12.0.4; Adobe Systems Software, San Jose, California, USA). Pixel percent coverage was then quantified using ImageJ (v. 1.42q; National Institutes of Health, Bethesda, Maryland, USA). The mass of copper particles was determined from the difference in mass of polymer control plugs and Cu-embedded polymers plugs ($n = 20$) using a balance (Adam Equipment Co. Ltd. AAA 250LE). The two polymers were also examined in cross section to estimate embedment depth of copper particles. Using a scalpel, a slice was taken from each polymer ($n = 3$) and photographed using a microscope (Olympus SZ61) and digital camera (Olympus DP25). Each image was then split into 10 equal segments within which one random particle depth was measured. Medians were obtained from each image and depth of embedment was quantified from images using ImageJ (v. 1.42q).

The copper metal control surfaces (copper plate) consisted of electrolytic tough pitch copper disks (C11000; 34 mm diameter) that were wet ground with P400 SiC paper to an average roughness of 0.24 ± 0.03 Ra (measured using a perthometer [Mahr GmbH, Göttingen, Germany]). Perspex was used as a positive control as this material fouls rapidly under field conditions at the study site (Scardino and de Nys 2004).

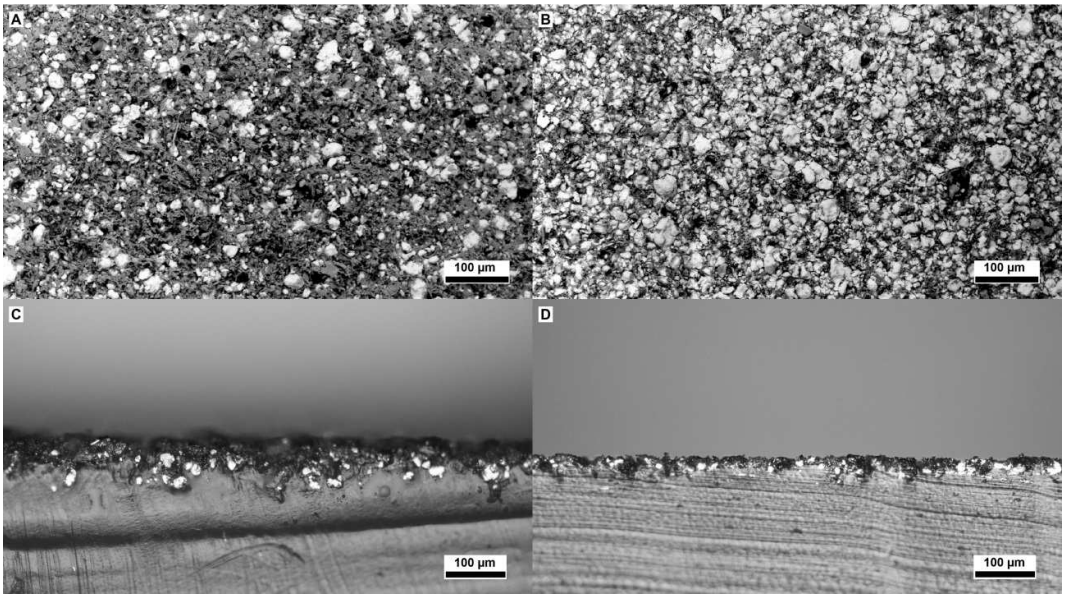

Figure 4.1. Backscattered scanning electron micrographs of polymers embedded with copper particles using cold spray technology. Light coloured surfaces are copper particles and dark coloured surfaces are polymer. (**A**) Surface view of Cu-embedded HDPE showing area coverage of copper particles; 150 times magnification; EHT, 10 kV. (**B**) Surface view of Cu-embedded nylon showing area coverage of copper particles; 150 times magnification; EHT, 10 kV. (**C**) Cross section of Cu-embedded HDPE showing embedment depth of copper particles. (**D**) Cross section of Cu-embedded nylon showing embedment depth of copper particles. Polymers were metallised by cold spray using a Kinetics 4000 cold spray system (Cold Gas Technology GmbH, Ampfing, Germany) with AEE-112 copper powder as the feedstock material.

4.2.3 Polymer surface field trials

Test surfaces were randomly attached to a Perspex backing plate (1115 x 275 mm) using super glue. Treatments were HDPE, Cu-embedded HDPE, nylon, Cu-embedded nylon, copper plate and a Perspex control ($n = 8$). Once attached, two coats of antifouling paint (Wattyl® SEAPRO® CU120) were applied around the plugs to prevent edge effects where fouling organisms would foul the Perspex plate and move onto the plugs without directly attaching (false fouling). The application of antifouling paint does not affect settlement on the surfaces with fouling occurring immediately adjacent to the paint (Scardino 2006). Holes were drilled along the length and width of the Perspex plate and the plate was attached to a PVC tube frame (25 mm diameter)

using cable ties with a 20 mm gap between the Perspex plate and the frame. The uncaged frame was placed vertically in the water, 200 mm below the surface at the Townsville Yacht Club (Queensland, Australia) in mid-December (summer). Given this dry tropical location, although fouling species vary throughout the year, there is consistent, heavy fouling year round. Photographs were taken weekly to track the course of fouling and using this method, individual fouling species and changes in the fouling community were quantified. Prior to taking photographs, all surfaces were lightly sprayed (no more than 2.5 N of force) using a conventional garden hose to remove the build-up of silt. Total fouling coverage (soft [*Ulva* sp.] and hard [bryozoans, barnacles, mussels and polychaetes] fouling), total hard fouling coverage and total number of hard foulers were first quantified and presented graphically after 181 days of continuous exposure when obvious differences in total fouling coverage on metallised polymer surfaces were observed, and after 250 days of continuous exposure when the first metallised polymer failed as determined by the settlement of hard fouling. In addition, critical quantitative changes in the species composition and structure of the fouling community at these two times are described. Percent fouling coverage and total hard fouler numbers were quantified from digital images using ImageJ (v. 1.42q).

To characterise the surface of Cu-embedded HDPE and Cu-embedded nylon after 250 days in the field, a dual focussed ion beam (FIB)/SEM (FEI Helios Nanolab 600i) was used. FIB/SEM was used to examine organisms at the surface, and individual particle characteristics below the surface, from pieces (5 x 5 mm; sputter-coated with iridium) cut from each plug. Rectangular trenches (20–30 μm wide) were milled into the surface using a Ga^+ ion beam so that when viewed in SEM mode at a 52° tilt, the exposed face showed a cross-section below the surface. This technique allowed careful sectioning through the soft polymer and brittle, reacted particles without the smearing, pore closure and particle pull-out that occur during standard mechanical polishing. In addition, energy-dispersed X-ray spectroscopy (EDS; JEOL JXA-8200) was used to quantify basic elements dominating the metal patina from scrapings of the copper embedded layer of the plugs to determine changes in the elemental composition

related to the release of copper ions from the metallised polymers. Test material was scraped from the plugs using a scalpel until only polymer was visible, and crushed using a mortar and pestle for examination using EDS.

4.2.4 Statistical analysis

To test for significant differences in copper loading, copper particle surface area, and particle depth of embedment between HDPE and nylon Cu-embedded surfaces, independent samples t-tests were used. To test the effects of polymers (HDPE and nylon), metallised polymers (Cu-embedded HDPE and Cu-embedded nylon) and metals (copper plate) on total fouling coverage, total hard fouling coverage and total number of hard foulers after 181 and 250 days in the field, one-factor permutational multivariate analysis of variances (PERMANOVA) with 9,999 permutations followed by pair-wise *a posteriori* comparisons (α = 0.05) were used, where applicable. Perspex was not included in any analysis and was solely used as a positive control to ensure active biofouling.

All proportions of total fouling coverage and macrofouling coverage data were arcsin$\sqrt{x}$ transformed, and all total macrofouler number data was $\log_{(x+1)}$ transformed prior to analysis using PERMANOVA. Proportions of particle surface area coverage were also arcsin$\sqrt{x}$ transformed prior to analysis to satisfy the assumptions of independent samples t-test. Independent samples t-tests were performed using SPSS (v. 17). All other statistical analyses were performed using PRIMER 6 (v. 6.1.13; Ivybridge, United Kingdom) and PERMANOVA+ (v. 1.0.3 [Clarke and Gorley 2006]). All data are presented as mean ± standard error.

4.3 Results

4.3.1 Polymer surface characterisation

Cold spray effectively embedded copper particles into HDPE and nylon. There was no significant difference (independent samples t-test, $t_{(38)} = 1.58$, $p = 0.122$) in the copper loading between Cu-embedded HDPE (125 ± 12 g m^{-2}) and Cu-embedded nylon (115 ± 10 g m^{-2}). There was however, a significant difference in copper particle surface area coverage (independent samples t-test, $t_{(24.2)} = -0.96$, $p < 0.001$) where Cu-embedded HDPE (33.6 ± 0.8%; Figure 4.1A) had fewer copper particles as a proportion of the total surface area than Cu-embedded nylon (60.1 ± 2.2%; Figure 4.1B). Consequently, there was also a significant difference (independent samples t-test, $t_{(4)} = 27.74$, $p < 0.001$) in copper particle depth of embedment between Cu-embedded HDPE (85 ± 1.5 μm; Figure 4.1C) and Cu-embedded nylon (40.6 ± 0.4 μm; Figure 4.1D) with particles being embedded more deeply into HDPE. To determine polymer properties associated with a high degree of copper retention, and affecting depth of embedment, HDPE and nylon were compared in relation to elastic modulus and hardness. HDPE had higher elastic modulus properties ($1{,}813.5 \pm 12.5$ MPa) and lower hardness levels (64.3 ± 0.2 D) than nylon, which had lower elastic modulus properties (1097.2 ± 33.4 MPa) and higher hardness levels (73 ± 0.5 D).

4.3.2 Polymer surface field trials

Biofouling was first recorded after 17 days with *Ulva* sp. occurring on all non-metallised polymers. Subsequently, first hard fouling occurred after 25 days on HDPE and nylon controls. Fouling was first quantified after 181 days of field exposure when there were obvious differences in the settlement of soft fouling (*Ulva* sp.) on Cu-embedded polymers (Figure 4.2A). After 181 days exposure, mean total fouling coverage (soft [*Ulva* sp.] and hard [bryozoans *Bugula neritina* (Linnaeus 1758) and *B. stolonifera* (Ryland 1960), barnacles *Amphibalanus reticulatus* (Utinomi 1967), mussels *Xenostrobus secures* (Lamarck 1819) sabellid polychaetes *Branchiomma nigromaculatum* (Baird 1865), spirorbid polychaetes *Simplaria pseudomilitaris* (Thiriot-Quievreux 1965)

and serpulid polychaetes *Hydroides elegans* (Haswell 1883)] foulers) on polymers, metallised polymer surfaces and copper plate, ranged from no fouling (0%; copper plate) to a maximum of 54.3 ± 11.7% (Cu-embedded nylon). There was a significant effect of surface type (PERMANOVA, pseudo-$F_{(4,34)} = 14.22$, $p < 0.001$) on total fouling coverage after 181 days in the field (Figure 4.2A) where Cu-embedded HDPE and copper plate had less total fouling coverage than all other surfaces including Cu-embedded nylon. Notably, all fouling on Cu-embedded polymer surfaces was *Ulva* sp., a copper-resistant green alga (Callow 1986).

When examining hard foulers alone, the effects of cold spray were even stronger with all copper treatments having neither hard fouling coverage nor individual hard foulers. After the 181 days exposure, mean hard fouling coverage on polymers, metallised polymer surfaces and copper plate ranged from no fouling (0%; Cu-embedded HDPE, Cu-embedded nylon and copper plate) to 15 ± 4% surface area coverage (nylon). There was a significant effect of surface type on mean total hard fouling coverage (PERMANOVA, pseudo-$F_{(4,35)} = 36.48$, $p < 0.001$; Figure 4.2B). Cu-embedded HDPE, Cu-embedded nylon and copper plate had significantly less coverage than polymer controls (HDPE and nylon) with the biofouling community occupying approximately 15% of the surface area available on Perspex, HDPE and nylon (Figure 4.2B). Of this, the sabellid polychaete *B. nigromaculatum* (large, parchment-shelled tubeworms) was the dominant species and although present in low numbers, because of their size, represented 87% of the hard fouling surface area coverage. *B. neritina*, *A. reticulatus*, *S. pseudomilitaris* and *H. elegans* were also present, but only accounted for 13% of the hard fouling surface area coverage.

Consequently, the mean number of hard foulers ranged from zero (Cu-embedded HDPE, Cu-embedded nylon and copper plate) to 3.7 ± 0.8 (HDPE). There was a significant effect of surface type on mean number of hard foulers (PERMANOVA, pseudo-$F_{(4,30)} = 20.51$, $p < 0.001$; Figure 4.2C) where Cu-embedded HDPE, Cu-embedded nylon and copper plate had significantly fewer individuals than polymer controls (HDPE and nylon).

The second major fouling event on metallised polymers occurred after 250 days of field exposure with the failure (settlement of hard foulers) of Cu-embedded nylon (Figures 4.2E and F). Mean total fouling coverage on polymers, metallised polymer surfaces and copper plate ranged from a minimum of no fouling (0%; copper plate) to a maximum of 63.6 ± 5% (Cu-embedded nylon), with the majority of fouling again being *Ulva* sp.. There was a significant effect of surface type (PERMANOVA, pseudo-$F_{(4,32)} = 55.55$, $p < 0.001$) on total fouling coverage (Figure 4.2D) where Cu-embedded HDPE and copper plate had less total fouling coverage than all other surfaces and Cu-embedded nylon had more total fouling than all other surfaces.

When examining hard fouling alone, mean hard fouling coverage on polymers, metallised polymer surfaces and copper plate, ranged from no fouling (0%; Cu-embedded HDPE and copper plate) to 22.3 ± 4% coverage (HDPE). There was a significant effect of surface type on mean total hard fouling coverage (PERMANOVA, pseudo-$F_{(4,35)} = 91.64$, $p < 0.001$; Figure 4.2E). Importantly, Cu-embedded HDPE and copper plate maintained their efficacy against hard fouling and had significantly less hard fouling coverage (0%) than Cu-embedded nylon (5.8 ± 2.1%), which in turn had significantly less coverage than polymer controls (HDPE [22.3 ± 4%] and nylon [13.6 ± 2.2%]). Although the biofouling community had changed over the period from 181 to 250 days, it still occupied approximately 15% (combined average) of the surface area available on Perspex, HDPE and nylon (Figure 4.2E). The serpulid polychaete *H. elegans* and the spirorbid polychaete *S. pseudomilitaris* (small, calcium carbonate-shelled tubeworms) were the dominant species, and although small in size, settled in high numbers and accounted for 75% of the hard fouling surface area coverage, replacing the previously dominant sabellid polychaete *B. nigromaculatum*. In addition, *B. neritina*, *B. stolonifera*, *B. nigromaculatum* and *A. reticulatus* were also present, but only accounted for 25% of the hard fouling surface area coverage.

Consequently, the mean number of hard foulers ranged from zero (Cu-embedded HDPE and copper plate) to 20.1 ± 5.0 individuals (HDPE), the majority of which were *S. pseudomilitaris* (up to 45 individuals on a single plug). There was a significant effect of surface type on mean number of hard foulers (PERMANOVA, pseudo-

$F_{(4,35)} = 138.28$, $p < 0.001$; Figure 4.2F) where Cu-embedded HDPE and copper plate had significantly fewer individuals (0) than Cu-embedded nylon and polymer controls (HDPE and nylon).

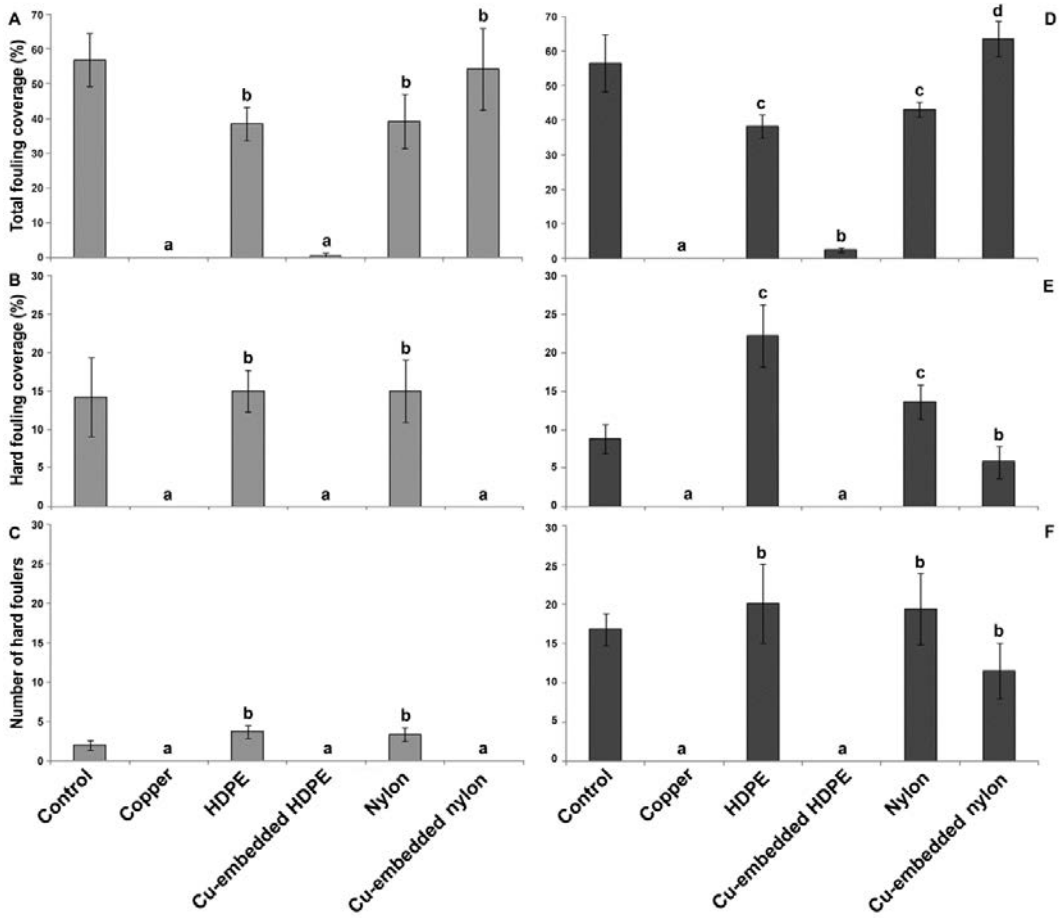

Figure 4.2. Fouling response to different metals, polymers and metallised polymer surfaces after 181 (**A–C**) and 250 (**D–F**) days in the field. (**A**) Total coverage (soft and hard foulers) of fouling organisms. (**B**) Hard fouler coverage. (**C**) Number of hard foulers. (**D**) Total coverage (soft and hard foulers) of fouling organisms. (**E**) Hard fouler coverage. (**F**) Number of hard foulers. N.B. Superscript letters above bars indicate significant groupings; all data displayed as means ± S.E.; Control, Perspex.

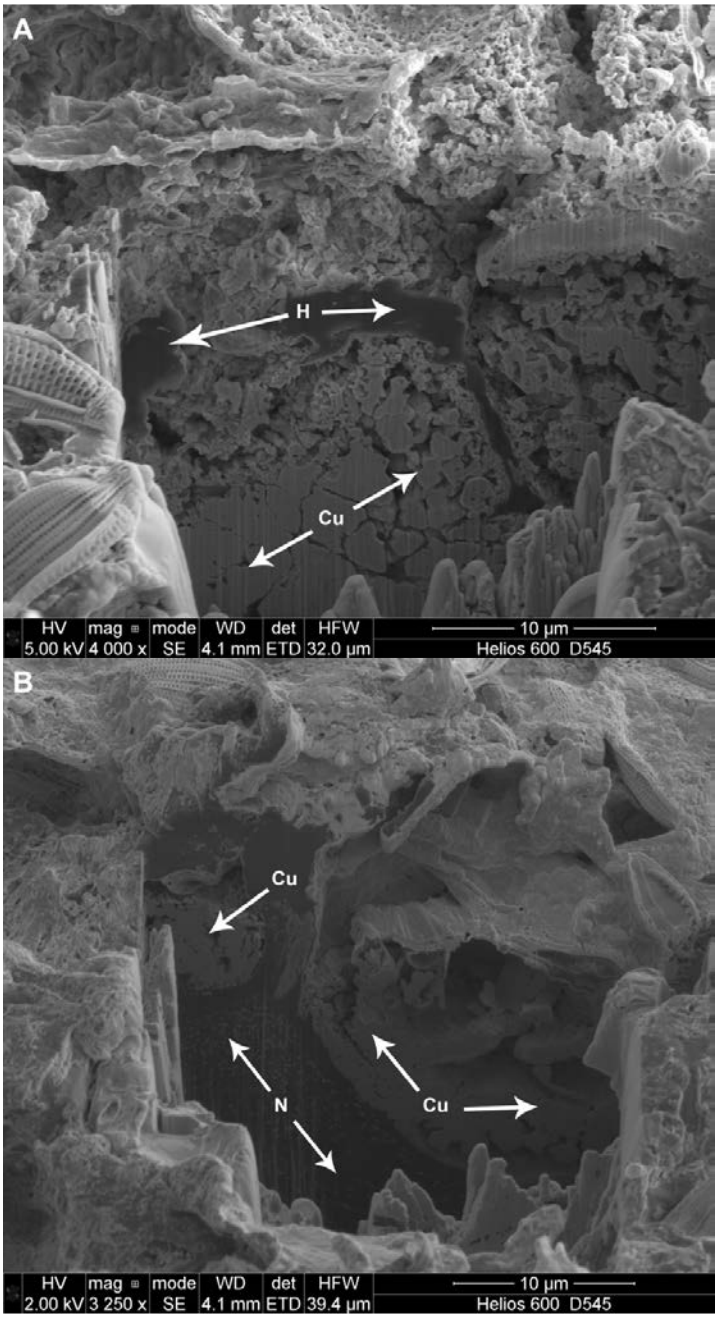

Figure 4.3. Cu-embedded polymers analysed using FIB/SEM after 250 days in the field under heavy fouling conditions. (**A**) Copper particle embedded into HDPE is porous near the top of the particle but remains intact moving deeper along the particle. In addition, the particle occupies most of the area under the surface of the polymer. (**B**) Two copper particles embedded into nylon. The larger particle, on the right, is highly degraded near the top of the particle and porous all the way through. N.B. H, HDPE; N, nylon; Cu, copper particles.

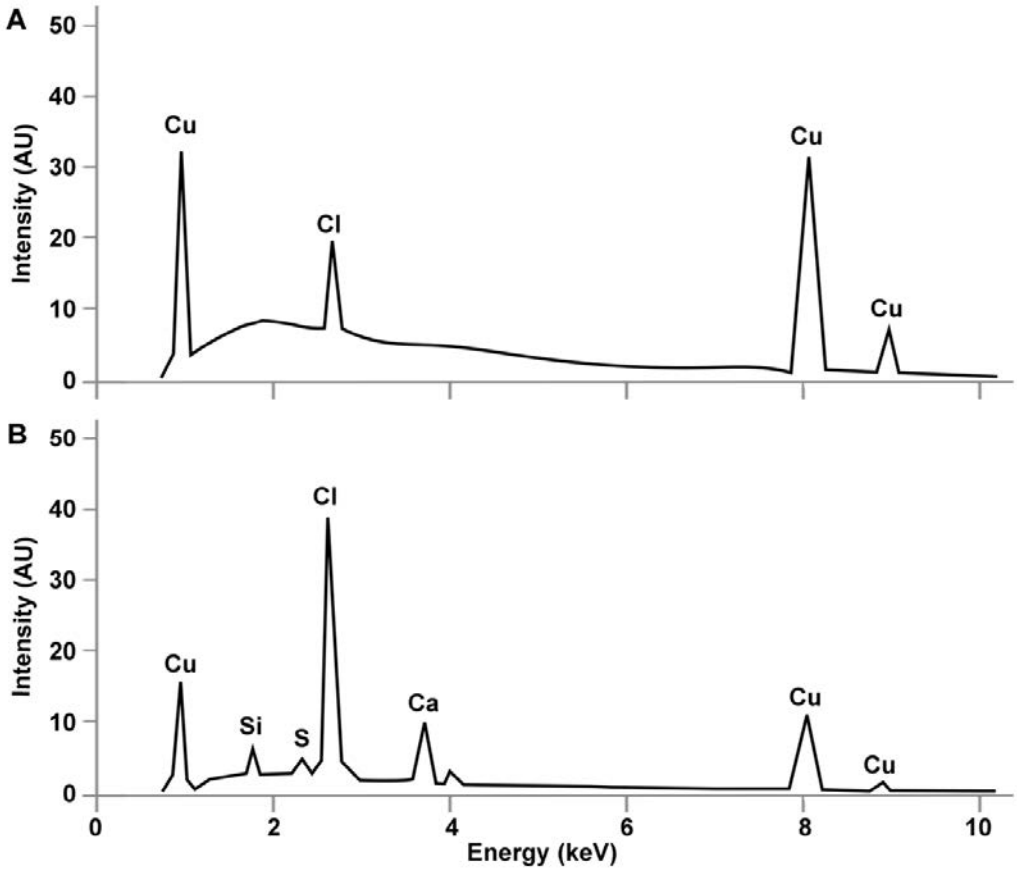

Figure 4.4. EDS spectra of the patina from cold-sprayed polymer plugs after 250 days in the field under intense fouling conditions. (**A**) Cu-embedded HDPE. (**B**) Cu-embedded nylon.

Upon closer examination of the surfaces using SEM after 250 days in the field, Cu-embedded HDPE and Cu-embedded nylon were covered in a biofilm layer consiting of the green alga *Ulva* sp. and the diatoms *Amphora* sp., *Surirella* sp., and *Achnanthes* sp.. In addition, Cu-embedded nylon was covered in serpulid and spirorbid polychaetes. FIB analysis demonstrated that particles embedded into HDPE were porous near the top of the particle but remained intact moving deeper along the particle (Figure 4.3A). In contrast, particles embedded into nylon were highly degraded near the top of the particle and porous all the way through (Figure 4.3B). EDS supported these findings where the EDS spectra of the patina for Cu-embedded HDPE is dominated by Cu peaks (96.85% combined mass) with a secondary signal from Cl (3.15% mass) consistent with a small presence of chlorocupric complexes with large amounts of copper available for speciation (Figure 4.4A). In contrast to Cu-

embedded HDPE, the EDS spectra for Cu-embedded nylon is dominated by Cu (70.07% combined mass) and Cl (18.33% mass) peaks with secondary signals from Ca (8.08% mass), Si (2.4% mass) and S (1.12% mass) consistent with a larger presence of chlorocupric complexes as well as smaller amounts of copper available for speciation (consistent with FIB analysis). The Si and Ca signals are most likely related to diatoms (Si), *H. elegans* (Ca) and *S. pseudomilitaris* (Ca) (Figure 4.4B).

4.4 Discussion

Cold spray technology used to embed copper particles into polymers is an innovative and effective mechanism to deliver antifouling properties to materials that have a high utility in aquaculture and marine industries but may be difficult to treat with standard antifouling coatings. Although the technique is applicable to multiple polymer types, substrate material properties are key factors in developing and refining this technique across applications.

Cu-embedded HDPE plugs have similar antifouling properties to copper plate after 250 days. Both performed equally well and in comparison to Cu-embedded nylon, strongly deterred soft fouling (algae) and completely deterred hard fouling, the most important component of the biofouling community from an economic perspective. Deterrence was maintained for 250 days in the field, regardless of changes in the biofouling community. In contrast, total fouling coverage on Cu-embedded nylon plugs (54.3 ± 11.7%) was two orders of magnitude higher than Cu-embedded HDPE (0.6 ± 0.6%) or copper plate (0%) after 181 days. Similarly, Cu-embedded nylon failed the critical test of inhibiting hard fouling after 250 days with significant settlement of polychaetes (*S. pseudomilitaris* and *H. elegans*). All surfaces were exposed to the same fouling pressures, however, Cu-embedded nylon performed less well than Cu-embedded HDPE and copper plate suggesting that Cu-embedded nylon was releasing ions at a level below which prevent the settlement of propagules and larvae of fouling organisms. There are differences in elastic modulus and hardness properties of HDPE and nylon and an interaction between those properties and the cold spray process.

Metal particle depth of embedment and surface area coverage differ with each polymer used, and therefore unique polymer characteristics produce specific copper release and retention rates that ultimately affect antifouling efficiency in the field. The effect of polymer can be seen clearly in the difference between HDPE and nylon which were cold sprayed using the same traverse speed of 0.1 m s^{-1} giving the same copper loadings (Cu-embedded HDPE, 125 ± 12 g m^{-2}; Cu-embedded nylon, 115 ± 10 g m^{-2}) but different depths of embedment (Cu-embedded HDPE, 85 ± 1.5 μm; Cu-embedded nylon, 40.6 ± 0.4 μm) and different surface area coverage (Cu-embedded HDPE, 33.6 ± 0.8%; Cu-embedded nylon, 60.1 ± 2.2%), resulting in significantly different fouling rates. HDPE is softer than nylon with a higher elastic modulus, and these characteristics allowed copper particles to embed deeper into HDPE than into nylon. Because Cu-embedded HDPE initially contains more deeply embedded copper, particles may be protected and less susceptible to erosion in the field, therefore lasting longer (lower dissolution). In contrast, Cu-embedded nylon, which had high particle surface area coverage and shallower depth of embedment, is hypothesised to have a higher dissolution rate compared to HDPE. This was supported after examining the samples after 250 days of fouling exposure using EDS, with the patina for Cu-embedded HDPE being dominated by Cu peaks with a secondary signal from Cl (Figure 4.4A). In contrast, the patina for Cu-embedded nylon had less Cu and more Cl signals (Figure 4.4B). In further support, FIB showed that particles embedded into HDPE were porous near the surface but remained intact moving away from the surface, while particles embedded into nylon showed high degradation and porosity throughout the particle (Figure 4.3). Therefore, for Cu-embedded HDPE which prevents macrofouling for more than 250 days, sufficient amounts of Cu^{+} and Cu^{2+} ions remain available for release into the water.

These findings demonstrate that the physical properties of the polymers, as shown by elastic modulus and hardness values, affect copper embedment depth for the same cold spray operating conditions. It should however be noted that this analysis is not exhaustive and other polymer properties (glass transition, response rate to high strain and impact, moisture content, percent crystallinity and melting point), as well as

interactions between polymer properties and heating of the surface during the spray process which may cause bonding between the polymer and the copper particles, should be examined. In addition, environmental conditions and experimental methods (spraying to remove silt) may also affect antifouling efficacy. Test surfaces were exposed to heavily silted conditions which could hinder the dissolution of copper particles. However, under most applications these surfaces would not be kept in low-flow, heavy-silt environments. For example, seismic streamers, a key target application used in the exploration industry, are only used under flow at a constant 4–5.5 knots which will produce different outcomes and requires *in situ* trials for these specific conditions. However, clear proof-of-concept has been achieved for an antifouling technology for polymers. Furthermore, as a comparison, the complete prevention of fouling for at least 250 days for HDPE exceeds that reported for antifouling coatings used on aquaculture nets in temperate latitudes, where coatings typically fail after six to nine months (reviewed in Braithwaite and McEvoy 2005; Braithwaite et al. 2007; Svane et al. 2007; reviewed in de Nys and Guenther 2009; Guenther et al. 2010).

As knowledge of the cold spray process is expanded and its role in antifouling technology is developed, it will be important to establish baseline data for the most common polymers used in aquaculture and marine industries. Given polymers have unique properties (Gnanou and Fontanille 2008), they will each need specific cold spray parameters to optimise effective copper retention. These are proximity of the cold spray nozzle, machine traverse speeds, carrier gas type, gas temperature, powder size, powder type and powder flow rate. Alternatively, the type and density of metal particles used to spray polymers will affect the interaction between polymer and cold spray parameters, which will ultimately affect antifouling efficiency (discussed further in Chapters 5 and 6).

In conclusion, cold spray is an innovative antifouling technology and its effectiveness has been demonstrated where Cu-embedded polymers, produced using cold spray technology, can prevent fouling with similar efficacy as copper plate for at least 250 days. The cold spray process is amenable to a diversity of metals that are alternatives

to pure copper, including zinc, brass and bronze (WHOI 1952b; Stoltenhoff et al. 2002; Papyrin et al. 2007), and it is advantageous as only a thin layer of metal particles is applied to the surface for antifouling purposes. Because of this, bulk polymer properties such as flexibility are not sacrificed and although further study is needed, the technology can potentially be used on polymers, polymer-hulled vessels, seismic exploration equipment, and aquacultures cages and netting, where fouling impedes functional capacity.

Chapter 5

Polyurethane seismic streamer skins:

an application of cold spray metal embedment*

5.1 Introduction

Cold spray is a deposition process whereby small metal particles (typically < 50 μm diameter) are accelerated to supersonic velocities in an inert gas flow and impact onto a receiving surface (Stoltenhoff et al. 2002; Papyrin et al. 2007). Applications of this process include the development of wear- and corrosion-resistant coatings, the enhancement of heat and electrical conductivity (Gärtner et al. 2006), the reinforcement of structures, and the formation of freeform shapes without the use of moulds (Pattison et al. 2007). In an innovation of this technology, the cold spray process is being used to functionalise thermoplastic polymers (polymers) and give them antifouling properties by embedding copper particles into the substratum (Vucko et al. 2012; Chapter 4). The embedment of metal particles into polymers has been used to control marine biofouling with Cu-embedded high-density polyethylene preventing fouling with similar efficacy to copper plate, under intense marine fouling pressures, thereby providing an innovative and effective technology to prevent fouling on submerged polymer surfaces (Poole et al. 2012; Vucko et al. 2012; Chapter 4).

However, specific polymer properties affect metal particle embedment depth and particle surface area coverage differently, and upon submersion into water these properties affect metal ion release and retention rates which ultimately control antifouling efficacy (Vucko et al. 2012; Chapter 4). In addition, the density of metal

*Chapter 5 adapted from Vucko MJ, King PC, Poole AJ, Jahedi MZ and de Nys R (2013). Polyurethane seismic streamer skins: an application of cold spray metal embedment. Biofouling 29: 1-9.

particles per unit area, or particle loading, will be an important factor affecting overall antifouling efficacy since a greater number of layered particles may provide longer periods of protection against fouling organisms. Understanding these factors and their interactions is critical to developing and refining the technique of cold spray metal embedment and its deployment across applications, with the process requiring tailoring for specific polymer products.

In this Chapter, cold spray metal-embedded seismic streamer skins were developed and tested, representing the first application of this technology in the marine industry. Streamers form part of seismic arrays used in the geophysical exploration industry and have robust polyurethane (PU) coverings which protect sensitive electronic equipment for recording seismic signals (Harrick and Stenzel 2011). Streamers are towed at a pre-set depth between 5–7 m at speeds of between 4–5.5 knots and record seismic feedback from sub-surface strata to identify offshore oil and gas bearing geological features (Elboth et al. 2010). In these remote offshore environments, pelagic goose barnacles are a major fouling organism settling on seismic streamer skins resulting in dense mono-specific communities which cause equipment failure and a reduction in seismic data quality (Harper 1995; Vignaux 2010). Goose barnacles add weight to streamers, thereby reducing their capacity to float, while increasing seismic feedback noise, hydrodynamic drag and therefore fuel consumption, as well as time lost as a result of cleaning regimes (Harper 1995; Vignaux 2010; Harrick and Stenzel 2011). Currently, no functional antifouling coatings are available for use on the flexible PU streamers due to economic and technical constraints associated with application procedures (Vignaux 2010). Proposed solutions are automatic cleaning devices (Hoogeveen 2006; Hoogeveen et al. 2008; Lepage and Dollon 2010) and foul-release materials (Lobe et al. 2010; Hartshorne et al. 2011) however, neither approach provides effective antifouling. Consequently, there is a clearly identified fouling problem with a demonstrated cost in a significant industry where specific polymer materials require effective protection against fouling. To directly address this problem, the utility and efficacy of metal particles embedded into PU seismic streamer skins was tested against

fouling using copper, the most common broad spectrum antifouling technology (Brooks and Waldock 2009; Finnie and Williams 2010).

Specifically, the aims of this Chapter were to firstly quantify the effects of copper particle density on antifouling longevity in the field under intense fouling conditions. Secondly, this Chapter aims to test, upon failure, whether settled fouling organisms could be removed from seismic streamers under a realistic flow of 4.5 knots.

5.2 Materials and methods

5.2.1 Seismic streamer skin surface preparation

Copper particles were embedded into PU seismic streamer skin sections (clear seismic PU; 600 mm length, 54.4 mm diameter and 3.5 mm thickness; Colex International Ltd., Leicestershire, UK). Streamers were metallised by cold spray using a Kinetiks 4000 cold spray system (Cold Gas Technology GmbH, Ampfing, Germany) with a cold spray nozzle mounted onto a robot arm (ABB IRB 2600) to give lateral movement. The streamer skins were fitted onto a 55 mm diameter aluminium rod and mounted onto a lathe and spun at 615 rpm during cold spray. The corresponding linear surface speed was 1.77 m s^{-1}, considerably faster than could be achieved by robot movement alone on a stationary streamer skin. Two different robot arm lateral traverse speeds of 0.033 m s^{-1} and 0.0083 m s^{-1} were used, producing a low and high density of copper particles, respectively. One half (300 mm) of each streamer section was sprayed while the other half was left untreated (Figure 5.1). AEE-112 copper powder (Atlantic Equipment Engineers, Bergenfield, NJ) was used as the feedstock material (see materials and methods in 'Chapter 4, 4.2.1 Polymer surface preparation'). Nitrogen was used as the carrier gas and was kept at a constant temperature of 400°C and pressure of 2.5 MPa throughout spraying. This temperature and pressure facilitated a gas velocity that was high enough for embedment of copper particles into the polymers. The fast relative movement between the cold spray nozzle, kept at a constant distance of 30 mm from the streamer skin surface, and the PU surface

permitted the use of a high spray temperature without the risk of polymer degradation.

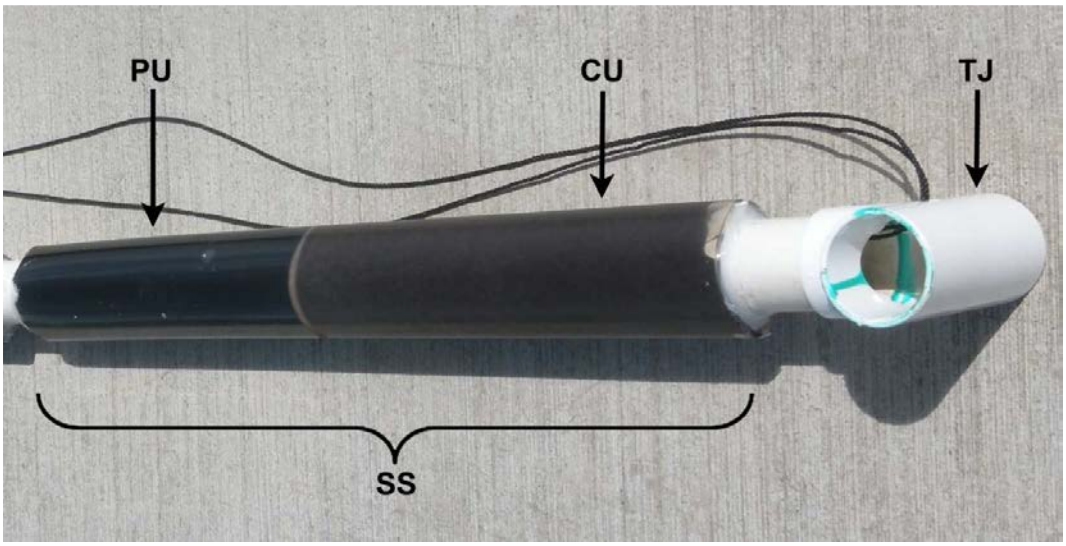

Figure 5.1. PU seismic streamer skin sections were embedded with copper particles (CU) using cold spray technology to produce low- and high-density treatments. One half (300 mm) of each streamer section (SS) was sprayed while the other half was left untreated. The inside surface of the streamer skins was painted black to provide contrast between the clear PU control and fouling. The skins were slipped over PVC tubes (40 mm diameter) with 50 mm between each replicate. A PVC T-joint (TJ) was attached to each end to prevent the streamers from touching the pier walls and polyethylene rope was threaded through the hole in the T-joint so the streamers could be tied to boat moorings.

5.2.2 Seismic streamer skin surface characterisation

Copper loading was quantified from the difference in mass of the PU streamer skins before and after spraying and wiping with a lint-free wipe. The surface area covered by copper particles (Figures 5.2A and B) was calculated from digital microscopy images of each treatment ($n = 5$), by inverting the colours and obtaining a black (copper particles) and white (polymer surface) pixel threshold (Photoshop v. 12.0.4; Adobe Systems Software, San Jose, California, USA). Pixel percent coverage was then quantified. Streamer skins were also examined in cross section to estimate embedment depth of copper particles (Figures 5.2C and D). Random slices were taken from each treatment type using a scalpel ($n = 5$) and digital microscopy images were obtained

from each slice. Subsequently, each image was split into 10 equal segments where one random particle depth was measured in each segment. Medians were obtained from each image and mean depth of embedment was quantified. Digital microscopy images were obtained using a microscope (SZ61; Olympus, Eagle Farm, Queensland, Australia) and digital camera (DP25; Olympus, Eagle Farm, Queensland, Australia) and all images were analysed using ImageJ (v. 1.42q; National Institutes of Health, Bethesda, Maryland, USA) software.

5.2.3 Seismic streamer skin field trials

The low- (n = 3) and high- (n = 4) density Cu-embedded streamer skins were placed in the water at the Townsville Yacht Club (Queensland, Australia) lengthwise along piers 200 mm below the surface in late January (summer). Although streamers *in situ* are towed between 5–7 m (Elboth et al. 2010), 200 mm was used to expose surfaces to the intense fouling pressures at this location. There is consistent, heavy fouling all year round at this dry tropical location and although fouling species vary throughout the year, many marine invertebrates have multiple spawning events (Bauer 1992). The inside surface of the streamer skins was painted black to provide contrast between the clear PU control and fouling. The skins were then fitted onto PVC tubes (40 mm diameter) leaving 50 mm between each replicate. The PVC tube extended 100 mm on each end to attach a PVC T-joint with a hole drilled into the top. The T-joint prevented the skins from touching the pier walls while polyethylene rope could be threaded through the hole and tied to boat moorings (Figure 5.1). Photographs were taken every two weeks of front- (facing outward) and back- (facing inward against the pier) facing streamer skin surfaces to track the development of fouling across the different conditions for each tube. Prior to photographs, all surfaces were sprayed with freshwater (no more than 2.5 N of force [measured with a force gauge; Extech® Instruments 475040]) using a conventional garden hose to remove the build-up of silt and immediately dip rinsed in seawater. Total fouling coverage (soft [*Ulva* sp.] and hard foulers), total hard fouling coverage and total number of hard foulers were quantified and presented graphically upon failure (defined as the settlement of hard foulers) of each Cu-embedded treatment. Both treatments failed differentially based

on initial copper density (see results in 'Seismic streamer skin field trials'). Percent fouling coverage and total hard fouler numbers were quantified from digital images using ImageJ (v. 1.42q) software. In addition, qualitative changes of the fouling community structure and composition are described at these two times.

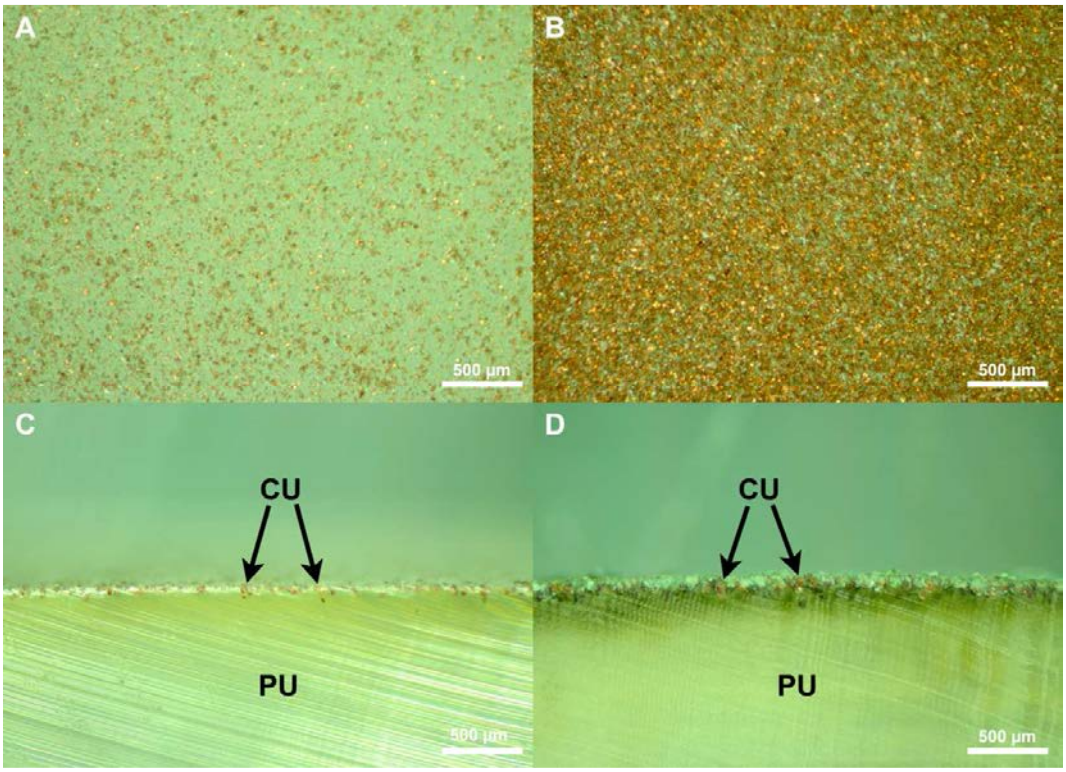

Figure 5.2. Digital microscopy images of PU streamers embedded with copper particles (CU) using cold spray technology. (**A**) Surface view of low-density Cu-embedded streamer skins showing area coverage of copper particles; (**B**) surface view of high-density Cu-embedded streamer skins showing area coverage of copper particles; (**C**) cross section of low-density Cu-embedded streamer skins showing embedment depth of copper particles; (**D**) cross section of high-density Cu-embedded streamer skins showing embedment depth of copper particles. Scale bars = 500 µm.

5.2.4 Adhesion strength

A flow chamber was used to quantify the effects of typical seismic array towing speeds on the removal of settled fouling organisms from treatment surfaces at the end of the field trial. The flow chamber, described in detail in Carl et al. 2012a, consists of a reservoir (1,000 L tank) from which filtered, natural seawater is pumped up into a channel and subsequently falls freely back into the reservoir for recirculation. Before

entering the channel, the water was dispersed through a fitting at a depth of less than 10 mm to create laminar-like flow (Enríquez and Rodríguez-Román 2006). At the end of the field trial, portions (50 x 50 mm) of the low- and high-density seismic streamers and PU controls were removed, placed into plastic tubs with natural seawater, and supplied with aeration for transport back to the laboratory. Test surfaces (n = 5) from each treatment were placed in the flow chamber (one surface at a time) and secured in the channel using customized fittings. A small Perspex ramp (6 mm) was placed in front of the test surfaces to ensure even flow over the surfaces. The removal of settled fouling organisms on seismic streamer skins was quantified by measuring the numbers of fouling organisms before and after exposure to a flow of 4.5 knots, equivalent to a velocity of 2.3 m s^{-1}, for 2 minutes.

5.2.5 Statistical analysis

To test for significant differences in copper density, copper particle surface area coverage and particle depth of embedment between low- and high-density Cu-embedded seismic streamer skins, independent samples t-tests were used (α = 0.05). To test the effects of copper density (no copper, low-density, high-density) and surface position (front- and back-facing) on total fouling coverage, total hard fouling coverage and total number of hard foulers on seismic streamer skins after 42 and 210 days in the field, two factor permutational multivariate analysis of variances (PERMANOVA) were used (α = 0.05).

All proportions of particle surface area coverage were arcsin$\sqrt{x}$ transformed and all copper loading and particle depth of embedment data were $\log_{(x+1)}$ transformed prior to analysis to satisfy the assumptions of independent samples t-tests. Independent samples t-tests were performed using S-PLUS (v. 8.0). All other statistical analyses were performed using PRIMER 6 (v. 6.1.13; Ivybridge, United Kingdom) and PERMANOVA+ (v. 1.0.3 [Clarke and Gorley 2006]). For PERMANOVA, the untransformed raw data were used to produce Bray-Curtis similarity matrices and p-values were calculated from 9,999 random permutations. All data are presented as mean ± standard error.

5.3 Results

5.3.1 Seismic streamer skin surface characterisation

The two robot traverse speeds used to embed copper particles into PU seismic streamer skins produced significantly different copper loadings (independent samples t-test, $t_{(4)} = 4.11$, $p = 0.015$). The faster robot speed of 0.033 m s^{-1} produced a significantly lower density of copper particles (22.1 ± 4.8 g m^{-2}) than the slower robot speed of 0.0083 m s^{-1} which produced a higher density of copper particles (101.1 ± 10.8 g m^{-2}). Consequently, there was also a significant difference in copper particle surface area coverage (independent samples t-test, $t_{(8)} = 19.94$, $p < 0.001$) where low-density Cu-embedded streamers (21.6 ± 1.4%; Figure 5.2A) had fewer copper particles as a proportion of the total surface area than high-density Cu-embedded streamers (64.7 ± 1.8%; Figure 5.2B). There was also a significant difference in mean depth of copper particle embedment (independent samples t-test, $t_{(104)} = 9.84$, $p < 0.001$) between low- (58.4 ± 1.9 μm; Figure 5.2C) and high- (85.6 ± 1.9 μm; Figure 5.2D) density Cu-embedded streamers with particles being embedded more deeply into high-density streamers.

5.3.2 Seismic streamer skin field trials

Biofouling first occurred after 14 days on PU controls with the settlement of *Ulva* sp. and the serpulid polychaete *Hydroides elegans* (Haswell 1883). Fouling was first quantified upon failure (defined as the settlement of hard fouling) of low-density Cu-embedded streamers after 42 days of field exposure. In contrast, high-density Cu-embedded streamers continued to deter all hard fouling at this time.

Mean total fouling coverage (soft and hard fouling) on streamers after 42 days in the field ranged from 1.1 ± 0.2% (back-facing, high-density Cu-embedded streamers) to 93.4 ± 1.4% (front-facing PU controls) and there was a significant interaction between copper density and surface position (two-factor PERMANOVA, pseudo-$F_{(2,22)} = 35.83$, $p < 0.001$; Figure 5.3A; Table 5.1). The interaction was mainly due to low- and high-

density Cu-embedded streamers having more total fouling on front-facing surfaces than on back-facing surfaces, while front- and back-facing PU controls had similar amounts of total fouling coverage. All fouling on high-density Cu-embedded surfaces was *Ulva* sp., a copper-tolerant green alga (Callow 1986). Overall, high-density Cu-embedded streamer skins had less total fouling coverage than low-density Cu-embedded streamer skins or PU controls, regardless of position.

Mean hard fouler coverage on streamers after 42 days ranged from 0% (front- and back-facing high-density Cu-embedded streamer skins) to 58.2 ± 3.4% (back-facing PU controls) and there was a significant interaction between copper density and surface position (two-factor PERMANOVA, pseudo-$F_{(2,22)} = 5.88$, $p < 0.001$; Figure 5.3B; Table 5.1). Mean number of hard foulers on streamers ranged from 0 (front- and back-facing high-density Cu-embedded streamer skins) to 1026.6 ± 36.6 (back-facing PU controls) and there was a significant interaction between copper density and surface position (two-factor PERMANOVA, pseudo-$F_{(2,22)} = 10.69$, $p < 0.001$; Figure 5.3C; Table 5.1). These interactions were mainly due to more hard foulers and hard fouling coverage on back-facing PU controls, while low- and high-density Cu-embedded streamers had similar amounts on front- and back-facing positions. High-density streamers also had significantly less hard fouling than low-density streamers or PU controls. The fouling community on PU controls was dominated by *H. elegans* while the barnacle *Amphibalanus reticulatus* (Utinomi 1967) dominated fouling on low-density Cu-embedded streamers. This was most probably due to seasonal spawning events, where *H. elegans* spawning began soon after streamer submergence and therefore larvae were immediately available for settlement onto PU controls. Spawning and settlement of *H. elegans* ended before 42 days when larvae of *A. reticulatus* were available for settlement onto the low-density streamers where, at this point, copper was depleted to levels below those which prevent fouling and the substratum became available for colonisation.

The second major fouling event occurred after 210 days of field exposure with the failure of high-density streamers. At this time mean total fouling coverage (soft and hard fouling) on streamers ranged from 38.7 ± 6.8% (back-facing, low-density Cu-

embedded streamers) to 94.6 ± 6.8% (back-facing PU control streamers) and there was a significant interaction between copper density and surface position (two-factor PERMANOVA, pseudo-$F_{(2,22)} = 28.64$, $p < 0.001$; Figure 5.3D; Table 5.1). The interaction was mainly due to the low-density Cu-embedded streamers having more fouling on front-facing surfaces while high-density Cu-embedded streamers and PU controls had more fouling on back-facing surfaces.

Mean hard fouler coverage on streamers after 210 days ranged from 0.4 ± 0.02% (front-facing high-density Cu-embedded streamer skins) to 93.3 ± 1.1% (back-facing PU controls) and there was a significant interaction between copper density and surface position (two-factor PERMANOVA, pseudo-$F_{(2,22)} = 44.63$, $p < 0.001$; Figure 5.3E; Table 5.1). Mean number of hard foulers on streamers ranged from 2.5 ± 0.7 (front-facing high-density Cu-embedded streamer skins) to 577.3 ± 44.6 (back-facing PU controls) and there was a significant interaction between copper density and surface position (two-factor PERMANOVA, pseudo-$F_{(2,22)} = 18.9$, $p < 0.001$; Figure 5.3F; Table 5.1). These interactions were mainly due to PU controls and low-density Cu-embedded streamers having more hard foulers and hard fouling coverage on back-facing surfaces, while high-density Cu-embedded streamers had similar but less hard foulers and hard fouling coverage in both positions. Although fouling on PU controls and low-density streamers was still dominated by *H. elegans* and *A. reticulatus*, respectively, both had additional settlement of the spirorbid polychaete *Simplaria pseudomilitaris* (Thiriot-Quievreux 1965), the stalked bryozoans *Bugula neritina* (Linnaeus 1758) and *B. stolonifera* (Ryland 1960), and the encrusting bryozoans *Hipporina indica* (Pillai 1978), *Watersipora subovoidea* (d'Orbigny 1852), and *Hippopodina iririkiensis* (Tilbrook 1999) in small proportions. More importantly, fouling on the high-density streamers was dominated by the encrusting bryozoan *W. subovoidea*.

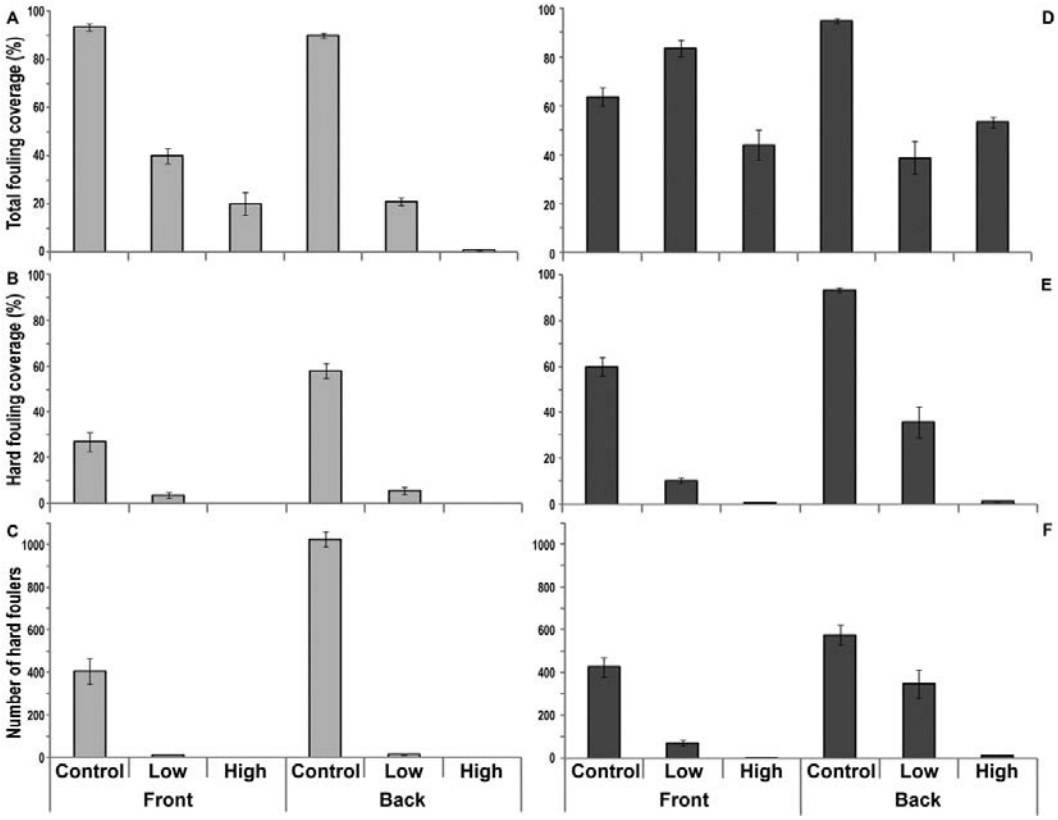

Figure 5.3. Fouling response to PU seismic streamer skins embedded with different densities of copper (low, high) and facing different directions (front- and back-facing) after 42 (**A, B, C**) and 210 (**D, E, F**) days in the field. (**A** and **D**) Total coverage (soft and hard fouling combined) of fouling organisms; (**B** and **E**) hard fouler coverage; (**C** and **F**) number of hard foulers. N.B. All data displayed as means ± S.E.; front, streamer surface facing away from the marina pier; back, streamer surface facing towards, but not touching, the marina pier.

Table 5.1. Two-factor PERMANOVA analysis with significant effects of position (Pos; back, front) and copper density (Den; no copper, low-density, high-density) on the settlement of fouling on seismic streamer skins after 42 and 210 days of continuous exposure in the field.

		Factor	df	Mean square	pseudo-*F*	*p*-value
42 days	Total fouling coverage	Pos	1	5,230	33.13	0.0001
		Den	2	15,379	97.42	0.0001
		Pos x Den	2	5,656	35.83	0.0001*
	Hard fouler coverage	Pos	1	842	3.24	0.0425
		Den	2	34,448	132.30	0.0001
		Pos x Den	2	1,530	5.88	0.0007*
	Number of hard foulers	Pos	1	1,229	7.71	0.0009
		Den	2	39,410	247.25	0.0001
		Pos x Den	2	1,703	10.69	0.0001*
210 days	Total fouling coverage	Pos	1	71	1.18	0.2896
		Den	2	1,408	23.14	0.0001
		Pos x Den	2	1,742	28.64	0.0001*
	Hard fouler coverage	Pos	1	2,789	32.21	0.0001
		Den	2	27,721	320.08	0.0001
		Pos x Den	2	3,864	44.63	0.0001*
	Number of hard foulers	Pos	1	3,848	12.55	0.0001
		Den	2	22,529	73.50	0.0001
		Pos x Den	2	5,792	18.90	0.0001*

Note: * denotes significant effect; $\alpha = 0.05$.

5.3.3 Adhesion strength

Removal of settled fouling organisms was tested using flow conditions typical for towed seismic arrays (4.5 knots) on Cu-embedded seismic streamer skins after the failure of high-density streamers (210 days). At this time fouling had been established for 196 days on PU controls (fouling recorded at 14 days), 168 days on low-density streamers (fouling recorded at 42 days) and less than 14 days on high-density streamers (fouling recorded at 210 days). The flow of 4.5 knots failed to remove hard foulers from any treatment, and barnacles, tubeworms, and bryozoans were unaffected.

5.4 Discussion

Cold spray metal embedment is an effective antifouling technology for application to seismic streamer skins. In this direct application, high-density Cu-embedded streamers, with approximately five times the amount of copper per unit area (101.1 ± 10.8 g m^{-2}), were significantly more effective than low-density Cu-embedded streamers (22.1 ± 4.8 g m^{-2}) and PU controls. The high density treatment deterred all hard fouling for 210 days under intense tropical fouling pressure in tidal currents. Notably, metal particle density, or copper loading, is a critical parameter in determining the antifouling properties of polymers embedded with copper particles using cold spray technology.

As a consequence of the differences in copper loading, the two treatments also differed in particle surface area coverage (low-density, 21.6 ± 1.4%; high-density 64.7 ± 1.8%) and particle depth of embedment (low-density, 58.4 ± 1.9 mm; high-density, 85.6 ± 1.9 mm). Both treatments were sprayed using identical cold spray parameters except for robot arm speed which was slower for high-density streamers. This increased the length of time the cold spray nozzle spent on any given spot on high-density streamers, thereby increasing the number of particles embedded into the substratum, pushing already-embedded particles further in, and in addition, heating the surface to a higher degree than on the low-density streamers. More heat provided greater plasticity in the polymer recipient and therefore particles embedded more deeply. Copper loading is not the only factor determining antifouling longevity in the field and there will inherently be an interaction between copper loading, surface area coverage and depth of embedment, and consequently the dissolution of copper ions. Low-density surfaces, which initially have fewer copper particles, will also release less copper ions per unit time and be depleted to amounts of copper below that which is needed to prevent hard fouling before high-density surfaces. The release rate of copper needed to prevent fouling on a surface is approximately 0.02 g m^{-2} h (Núñez et al. 2005) and after 42 days the copper release rates of low-density streamers were low enough to fail in deterring larvae of the barnacle *A. reticulatus*. In a similar manner, copper release rates of high-density streamers were low enough after 210 days to fail

in deterring larvae of the encrusting bryozoan *W. subovoidea*. Interestingly, fouling by *W. subovoidea* only occurred on the thickest patches of *Ulva* sp. and encrusted outwards to cover the streamer. However, the critical outcome is that high-density streamers remained free of hard foulers for longer than low-density or PU control streamers, meaning density can be manipulated to deliver surfaces with varying degrees of antifouling longevity. Importantly, pelagic goose barnacles, the major fouling organism settling onto seismic streamer skins (Harper 1995), although not found at the test site, have similar larval stages to the barnacles found here and therefore settlement should also be prevented.

Notably, all fouling on high-density streamers up to 210 days was *Ulva* sp., a copper-tolerant green alga (Callow 1986) which was also the predominant fouling organism on front-facing low-density Cu-embedded streamer skins compared to back-facing treatments, most likely due to light availability (Ramus and Venable 1987). For those streamer surfaces where significant fouling occurred, settlement position of hard foulers varied on seismic streamer skins with heaviest fouling occurring on the area of the streamer that was protected, against the pier, and towards the bottom of the streamer. This may be in part because some settling larvae avoid damaging ultraviolet light by moving deeper in the water column (Gleason et al. 2006) or because of the build up of silt on the top side of the streamers. While silt may reduce suitable surfaces for settlement or may deter settlement altogether (Babcock and Davies 1991; Gilmour 1999), the deposition of silt could also have hindered the dissolution of copper particles, making settlement possible for some organisms. However, under most applications these surfaces would not be kept in low-flow, heavy-silt environments and the results presented here should be treated as a proof-of-principle.

The seismic streamers used in this Chapter are towed at speeds of between 4–5.5 knots (Elboth et al. 2010). Therefore, after failure (defined as the settlement of hard foulers) of high-density streamers, all treatment surfaces were exposed to flow of 4.5 knots to determine whether settled fouling organisms could be removed under normal field conditions. However, once fouled, movement of water at 4.5 knots over the surfaces failed to remove biofouling, regardless of fouling type or the time fouling had been

established. This implies that fouling needs to be prevented and these surfaces do not have foul-release properties. Therefore, the question remains as to whether fouling would occur on these surfaces if moving at operational speeds, as opposed to trialling removal of fouling from streamers post-settlement, and this requires *in situ* trials. This will then also address pragmatic operational issues around cold spray technology. Regardless, Cu-embedded streamers produced using cold spray technology can provide effective antifouling. This technology is not expected to interfere with the transmission of acoustic signals through the PU, but rather, eliminating fouling organisms will reduce eddy formation and surface turbulence, thereby improving the signal-to-noise ratio (Harrick and Stenzel 2011). It is also unlikely that the relatively shallow metal particle depth of embedment ($< 100\ \mu m$) will affect bulk polymer properties such as flexibility, important in seismic exploration where streamers are handled mechanically on-board specialised exploration vessels. In addition, testing streamer skins *in situ* will be important to determine any interaction between copper loading, the increased dissolution rates of copper ions caused by flow and the ability of fouling organisms to settle under these conditions.

Release rate differences between low- and high-density surfaces and the interaction between those rates and other characteristics such as polymer and metal particle plasticity need to be determined and this is the next critical step to be undertaken. Release rate models have been developed for copper and copper alloys (Núñez et al. 2005; Zhu et al. 2008), however, the situation differs with cold spray metal embedment. Characteristics from existing antifouling materials or known corrosion rates cannot be extrapolated for use with cold spray antifouling surfaces since cold spray technology is applicable to multiple polymer types, which affect particle embedment depth and surface area coverage differently (Vucko et al. 2012; Chapter 4). By correlating release rate kinetics of copper with particle composition, size, density and depth of embedment, as well as with salinity, temperature and pH, which affect release rates and corrosion products (Farro et al. 2009), studies can move beyond proof of principle of key parameters and onto developing models specifically designed for

cold spray materials to deliver polymers with controlled release rates and longer, predictable lifespans.

In conclusion, copper loading (metal particle density) is a key parameter in antifouling efficiency in the field for Cu-embedded PU seismic streamer skins, and cold spray technology may provide a suitable method in the prevention of fouling organisms. Additionally, these surfaces do not have foul-release properties and flow has no effect on the removal of fouling organisms once established, so prevention is key. These outcomes support further development of copper release rate models to deliver improved antifouling surfaces, and *in situ* field trials to assess the effects of movement under operational conditions.

Chapter 6

Assessing the antifouling properties of cold spray metal embedment using particle concentration gradients*

6.1 Introduction

Biofouling has negative impacts on many aspects of marine industry that use thermoplastic polymers (polymers), exemplified by aquaculture and geophysical exploration. In finfish aquaculture, high-density polyethylene (HDPE) and nylon are major constituents used to fabricate cages and netting. Fouling on these polymers decreases cage volume, flow and buoyancy while it increases physical damage and deformation as well as cage weight and therefore mooring stress (Braithwaite and McEvoy 2005; Fredriksson et al. 2007; Moe et al. 2009; Fitridge et al. 2012). In geophysical exploration, polyurethane seismic streamers are used to protect sensitive electronic equipment. Fouling on streamers reduces seismic data quality and increases equipment failure, feedback noise, hydrodynamic drag and therefore fuel consumption (Harper 1995; Vignaux 2010; Harrick and Stenzel 2011). Consequently, it is important to optimise the efficacy of antifouling technologies used for polymers to control a broad range of fouling organisms.

The most widely used functional broad spectrum antifouling technologies are copper and copper-based coatings (Brooks and Waldock 2009; Finnie and Williams 2010). However, in many cases, copper-based coatings have poor adhesion to polymers. For example, standard boat paints, which are designed for inflexible surfaces, cannot be used on aquaculture netting which are coated in flexible waxy emulsions incorporating copper. The typical life span of these waxy emulsions prior to failure is between 6 and 9 months, much shorter than conventional paints which have a lifespan

*Chapter 6 adapted from Vucko MJ, King PC, Poole AJ, Hu Y, Jahedi MZ and de Nys R (2014). Assessing the antifouling properties of cold spray metal embedment using loading density gradients of metal particles. Biofouling 30: 651-666.

of approximately 36 months (reviewed in Braithwaite and McEvoy 2005; Braithwaite et al. 2007; Finnie and Williams 2010; Guenther et al. 2010). In addition, no functional coatings exist for seismic streamers where polyurethane, which is relatively soft, flexible and hydrophobic, is handled mechanically during operation on specialised exploration vessels (Poole et al. 2012). However, technologies such as cold spray metal embedment offer an alternative.

Cold spray is a metal spray process where small, solid metal particles (typically < 50 μm) are accelerated to supersonic velocities using high pressure gas (1.5–3.5 MPa) and heat (less than the melting point of the metal being used), and deposited onto a receiving surface (Stoltenhoff et al. 2002; Papyrin et al. 2007). This process has been applied to developing wear- and corrosion-resistant coatings, enhancing heat and electrical conductivity (Gärtner et al. 2006), reinforcing structures, forming shapes without the use of moulds (Pattison et al. 2007) and giving antifouling properties to polymers by embedding metals that prevent fouling (Vucko et al. 2012; King et al. 2013; Vucko et al. 2013a; Chapters 4 and 5).

Metals including zinc, and copper and its alloys, prevent fouling due to their toxicity towards the settlement phase of marine invertebrate fouling larvae (WHOI 1952b; Mance 1987; Fitridge et al. 2012), which is an essential step in establishing fouling communities. The toxicity towards marine invertebrates occurs through the direct absorption of waterborne metal ions, arguably the most toxic form of the metal (Pinho et al. 2007; Thomas and Brooks 2010). The toxicity of copper is associated with the inhibition of Na^+- and K^+-ATPase activity, which causes imbalances in intracellular ions and the inhibition of the activity of carbonic anhydrase enzymes, while impairing gas exchange and acid–base regulation (Grosell et al. 2007; Lopes et al. 2011). In contrast, the toxicity of zinc is associated with the inhibition of Ca uptake, resulting in the reduction of total body Ca, causing decreases in food uptake and therefore reduced growth, and eventual death due to hypocalcaemia (Muyssen et al. 2006). Zinc can also decrease oxygen consumption, impair carbohydrate metabolism and the use of proteins (Devi 1995). Most importantly, the effectiveness of these metals is highest within surface boundary layers, while they are less toxic when released into the

environment as a result of low bioavailability within sediments and complexation with dissolved organic carbon (Brooks et al. 2008; Brooks and Waldock 2009; Thomas 2009; Howell and Behrends 2010; Thomas and Brooks 2010).

Overall, cold spray metal-embedded polymers exhibit effective antifouling properties. However, upon submersion into water, the loading density of metal particles (metal particles per unit area) and depth of embedment affect the release rates of metal ions and ultimately, antifouling efficiency (Vucko et al. 2012; Vucko et al. 2013a; Chapters 4 and 5). Specific release rates of metal ions can be used to determine the minimum effective release rate (MERR), defined as the point when the release rate of metal ions becomes low enough such that the surface fails to prevent fouling. Understanding the interaction between metal loadings and metal ion release rates is therefore critical to refining cold spray technology and its deployment across antifouling applications. Upon exposure to field conditions and a natural fouling community, the recruitment of fouling will depend upon the interaction between the species available for recruitment and the MERRs for their deterrence. Marine invertebrate species display different tolerances to metal toxicity (Bellas et al. 2001; Brown et al. 2004; Rivera-Duarte et al. 2005; Brooks and Waldock 2009; Pineda et al. 2012) and by determining which species are most resilient to metal ions being released from metal-embedded polymers, antifouling materials can be tailored to specific, complex fouling communities. To determine the MERR needed to deter fouling organisms, a gradient of metal loading densities within the same surface was used, where the low loading densities of the gradient should become fouled first. Overall, release rates will decrease over time, and the rate of release from a high density section of the tube at a later time should have a similar release rate to a low density section of the tube at an earlier time. Consequently, when examining a single species through time along the length of the gradient, with a range of loading densities of metal particles, the tolerance of a species should remain constant given the decrease in metal ion release rates.

The specific aims of this Chapter were to, first, use cold spray metal embedment of HDPE tubes to produce a gradient of copper, bronze and zinc metal particles ranging

from low to high loading densities. Second, to determine which species, from a natural fouling community, were the first to recruit to the metal-embedded HDPE tubes (most tolerant species) and consequently establish the MERRs of copper ions (from copper- and bronze-embedded tubes) and zinc ions (from zinc-embedded tubes) needed to prevent the recruitment of the most tolerant fouling organisms. Third, to examine the release rates of copper ions from copper- and bronze-embedded tubes to establish whether there was a difference between the two metals.

6.2 Materials and methods

6.2.1 Gradient tube surface preparation

Metal particles were embedded into sections of black HDPE tube (500 mm length, 57.5 mm diameter and 3 mm thickness; Geberit Pty. Ltd., North Ryde, New South Wales). The HDPE tubes were metallised by cold spray using a Kinetics 4000 cold spray system (Cold Gas Technology GmbH, Ampfing, Germany) where a cold spray nozzle was mounted onto a robot arm (ABB IRB 2600) to give lateral movement. The tubes were fitted onto a 55 mm diameter aluminium rod, mounted onto a lathe, and spun at 1,156 rpm during cold spray, which corresponded to a linear surface speed of 3,390 mm s^{-1}. The traverse speed of the robot arm was linearly increased from 1.67 to 60 mm s^{-1} during spraying to produce a gradient along the length of the tube from a high loading density to a low loading density (Figure 6.1). Only the middle 400 mm portion of the tube was sprayed leaving 50 mm bare on either end. Copper (Atlantic Equipment Engineers Inc, Bergenfield, New Jersey; 99.99% purity on a metal-basis), bronze (Automotive Components Ltd., Launceston, Tasmania; 90% Cu and 10% Sn on a metal-basis) and zinc (Umicore, Melbourne, Victoria; 98% purity on a metal-basis) powders were used as the feedstock materials to produce copper, bronze and zinc gradient treatments. The as-supplied powders were -325 mesh, being passed through a 45 μm sieve. Size analysis of the particles was done using a Mastersizer Laser Analyser (Malvern Instruments Ltd., Malvern, Worcestershire, UK). The average particle size (d_{50}) for copper was 26.9 μm, while d_{10} and d_{90} were 12.8 and 49.7 μm,

respectively. The average particle size (d_{50}) for bronze was 22.1 μm, while d_{10} and d_{90} were 7.1 and 45.8 μm, respectively. The average particle size (d_{50}) for zinc was 22.9 μm, while d_{10} and d_{90} were 5.6 and 45.3 μm, respectively. The metal powders were characterised using inductively coupled plasma optical emission spectroscopy (ICP-OES) to demonstrate their purity by determining which elements were present at concentrations greater than 10 ppm (Table 6.1). Nitrogen was used as the carrier gas and was kept at a constant temperature (150°C) and pressure (2.5 MPa) throughout spraying, which facilitated a gas velocity that was high enough for embedment of metal particles into the HDPE tubes. The flow rate of particles was calculated from the difference in mass of the powder feeder before and after spraying. The flow rate for copper was 735 g h^{-1}, the flow rate for bronze was 877 g h^{-1}, and the flow rate for zinc was 814 g h^{-1}.

Table 6.1. Elemental characterisation of metal powders used for cold spray metal embedment of HDPE tubes. Results were obtained using ICP-OES and are expressed as parts per million or as a percent where specified.

	Metal powder type		
Element	Copper	Bronze	Zinc
Ag	189	11.1	< 0.1
Al	32	4.5	7.3
Cu	99.26%	90.16%	113
Fe	267	83	8.3
Mg	10.5	1.3	0.4
Na	97	17	5.5
Ni	221	30	< 0.1
Pb	27	162	196
Si	27	346	72
Sn	< 0.1	9.84%	< 0.1
Ti	1.4	31	2.6
Zn	< 0.1	< 0.1	99.9%

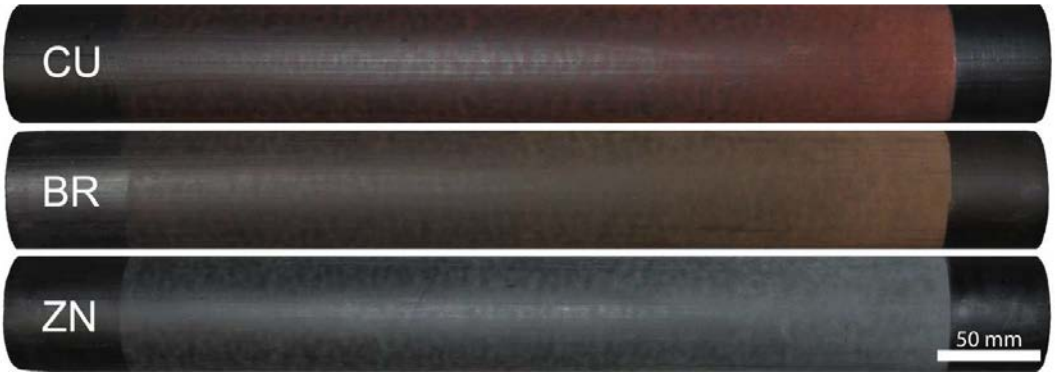

Figure 6.1. Black HDPE tubes embedded with copper (CU), bronze (BR) and zinc (ZN) metal particles (< 50 μm diameter) using cold spray technology. Particles vary in loading density from low (left) to high (right) along their lengths and only the middle 400 mm of the 500 mm tube was sprayed.

6.2.2 Gradient tube surface characterisation

The surface area coverage of metal particles was examined along the length of the gradient tubes. The surface area covered by metal particles was calculated from 16 sections along the length of the tube using digital microscopy images of each metal type ($n = 4$), where section 1 had the lowest loading density of metal particles and section 16 had the highest loading density of metal particles. Sixteen sections were chosen since a gradient length of 400 mm could be cut into sixteen equal parts of 25 mm, coinciding with the size of the hole saw (Cobalt Bi-metal; Sutton Tools Pty. Ltd., Thomastown, Victoria, Australia) used to drill out plugs for release rate analysis (see materials and methods in '6.2.3 Initial release rates from gradient tubes'). Digital images of the plugs were obtained using a microscope (SZ61; Olympus, Eagle Farm, Queensland, Australia) and digital camera (DP26; Olympus, Eagle Farm, Queensland, Australia). For copper and bronze, metal particle surface area coverage was calculated by inverting the colours of the digital image and obtaining a black (metal particles) and white (polymer surface) pixel threshold. For zinc, metal particle surface area coverage was calculated by inverting the colours of the digital image, increasing the contrast of the image to 100% five times and then obtaining a black (metal particles) and white (polymer surface) pixel threshold. Pixel threshold images were obtained using Photoshop (v. 12.0.4; Adobe Systems Software, San Jose, California, USA) and

pixel percent coverage of those images was quantified using ImageJ (v. 1.42q; National Institutes of Health, Bethesda, Maryland, USA).

6.2.3 Initial release rates from gradient tubes

The initial release rates of metal ions were examined along the length of gradient tubes prior to submersion. For sections 1, 4, 7, 10, 13 and 16 (n = 4), release rates were determined from the concentrations of metal ions from plugs drilled out of each section. Concentrations of metal ions were measured by spinning the plugs in filtered seawater (FSW) for 60 min according to the ASTM D6442-06 standard (ASTM 2011). The following alterations to the standard were made to suit the materials used. The plugs (25 mm in diameter) were inserted into a hole cut out of sections of HDPE tube (100 mm length, 57.5 mm diameter) and secured using a thin piece of clear tubing. The HDPE tubes were attached to motors (70 rpm 12V DC reversible gearhead) using customized polyvinyl chloride (PVC) fittings and the tubes were placed into 1,000 mL polypropylene beakers (Livingstone International Pty. Ltd., Rosebery, New South Wales, Australia) filled with 500 mL of FSW. All FSW used in release rate quantification was passed through 0.35 μm, 0.2 μm and activated carbon filters, UV treated, autoclaved at 121°C for one hour, and then stored for five days. The mean temperature, salinity, pH and dissolved organic carbon for FSW used throughout the experiment was 24.78 ± 0.23°C, 38.00 ± 0.00 ppt, 8.55 ± 0.03 and 5.08 ± 0.95 mg L^{-1}, respectively. A speed controller (KC5502; Jaycar Electronics, Rydalmere, New South Wales, Australia) was used to adjust the rotational speed of the motors to 67 rpm in order to achieve a peripheral speed of 0.2 m s^{-1} (ASTM 2011). After 60 min the FSW sample was agitated, acidified, and filtered at which point the concentration of metal ions released into the water could be measured. The concentration of copper ions was measured from copper and bronze treatments while the concentration of zinc ions was measured from zinc treatments.

The concentration of metal ions of each water sample was quantified using an inductively coupled plasma mass spectrometer (ICP-MS; Bruker 820-MS formerly Varian 820-MS, Melbourne, Australia). Sample analysis was carried out at the

Advanced Analytical Centre at James Cook University (JCU; Townsville, Queensland, Australia). All samples were diluted ten-fold with 1% double distilled HNO_3 before ICP-MS analysis, and ^{65}Cu and ^{67}Zn were used for quantification. A high purity multi-element standard solution (Choice Analytical Sydney, Australia) was used to calibrate the instrument and an internal standard (yttrium) was added on-line through a Y-piece (three-way tubing connector) to correct for the instrument drift and potential matrix effects. An untreated FSW sample was also diluted ten-fold with 1% double distilled HNO_3 and measured along with all other samples to be used for subtraction of the background FSW concentrations of metal ions. For the purposes of quality control, one sample from every batch was spiked with 1 ppb Cu or 1 ppb Zn before analysis. The recovery was found to be greater than 95% for Cu and Zn.

For all analyses, the release rates (g $m^{-2} h^{-1}$) could be calculated using the concentrations of metal ions (μg L^{-1}) measured. In addition, a conversion factor of 2,400 can be used to convert g $m^{-2} h^{-1}$ to μg $cm^{-2} d^{-1}$, which is commonly used in studies reporting the release rates of metal ions (Valkirs et al. 2003; Finnie 2006; Earley et al. 2014). To compensate for any variation in pH, which has a substantial effect on release rates (Howell and Behrends 2010), between the seawater where the samples were deployed (see materials and methods in '6.2.4 Gradient tube field trials') and the FSW used for release rate measurements in the laboratory, a standard calibration curve was used. Calibration curves were produced by testing the metal ion release rates of copper (copper ions), bronze (copper ions) and zinc (zinc ions) plugs (n = 3) at pH 7.9, 8.5 and 9.1. For all three, release rates decreased as pH increased and exponential models were used to describe the relationships. The models used for copper, bronze and zinc were $y = 373.22e^{-1.166x}$ (R^2 = 0.999), $y = 15.478e^{-0.734x}$ (R^2 = 0.966) and $y = 39.128e^{-0.561x}$ (R^2 = 0.930), respectively.

6.2.4 Gradient tube field trials

Gradient tubes were deployed in the field to determine the MERR needed to prevent the recruitment of tolerant fouling species from a natural fouling community, as well as how both the release rates and the recruitment of those species were affected

through time. Surfaces were submerged at the Townsville Yacht Club (Queensland, Australia) in late September (Australian spring) and remained in place until all sections of the gradient tubes were fouled. At this dry, tropical location, there is intense, consistent fouling pressure year round. The mean temperature, salinity, pH and dissolved organic carbon throughout the course of the trial was 28.35 ± 0.05°C, 37.83 ± 0.17 ppt, 7.93 ± 0.02 and 1.92 ± 0.42 mg L^{-1}, respectively. Copper, bronze and zinc gradient tubes (n = 4), and unsprayed HDPE controls (n = 4), were randomly positioned horizontally within six PVC tube frames (675 x 1,270 mm; 25 mm tubing diameter) and spaced 100 mm apart from each other. It should be noted that the four replicates of copper, bronze and zinc gradient tubes used for field trials were different than the four replicates used for initial release rate measurements. The tubes were secured within the frames using cable ties to ensure consistent orientation of each tube throughout the trial. The frames were secured to boat moorings using polyethylene rope and the uppermost tube was 600 mm below the surface of the water while the lowermost tube was 1,200 mm below the surface of the water. The HDPE tubes were checked every two weeks for the occurrence of fouling and photographed using a digital camera. For all subsequent image analyses, images were split into sixteen equal sections, each 25 mm in length, which coincided with the diameter of the plugs being removed (see materials and methods in '6.2.3 Initial release rates from gradient tubes').

6.2.4.1 MERR to prevent the recruitment of tolerant fouling species

When fouling recruited to a gradient tube, it invariably occurred up to a 'leading edge', defined as the line of fouling closest to the high-density end of the gradient tube, after which fouling did not occur. This leading edge was assumed to be the loading density of metal, and resulting metal ion release rate, that fouling could tolerate, above which fouling was prevented. In all instances, the plug was removed from an unfouled portion of the tube adjacent to the leading edge of fouling (Figure 6.2). Throughout drilling, the tube was held in place using customized fittings, which prevented the tubes from being damaged. Plugs were placed into individual plastic jars with natural seawater and brought back to the laboratory where release rates were measured within 24 hours (see materials and methods in '6.2.3 Initial release rates

from gradient tubes'). The gradient tubes were subsequently left in the water until fouling occurred at a further point along the tube towards the high-density end, and the procedure was repeated. As there was rapid colonization of the surfaces, only the first two most tolerant fouling species were identified during the initial 12 weeks of the gradient tube field trial. After 12 weeks, the gradient tubes had become completely fouled up to section 15 and were left in the water to determine the time to fouling of the final section (section 16). The two most tolerant species, in order of recruitment, were the encrusting bryozoan *Watersipora* sp. and the spirorbid polychaete *Simplaria pseudomilitaris* (Thiriot-Quievreux 1965). The section upon which the leading edge of fouling occurred was recorded to determine whether fouling recruited to similar sections within each gradient treatment each week and the progression over time. In addition, regardless of the time that fouling occurred, plugs removed from the leading edge of fouling were used to determine the release rates of these sections and to estimate the MERR for each of the two species (defined as the highest release rate measured). For one treatment, results are not presented graphically as fouling occurred over the full length of the tube for all replicates at the first time point (*Watersipora* sp. on zinc at week 2). Finally, the mean copper ion release rates from of copper- and bronze-embedded gradient tubes for each species were compared to establish any difference between the two metal types.

6.2.4.2 Fouling through time

Although there was a focus on the leading edge of fouling to determine MERRs, it was assumed that if a species could tolerate release rates at the leading edge, then the same species could also tolerate release rates at any point towards the low loading density end of the gradient tube. Therefore, images were used to determine the effects of metal gradients (copper, bronze and zinc) on the progression of the two most tolerant fouling species through time along the length of the gradient tubes compared to controls without embedded metal. Fouling on copper, bronze and zinc gradient tubes as well as HDPE controls (n = 4) was quantified as a percent coverage for *Watersipora* sp. and as the number of individuals for *S. pseudomilitaris.* Quantitative changes of the tolerant fouling species on gradients were compared to HDPE controls and examined

at time points when release rate measurements were taken over the first 12 weeks. In addition, other species within the natural fouling community occurred on the control tubes, and images were used to determine the recruitment patterns of all fouling organisms through time along the length of the controls. Nine other species recruited to controls (n = 4), in addition to the two most tolerant species, and were quantified as the number of individuals of the barnacle *Amphibalanus reticulatus* (Utinomi 1967), the oyster *Pinctada imbricata* (Gould 1850), the stalked bryozoans *Bugula neritina* (Linnaeus 1758) and *Bugula stolonifera* (Ryland 1960), the sabellid polychaete *Branchiomma nigromaculatum* (Baird 1865) and the serpulid polychaete *Hydroides elegans* (Haswell 1883), as well as percent coverage of colonies of ascidians, the encrusting bryozoan *Hippopodina irrikensis* (Tilbrook 1999) and the stalked bryozoan *Zoobotryon verticillatum* (Delle Chiaje 1828). Quantitative changes in the total fouling community on controls were examined and major patterns are described through time over the first 12 weeks of the field trial. All results were quantified using ImageJ (v. 1.42q) and for graphical purposes were displayed as mean values without error bars for each of the sixteen sections.

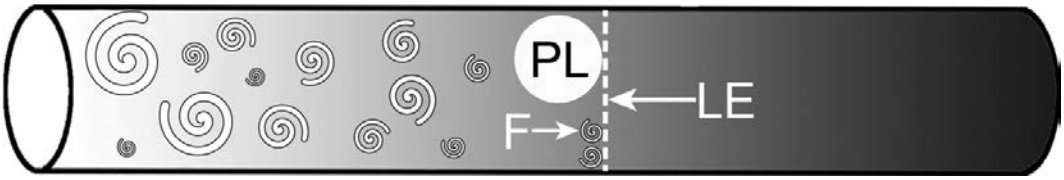

Figure 6.2. Plugs (PL) used for metal ion release rate measurements were removed from an unfouled portion of the gradient tubes adjacent the leading edge (LE) of fouling (F). N.B. spirals represent fouling by a spirorbid polychaete.

6.2.5 Statistical analysis

One-factor permutational analysis of variance (PERMANOVA) analyses were used to test for significant differences in the mean position of fouling on gradient tubes at different times (fixed factor) when measurements were obtained from three or more time points. Independent samples t-tests were used to test for significant differences in the mean position of fouling at different times (fixed factor) when measurements were obtained from only two time points. Since the MERRs were estimated from the highest

release rate measurements and the decrease of those rates over time, it was important to validate the MERR estimates by ensuring that the metal ion release rates remained constant regardless of time or section from which the plug was removed. To determine whether the release rates of each plug remained constant, Pearson's product-moment correlations were used to test for correlations between release rate and section. Independent samples t-tests were used to test for significant differences between the release rates of copper ions from copper- and bronze-embedded tubes (fixed factor) overall for each species. Two-factor repeated measures PERMANOVA analyses were used to test for significant differences in recruitment of fouling over time between treatments (fixed factor) across each section (fixed factor). Two-factor PERMANOVA analyses were used to test for significant differences in recruitment of fouling between treatments (fixed factor) across each section (fixed factor) when measurements were only taken at one time point, and there was no need for repeated measures. For PERMANOVA, pair-wise *a posteriori* comparisons were used to determine significant groupings ($\alpha = 0.05$), when a significant result was obtained.

All PERMANOVA analyses were performed using PRIMER 6 (v. 6.1.13; Ivybridge, United Kingdom) and PERMANOVA+ (v. 1.0.3 [Clarke and Gorley 2006]). For PERMANOVA, Bray-Curtis similarity matrices were produced using the untransformed raw data, *p*-values were calculated from 9,999 random permutations and dummy variables (0.0001) were used to account for zero values. All independent samples t-tests and Pearson's product-moment correlations were performed using the R language (v. 3.0.1 [R Core Team 2013]). For correlations, the assumptions of normality were checked with Q-Q plots and Shapiro-Wilk normality tests. All data are presented as mean ± standard error unless otherwise indicated.

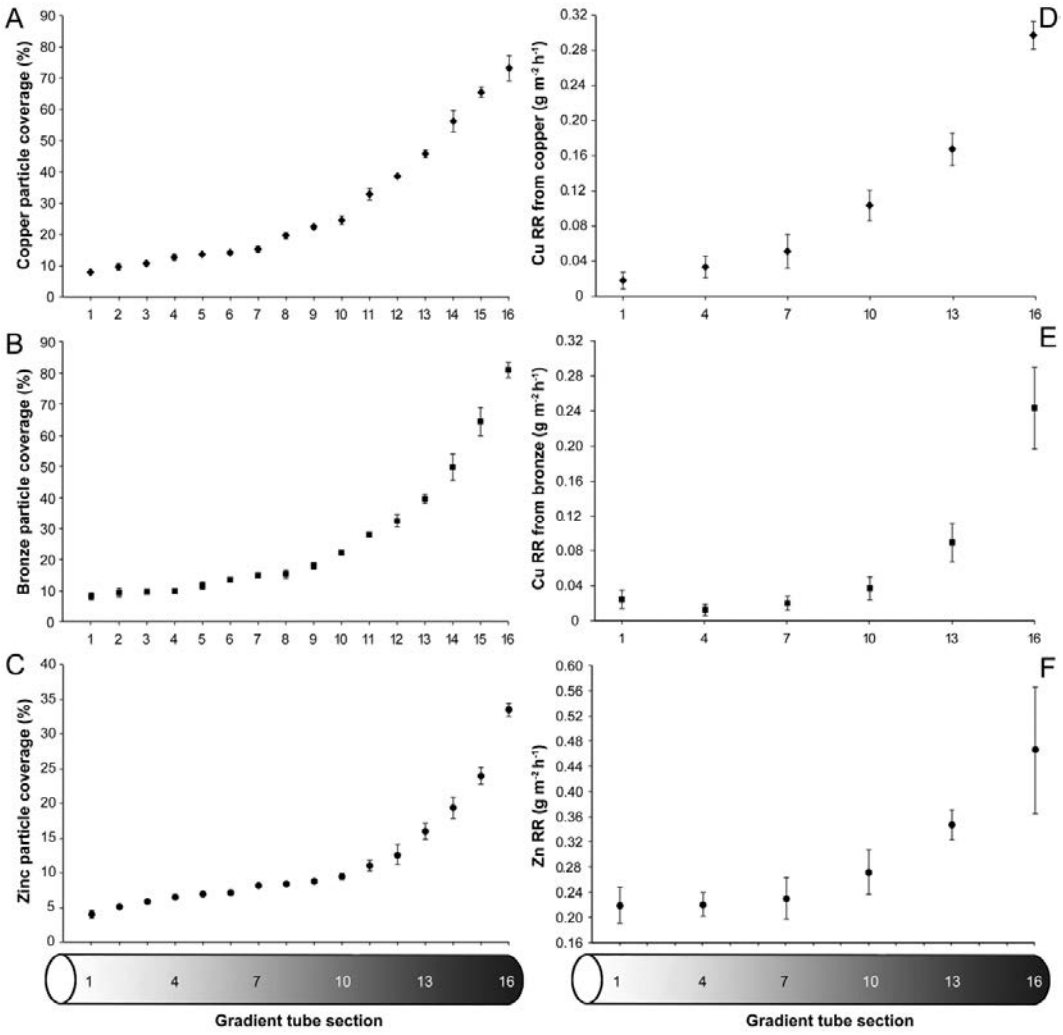

Figure 6.3. Gradient tube surface characterisation examining metal particle surface area coverage and initial metal ion release rates (from low to high loading density of metal particles). Metal particle surface area coverage from sixteen sections along the length of the gradient tubes for (**A**) copper, (**B**) bronze and (**C**) zinc and initial metal ion release rates from six sections along the length of the gradient tubes for (**D**) copper (copper ions), (**E**) bronze (copper ions) and (**F**) zinc (zinc ions). RR, release rates.

6.3 Results

6.3.1 Gradient tube surface characterisation

The surface area covered by metal particles increased along the length of the gradient tubes for copper (Figure 6.3A), bronze (Figure 6.3B) and zinc (Figure 6.3C) metal treatments. The section of the tube with the lowest loading density of metal particles for copper, bronze and zinc had 7.86 ± 0.44%, 8.22 ± 1.14% and 4.11 ± 0.58% mean particle coverage, respectively. The section of the tube with the highest loading density of metal particles for copper, bronze and zinc had 73.35 ± 4.01%, 81.10 ± 2.33% and 33.56 ± 0.95% mean particle coverage, respectively. The surface area covered by particles on the highest density end of the tube was approximately ten-fold higher than the lowest density end.

6.3.2 Initial release rates from gradient tubes

The initial metal ion release rates increased along the length of the gradient tube for copper (Figure 6.3D), bronze (Figure 6.3E) and zinc (Figure 6.3F) metal treatments. The section of the tube with the lowest loading density of metal particles for copper, bronze and zinc had initial mean release rates of 0.02 ± 0.01 g m^{-2} h^{-1}, 0.03 ± 0.01 g m^{-2} h^{-1} and 0.22 ± 0.03 g m^{-2} h^{-1}, respectively. The section of the tube with the highest loading density of metal particles for copper, bronze and zinc had initial mean release rates of 0.30 ± 0.02 g m^{-2} h^{-1}, 0.25 ± 0.05 g m^{-2} h^{-1} and 0.47 ± 0.10 g m^{-2} h^{-1}, respectively. For copper and bronze, the initial metal ion release rates from the highest density end of the tube were approximately ten-fold higher than the lowest density end.

6.3.3 Gradient tube field trials

6.3.3.1 MERR to prevent the recruitment of tolerant fouling species

For most treatments, initial fouling occurred at week 4 and progressed along the length of the gradient tube over time. Importantly, regardless of this progression, release rates remained constant, validating the estimated MERRs (defined as the

highest metal ion release rates). *Watersipora* sp. and *S. pseudomilitaris* were the first and second species that recruited to gradient tubes and subsequently had the highest tolerance to the release of metal ions. Copper and bronze gradient tubes were equal in their effectiveness against fouling with a similar MERR of copper ions. After 12 weeks, fouling had recruited to all sections of zinc tubes while fouling on copper and bronze tubes occurred up to section 15 with no progression to section 16 until week 44.

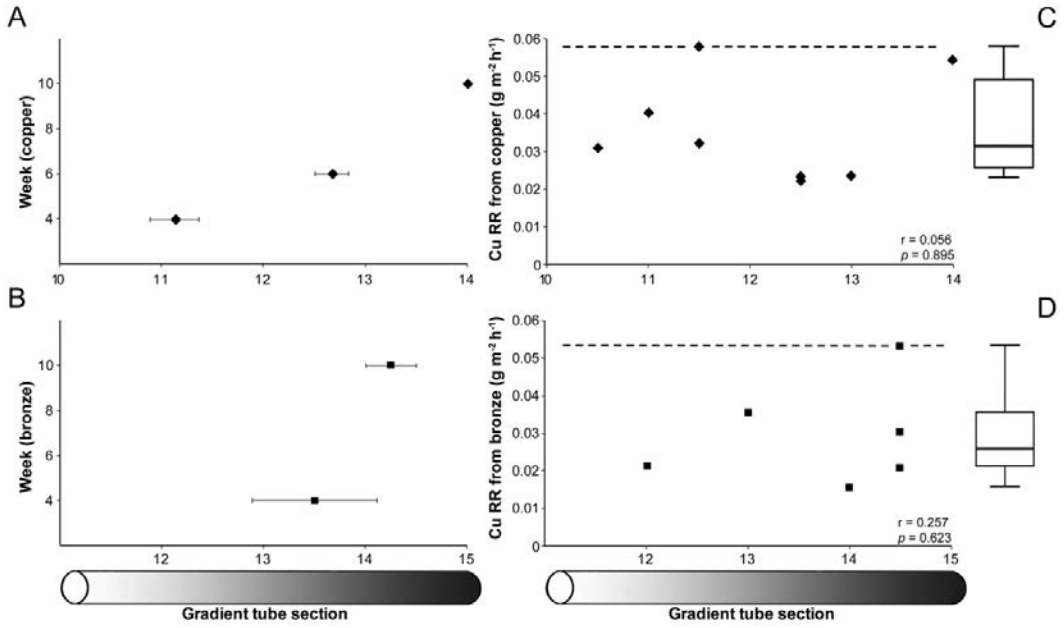

Figure 6.4. Recruitment of the most tolerant fouling species, *Watersipora* sp., on HDPE tubes embedded with a gradient of metal particles. Progression of the leading edge of *Watersipora* sp. recruitment through time along the length of (**A**) copper and (**B**) bronze gradient tubes. Release rates of leading edge sections where fouling occurred, regardless of time, along the length of (**C**) copper and (**D**) bronze gradient tubes. N.B. Boxplots indicate mean release rate for (**C**) copper and (**D**) bronze gradient tubes; dashed lines indicate the MERR for each metal type; RR, release rates.

There was a significant effect of time on the progression of *Watersipora* sp. on copper gradients (Figure 6.4A; Table 6.2A) where each occurrence of fouling was further along than the last. There was no effect of time on the progression of *Watersipora* sp. on bronze gradients (Figure 6.4B; Table 6.2A), although there was a trend where each occurrence of fouling was further along than the last. The position of the leading edge of recruitment for *Watersipora* sp. on zinc gradients was up to, and including, section 16 at week 2 for all replicates. There was no significant correlation between the release

rates from gradient tubes at the leading edge of fouling and the section from which the measurement was taken regardless of time for both copper (Figure 6.4C) and bronze (Figure 6.4D) gradients (Table 6.2B). The MERR of copper ions to prevent the recruitment of *Watersipora* sp. was 0.058 g m^{-2} h^{-1} from copper-embedded tubes (Figure 6.4C) and 0.054 g m^{-2} h^{-1} from bronze-embedded tubes (Figure 6.4D). In addition, there was no significant difference between the mean release rates of copper ions from copper- (0.036 ± 0.005 g m^{-2} h^{-1}) and bronze-embedded (0.030 ± 0.006 g m^{-2} h^{-1}) tubes overall (Figures 6.4C and D; Table 6.2C). The mean zinc ion release rate from zinc-embedded tubes (0.111 ± 0.035 g m^{-2} h^{-1}) could not be used to estimate the MERR as *Watersipora* sp. recruited up to the highest loading density of metal particles (section 16) after 2 weeks.

There was a significant effect of time on the progression of *S. pseudomilitaris* on copper (Figure 6.5A), bronze (Figure 6.5B) and zinc (Figure 6.5C) gradients (Table 6.2A), where each occurrence of fouling was further along than the last. There was no significant correlation between the release rates from gradient tubes at the leading edge of fouling and the section from which the measurement was taken regardless of time for copper (Figure 6.5D), bronze (Figure 6.5E) or zinc (Figure 6.5F) gradients (Table 6.2B). The MERR to prevent the recruitment of *S. pseudomilitaris* was 0.030 g m^{-2} h^{-1} of copper ions from copper-embedded tubes (Figure 6.5D), 0.025 g m^{-2} h^{-1} of copper ions from bronze-embedded tubes (Figure 6.5E) and 0.080 g m^{-2} h^{-1} of zinc ions from zinc-embedded tubes (Figure 6.5F). In addition, there was no significant difference between the mean release rates of copper ions from copper- (0.020 ± 0.002 g m^{-2} h^{-1}) and bronze-embedded (0.019 ± 0.002 g m^{-2} h^{-1}) tubes overall (Figures 6.5D and E; Table 6.2C).

Table 6.2. Statistical analyses surrounding the effects of copper (CU), bronze (BR) and zinc (ZN) metal particle gradients on fouling species. (**A**) the effect of time on the progression of fouling; (**B**) the correlation between release rate and the section from which measurements were obtained and (**C**) the difference in release rates between copper and bronze gradient tubes within *Watersipora* sp. and *S. pseudomilitaris* and between time points.

Species	Metal	Test	*df*	pseudo-*F* or *t*	r (*t*)	*p*
(A) Effect of time on progression						
Watersipora sp.	CU	P1	2,5	20.72		0.004*
	BR	T	1,4	-0.81		0.466
S. pseudomilitaris	CU	T	1,4	2.75		0.051*
	BR	T	1,4	7.92		0.001*
	ZN	P1	3,7	26.08		0.001*
(B) Correlation between release rate and section						
Watersipora sp.	CU	PPC	6		0.06 (0.14)	0.895
	BR	PPC	4		0.26 (0.53)	0.623
S. pseudomilitaris	CU	PPC	4		-0.61 (-1.53)	0.200
	BR	PPC	4		-0.49 (-1.11)	0.328
	ZN	PPC	9		0.38 (1.22)	0.254
(C) Difference in release rates between copper and bronze overall						
Watersipora sp.	CU x BR	T	1,12	0.86		0.406
S. pseudomilitaris	CU x BR	T	1,10	-0.21		0.838
Across time points	WK	P2	2,30	6.80		0.001*
	TR	P2	1,30	0.32		0.737
	WK x TR	P2	2,30	0.31		0.876

Notes: P1, one-factor PERMANOVA; P2, two-factor PERMANOVA; T, independent-samples t-test; PPC, Pearson's product-moment correlation; * denotes significant effect, $\alpha = 0.05$.

After week 12, fouling remained unable to recruit to section 16 (highest loading density of metal particles) of the copper and bronze gradient tubes until recruitment of *Watersipora* sp. at week 44. *Watersipora* sp. was able to recruit to the highest loading density of metal particles on both copper and bronze treatments where the mean release rates of copper ions were 0.017 ± 0.001 g m^{-2} h^{-1} and 0.023 ± 0.005 g m^{-2} h^{-1}, respectively.

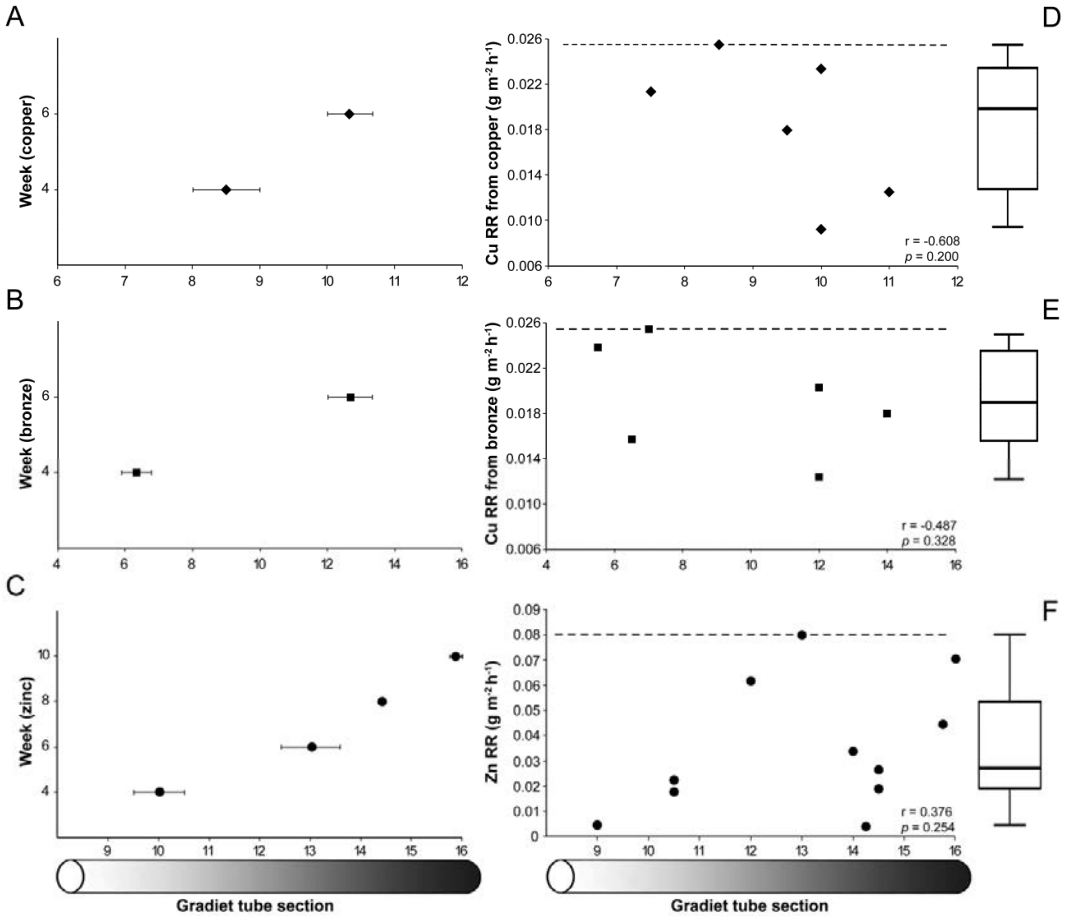

Figure 6.5. Recruitment of the second most tolerant fouling species, *S. pseudomilitaris*, on HDPE tubes embedded with a gradient of metal particles. Progression of the leading edge of *S. pseudomilitaris* recruitment through time along the length of (**A**) copper, (**B**) bronze and (**C**) zinc gradient tubes. Release rates of leading edge sections where fouling occurred, regardless of time, along the length of (**D**) copper, (**E**) bronze and (**F**) zinc gradient tubes. N.B. Boxplots indicate mean release rates for (**D**) copper, (**E**) bronze and (**F**) zinc gradient tubes; dashed lines indicate the MERR for each metal type; RR, release rates.

6.3.3.2 Fouling through time

The recruitment of *Watersipora* sp. and *S. pseudomilitaris* on controls increased in percent coverage and the number of individuals over time while covering the length of the tubes regardless of section. Conversely, for copper and bronze gradients, although recruitment of the two species increased in percent coverage and number of individuals over time, there was a decrease in fouling towards the high loading density end of the gradient tubes where, after 12 weeks, the highest loading densities

completely prevented settlement. Zinc gradient tubes were not as efficient at preventing fouling with recruitment of *Watersipora* sp. and *S. pseudomilitaris* along the full length of zinc gradients by week 2 and week 8, respectively. In addition, the natural fouling community, which, as a whole comprised eleven species on controls, generally increased over time and occurred along the length of the control tubes regardless of section.

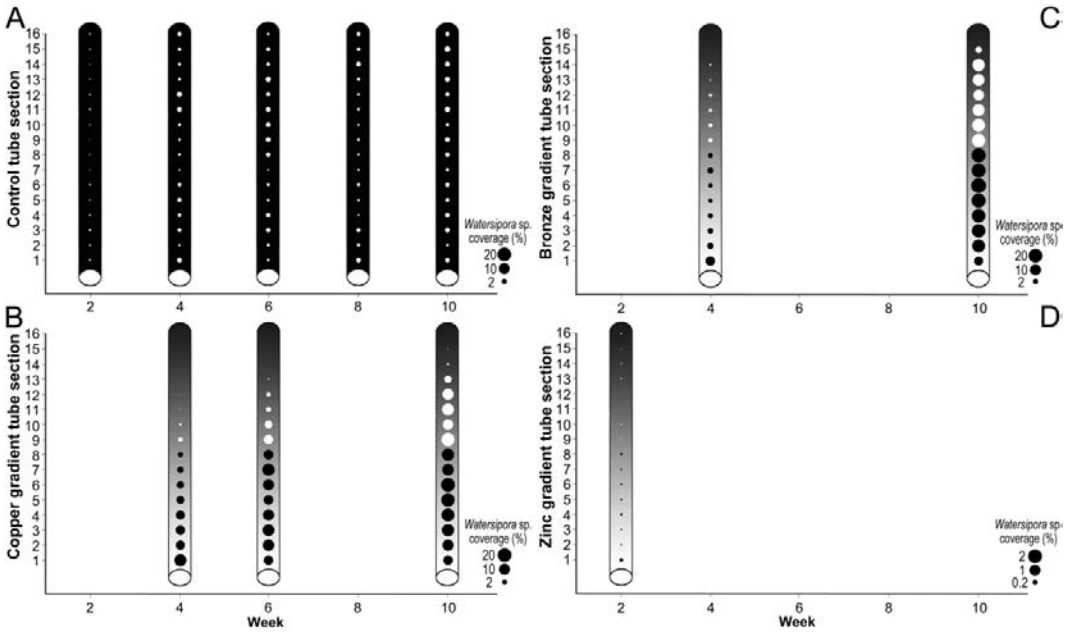

Figure 6.6. Recruitment of *Watersipora* sp. over time on HDPE tubes with and without embedment of metal particle gradients. Mean recruitment was quantified on sixteen sections of (**A**) control, (**B**) copper, (**C**) bronze and (**D**) zinc treatments at two-week intervals. Each circle (black and white) represents mean fouling coverage of *Watersipora* sp. per section. Quantification of fouling on gradient tubes was only done on weeks corresponding to the removal of plugs for release rate analysis. N.B. The scale for *Watersipora* sp. recruitment onto zinc tubes is an order of magnitude lower than the others due to low coverage.

For percent coverage of *Watersipora* sp., there was a significant interaction of section, treatment and week between controls and copper gradients (Figures 6.6A and B; Table 6.3) as well as between controls and bronze gradients (Figures 6.6A and C; Table 6.3). Recruitment of *Watersipora* sp. on controls and gradients (copper and bronze) occurred from week 2 and week 4, respectively, and fouling on all three treatments increased over time, albeit at different rates. In addition, there was equal coverage of *Watersipora*

sp. on all sections of controls while fouling coverage on copper and bronze gradients decreased along the length of the tubes, where recruitment was prevented more effectively, for longer, as loading densities of metal particles increased. Between controls and zinc gradients (Figures 6.6A and D), there was a significant effect of treatment (Table 6.3) on *Watersipora* sp. coverage. *Watersipora* sp. recruited to all sections of controls and zinc gradients after 2 weeks and zinc gradients had more fouling than controls.

Table 6.3. Two- and three-factor PERMANOVA analyses with effects of section (SE), treatment (TR) and week (WK) on the recruitment of fouling species on copper (CU), bronze (BR) and zinc (ZN) gradient tubes as compared to HDPE controls.

Species	Metal	Factors	Test	*df*	MS	pseudo-*F*	*p*
Watersipora sp.	CU	SE x TR x WK	P3	30,288	2,904	2.17	0.001*
	BR	SE x TR x WK	P3	15,192	2,584	1.91	0.001*
	ZN	SE	P2	15,96	2,114	1.19	0.218
		TR		1,96	43,544	24.51	0.001*
		SE x TR		15,96	1,929	1.09	0.347
S. pseudomilitaris	CU	SE x TR x WK	P3	15,192	2,405	3.59	0.001*
	BR	SE x TR x WK	P3	15,192	3,453	5.00	0.001*
	ZN	SE x TR x WK	P3	45,384	2,308	3.15	0.001*

Notes: P2, two-factor PERMANOVA; P3, three-factor PERMANOVA; * denotes significant effect, $\alpha = 0.05$.

For the number of individuals of *S. pseudomilitaris*, there were significant interactions of section, treatment and week (Table 6.3) between controls and copper gradients (Figures 6.7A and B), between controls and bronze gradients (Figures 6.7A and C) and between controls and zinc gradients (Figures 6.7A and D). Recruitment of *S. pseudomilitaris* on controls and gradients (copper, bronze and zinc) occurred from week 2 and week 4, respectively, and over time, fouling on gradients increased while fouling on controls remained equal. In addition, there were equal numbers of *S. pseudomilitaris* on all sections of controls while numbers on copper and bronze gradients decreased along the length of the tubes, where recruitment was prevented

more effectively, for longer, as loading densities of metal particles increased. *S. pseudomilitaris* recruited to all sections of zinc gradients by week 8.

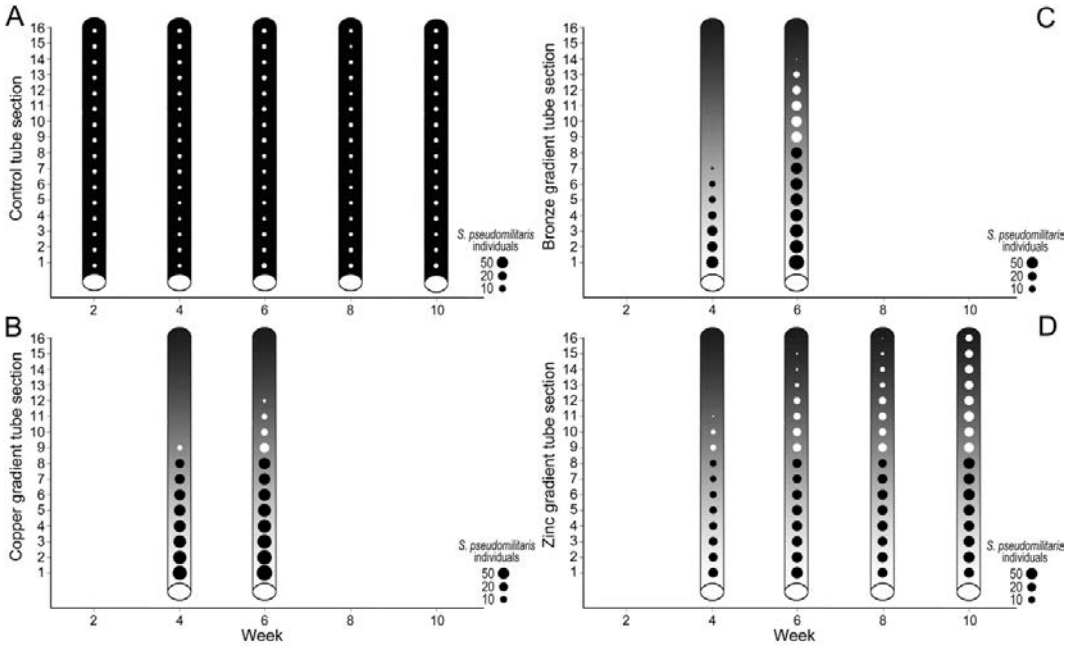

Figure 6.7. Recruitment of *S. pseudomilitaris* over time on HDPE tubes with and without embedment of metal particle gradients. Mean recruitment was quantified on sixteen sections of (**A**) control, (**B**) copper, (**C**) bronze and (**D**) zinc treatments at two-week intervals. Each circle (black and white) represents mean number of individuals of *S. pseudomilitaris* per section. Quantification of fouling on gradient tubes was only done on weeks corresponding to the removal of plugs for release rate analysis.

The natural fouling community comprised eleven species that recruited to controls. These were individuals of *A. reticulatus* (Figure 6.8A), *B. neritina* (Figure 6.8B), *B. stolonifera*, *B. nigromaculatum* (Figure 6.8C), *H. elegans* (Figure 6.8D), *S. pseudomilitaris* (Figure 6.8E) and *P. imbricata* (Figure 6.8F), as well as colonies of ascidians (Figure 6.8G), *H. irrikensis* (Figure 6.8H), *Watersipora* sp. (Figure 6.8I) and *Z. verticillatum* (Figure 6.8J). *B. stolonifera* was not presented graphically as only three individuals were recorded from weeks 2 to 8. In general, individual numbers and percent coverage of fouling species increased over time, except for *B. neritina*, which decreased over time and ascidians which began decreasing at week 12. The two most tolerant species as well as *A. reticulatus*, *B. neritina*, *H. elegans* and the ascidians were present throughout the initial 12 weeks of the field trial while *B. nigromaculatum*, *P. imbricata*

and *Z. verticillatum* were not present from weeks 2 to 6. Although there was potential for these three species to recruit to available portions of the gradient tube from weeks 8 to 12, they consistently occurred on already established organisms and never on the tube itself. Most importantly however, fouling on controls occurred across the length of the tubes, regardless of section compared to gradient tubes where, in general, less fouling was found on sections of the tube with higher loading densities of metal particles.

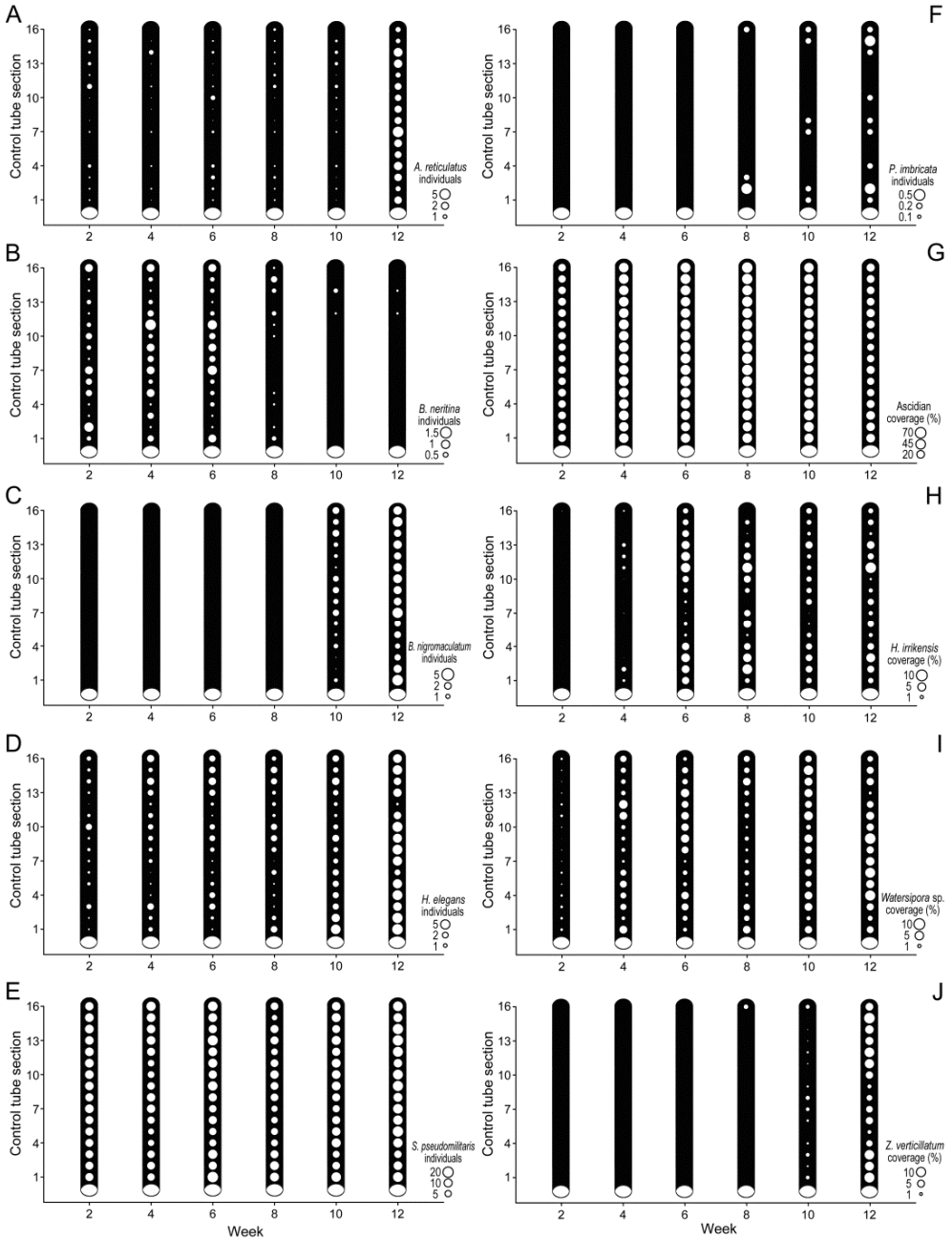

Figure 6.8. Recruitment of all fouling over time on HDPE control tubes, without embedment of metal particles. Mean recruitment was quantified on sixteen sections for each control tube at two-week intervals for 12 weeks. Fouling on controls included mean number of individuals of (**A**) the barnacle *A. reticulatus*; (**B**) the stalked bryozoan *B. neritina*; the polychaetes (**C**) *B. nigromaculatum*, (**D**) *H. elegans* and (**E**) *S. pseudomilitaris*; (**F**) the oyster *P. imbricata*; and mean percent coverage of (**G**) ascidians; the encrusting bryozoans (**H**) *H. irrikensis* and (**I**) *Watersipora* sp. and (**J**) the stalked bryozoan *Z. verticillatum*. White circles represent mean number of individuals or mean percent coverage of fouling per section.

6.4 Discussion

Loading density gradients of metal particles, produced using cold spray metal embedment, proved to be an effective method to establish the MERRs of metal ions needed to prevent fouling, even by the most tolerant species. These species, *Watersipora* sp. and *S. pseudomilitaris*, in order of highest tolerance, withstood the highest release rates of metal ions over the first 12 weeks of the field trial. After 12 weeks, fouling on copper and bronze gradient tubes, nominally split into 16 sections for analyses, occurred up to section 15. It was only at week 44 when the section with the highest loading density of metal particles (section 16) was no longer effective as an antifoulant and was again colonized by *Watersipora* sp.. Copper and bronze gradient tubes were equal in their effectiveness against each of the most tolerant species, with a similar MERR of copper ions and similar mean release rates of copper ions overall. In contrast, zinc was not efficient as an antifoulant with failure after the recruitment by *Watersipora* sp. and *S. pseudomilitaris* at week 2 and week 8, respectively. Importantly, fouling on control tubes, without embedded metal, occurred on all sections compared to gradients where fouling decreased as loading densities of metal particles increased at each time point. Nine additional fouling species were found only on control tubes, demonstrating that cold spray metal embedment proved an effective antifouling material for those species for at least 44 weeks.

Recruitment of the most tolerant species occurred on subsequent sections further along the length of the gradient tubes over time. Importantly, regardless of this progression, release rate measurements remained constant at each section, albeit sometimes wide ranging. That is, species were only able to recruit to sections with release rates below a constant minimum effective level. Therefore, the MERR obtained from the release rate data were an accurate representation of the tolerance of each species under field conditions. The first two species to recruit to gradient tubes are not endemic to Australia (Knight-Jones 1984; Dafforn et al. 2008) and notably, many non-endemic marine fouling species are less affected by modern antifouling technologies than their endemic counterparts who are deterred from recruitment, leaving open

space for tolerant species (Dafforn et al. 2008; Piola and Johnston 2008; Piola et al. 2009).

Watersipora sp., the most tolerant species, withstood the highest concentrations of metal ions compared to the second most tolerant species and the nine species found on controls. Subsequently, *Watersipora* sp. withstood the highest release rates (MERRs) of 0.058 g m^{-2} h^{-1} of copper ions for copper-embedded tubes and 0.054 g m^{-2} h^{-1} of copper ions for bronze-embedded tubes, which equates to concentrations of 41.5 and 38.5 μg L^{-1}, respectively, according to the ASTM D6442-06 standard (ASTM 2011). These MERRs are similar to previous findings where *Watersipora subtorquata* could withstand exposure to copper ion concentrations of 40 μg L^{-1} under laboratory conditions (McKenzie et al. 2011). Interestingly, McKenzie et al. (2011) also found that larvae were able to withstand concentrations of 80 μg L^{-1} and settle/metamorphose successfully, albeit significantly less so than the lower concentration of 40 μg L^{-1} or controls. Moreover, *W. subtorquata* larvae, that were able to settle and survive in the laboratory in concentrations of 50 and 100 μg L^{-1} of copper, had significantly reduced growth compared to those treated with no copper or low copper concentrations when transferred to the field (Piola and Johnston 200**6**a). Under natural conditions, it is likely that larvae would move to a surface without (or with less) copper ion diffusion if they had the opportunity to do so, even though under no-choice laboratory assays, higher release rates could be tolerated. Therefore, a release rate of 0.058 g m^{-2} h^{-1} of copper ions is suitable as a MERR for *Watersipora* sp. under field conditions where fouling organisms presumably have options. The MERR quantified here for *Watersipora* sp. was established from the first 15 sections on the gradient tubes while larvae were only able to recruit to the highest loading density of copper and bronze gradient tubes (section 16) after week 44. However, the release rates from the highest loading density at this time were lower than on previous sections. This may have been due to the absence of larvae of *Watersipora* sp. for the weeks leading up to recruitment at week 44 or, because the surfaces were only being checked every month, recruitment may have occurred up to four weeks earlier when release rates of copper ions would have been higher. In a previous study examining the antifouling longevity of copper

particles embedded into polyurethane, failure occurred after 30 weeks with the recruitment of *Watersipora subovoidea* (Vucko et al. 2013a; Chapter 5). The percent coverage of copper particles in that study was 64.7 ± 1.8%, similar to section 15 here (65.6 ± 1.7%), which failed after 12 weeks. The difference in longevity was most likely due to unique polymer properties such as elastic modulus and hardness, which affect particle embedment depth and therefore the release of copper ions (Vucko et al. 2012; Chapter 4). The MERR of zinc ions for *Watersipora* sp. could not be established as recruitment occurred on all zinc gradient sections by week 2 and consequently, the highest loading density of zinc metal particles, and therefore the highest zinc ion release rate had little, if any, effect on the settlement of larvae. This was also true for *S. pseudomilitaris*, which recruited to all sections of zinc gradient tubes regardless of loading density by week 8. Rapid colonization of the two species left little room on the zinc gradient tubes to establish the MERR for any other species. Although zinc on its own has been considered as an antifouling agent (WHOI 1952b), and is toxic towards marine invertebrates by inhibiting Ca uptake, decreasing oxygen consumption and impairing both carbohydrate metabolism and protein use (Devi 1995; Muyssen et al. 2006), it was not effective here. *S. pseudomilitaris*, the second most tolerant species, demonstrated its ability to withstand higher concentrations of metal ions compared to all other species on controls. There is little known about the tolerance to metal toxicity of *S. pseudomilitaris*, and to the authors knowledge, this is the first study examining MERRs needed to prevent this species.

In general, coverage and individual numbers of the two most tolerant species were greater on copper, bronze and zinc gradient tubes than on controls. This may have been due to the presence of other species on control tubes or the difference in roughness between gradients and control surfaces. While controls had eleven species competing for space, gradients prevented recruitment of most of the available species within the fouling community leaving more space for those with the highest tolerance. Alternatively, during the cold spray process the metal particles embed into, and cause deformations of the HDPE polymer, which partially flows around the particles to hold them in place (King et al. 2013), thereby creating a surface which would be rougher

than an unsprayed control. In addition, when exposed to field conditions, metal ions are released from the particles over time and become porous, sometimes leaving a gap or hole (Vucko et al. 2012; Chapter 4). If these holes are large enough, there may be further increases in roughness and therefore surface area of the gradient tubes leading to an increase in attachment points. There is a positive correlative effect between higher numbers of attachment points and settlement/attachment success of fouling organisms (Scardino et al. 2008; Vucko et al. 2014; Chapter 2) which, in this study, may have led to higher amounts of fouling on gradients. Most importantly however, regardless of the differences in fouling numbers between controls and gradients, controls exhibited equal fouling along the length of the tube whereas gradients exhibited decreased fouling as loading densities of metal particles increased.

Copper and its alloys prevent fouling due to the toxicity of metal ions towards marine invertebrate fouling larvae (Mance 1987; Fitridge et al. 2012), and the rate of copper ion release from a surface needed to prevent overall fouling is ~0.02 g m^{-2} h^{-1} (Núñez et al. 2005). However, the MERR for *Watersipora* sp. and *S. pseudomilitaris* found here were 1.5 to 3 times higher. This is likely due to marine invertebrate species having varied tolerances to metal toxicity where some species are less sensitive than others (Bellas et al. 2001; Brown et al. 2004; Rivera-Duarte et al. 2005; Brooks and Waldock 2009; Pineda et al. 2012). Tolerance to metal toxicity can also differ within species and even within individuals of the same population depending on the tolerance coping mechanism being employed (McKenzie et al. 2011). Copper and its alloys are effective against a variety of marine fouling invertebrates including barnacles (Johnston and Keough 2000), bryozoans (Piola and Johnston 2006a; Piola and Johnston 2006b), mussels (Dormon et al. 1996) and ascidians (Bellas et al. 2001; Agell et al. 2004; Pineda et al. 2012) while copper-tolerant species include polychaetes (Johnston and Keough 2000; Bao et al. 2010) and bryozoans (Piola and Johnston 2006a). In general, these findings are comparative to the ones in this Chapter, where similar intolerant and tolerant organisms were present on either controls or gradient tubes, respectively. Importantly, the use of controls confirmed the presence of a larval supply for each species and subsequently, facilitated the identification of species which were most

strongly deterred. By establishing which species are easily deterred as well as the concentrations of metal ions needed to prevent all fouling, the negative impacts of biofouling can be avoided or mitigated by using materials that consistently release ions at a rate above the MERR for the most tolerant species.

There was no difference between copper and bronze gradient tubes with respect to their mean release rate of copper ions and their effectiveness against the recruitment of fouling, where the longevity of section 16 of both treatments was approximately 10 months (44 weeks) prior to failure. Since both treatments had similar initial copper ion release rates at section 16 and they both failed at the same time, this suggests that they had similar rates of release of copper ions during that 44 week period, even though bronze was expected to release copper ions at a lower rate due to the formation of an insoluble tin oxide layer (Drach et al. 2013). The similarities between copper and bronze gradient tubes allow them to be used interchangeably, and as an alternative to current polymer-based technologies (Braithwaite and McEvoy 2005; Braithwaite et al. 2007; Guenther et al. 2010). Importantly, the presence of tin in bronze materials should not obstruct their use in the natural environment since the bioavailability of inorganic tin compounds is low (Rüdel 2003).

In conclusion, metal particle gradients were effective in establishing the MERRs of metals and showed how the recruitment of fouling species depended on metal ion release rates and which species were most tolerant to the release of metal ions from polymer surfaces. These outcomes support further development of cold spray antifouling materials that can remain above the MERR, based on the most tolerant species, to prevent all fouling for longer periods, either by layering metal particles, using larger metal particles to slow the initial release of metal ions, or embedding more particles, more deeply into the polymers in an effort to regulate ion release rates.

Chapter 7

General discussion

This thesis successfully establishes the effectiveness of several innovative antifouling technologies as potential alternatives to copper-based biocide paints across niche and broad spectrum applications. Textured polydimethylsiloxane (PDMS) with and without photocatalytic TiO_2, and the use of cold spray technology as a method to give antifouling properties to thermoplastic polymers (polymers), have been thoroughly investigated. The outcomes of this research are synthesized below and discussed in the broader context of the development of innovative antifouling technologies.

7.1 Chapter 2. Using textured PDMS to prevent settlement and enhance foul-release of marine fouling organisms

The antifouling and foul-release properties were quantified for a range of 18 textured (0.2–1,000 μm) and non-textured (0 μm) surfaces, produced using a known foul-release material, PDMS (Townsin and Anderson 2009). In short-term laboratory assays the diatoms *Nitzschia closterium* and *Amphora* sp. were deterred by all surface topographies regardless of texture type. In contrast, the settlement of propagules of *Ulva* sp. was lower on texture sizes less than the propagule size, and the settlement of larvae of *Saccostrea glomerata* and *Bugula neritina* was lower on texture sizes closest to, but less than, the sizes of larvae, supporting attachment point theory. However, after exposing the textured surfaces to field conditions and a natural fouling community for six months, all textured surfaces lost their deterrent effect with similar, high coverage of fouling. More importantly, after losing deterrence, the textured surfaces were

sprayed with a pressure washer to simulate hydrodynamic flow, and the foul-release properties of some textures (300, 400, 600 and 800 μm) were more effective than others (2 and 4 μm). There was a positive correlation between initial attachment and fouling remaining, where fouling organisms recruited in higher numbers to surfaces upon which they attached most strongly. Textured surfaces for use in antifouling have been examined thoroughly in the past but generally in the context of laboratory assays alone (Schumacher et al. 2007b; Scardino et al. 2008; Aldred et al. 2010; Cooper et al. 2011; Carl et al. 2012a). While those studies provide the basis of understanding for how texture facilitates the settlement, attachment and metamorphosis of fouling organisms, there is a paucity of comparisons between laboratory assays and field trials (Thomason et al. 2002; Bers and Wahl 2004). When exposed to a natural fouling community, the deterrent effect of texture can be diminished with conditioning and exposure to a natural fouling community consisting of a multitude of differently-sized organisms (Molino and Wetherbee 2008; Molino et al. 2009a; Molino et al. 2009b; Bers et al. 2010; Zargiel et al. 2011; Martinelli et al. 2012). In addition, although the release of fouling from surfaces has been well documented, it has been done using newly-settled fouling larvae and not conditioned surfaces with older fouling communities (Aldred et al. 2010; Carl et al. 2012a). Here, in addition to providing a link between laboratory assays and field trials, this research highlights the importance of carrying out one method in conjunction with the other, and establishes that the release of fouling organisms from specific textures may be more effective than others, even after long conditioning periods. These results are notable and reinforce two applied outcomes. The first is that specific textures can be used effectively to enhance the settlement of larvae of a particular dimension and therefore may have applications in controlling settlement in aquaculture, where the timing and density of settlement are key factors to the success of the industry (Hickman 1992; Köhler et al. 1999; Gribben et al. 2011; Carl et al. 2012a). The second is that texture alone is inadequate for the purposes of antifouling against a natural fouling community and the addition of an alternative broad spectrum technology, such as a photocatalyst may prevent fouling (Carl et al. 2012b), while maintaining the benefit of a foul release surface.

7.2 Chapter 3. Combining a photocatalyst with microtopography to develop effective antifouling materials

To test the use of photocatalysts in the prevention of fouling, PDMS surfaces, textured with a square-wave linear grating profile (0, 20, 200, 300 and 600 μm), were embedded with a range of photocatalytic TiO_2 nanoparticle loadings (3.75, 7.5, 11.25 and 15 wt%). The resulting surfaces were used to test the combined efficacy of these technologies as antifouling materials in the laboratory and in the field against the common fouling bryozoan, *B. neritina*. In laboratory assays, although the lowest settlement rates were observed on 20 μm surfaces, the effects of texture were not as critical to larval settlement as the presence of TiO_2. TiO_2, activated by UV light, was highly effective against larvae of *B. neritina* demonstrating complete inhibition of larval growth and maturation, with no detrimental effect on larvae exposed to non-activated TiO_2. Similarly, there was a strong deterrent effect of TiO_2 on the recruitment of *B. neritina* and *Hydroides elegans* after 28 days in the field where TiO_2 was activated by natural sunlight. These results show that although all loadings (3.75, 7.5, 11.25 and 15 wt.%) of embedded TiO_2 were equally effective, 3.75 wt% TiO_2 is sufficient for use as a minimum inhibitory concentration to deter larval settlement, and the addition of a 20 μm texture further increases this deterrent effect. Photocatalysts are lethal to invertebrate larvae, bacteria, fungi, viruses, prions, protozoans, spores, oocysts and cancer cells (Watts et al. 1995; Lonnen et al. 2005; Xu et al. 2007; Paspaltsis et al. 2009; Zhao et al. 2009; Carl et al. 2012b) and have the clear potential to decrease the adhesion strength of fouling larvae and prevent larval settlement and adult recruitment in the photic zone (Carl et al. 2012b) while not being persistent in the environment (Bhatkhande et al. 2002). However, they are currently not used in marine antifouling applications but are used extensively in antifouling membranes (Choi et al. 2007; Madaeni and Ghaemi 2007), heat exchange surfaces (Gopal et al. 2007), self-sterilising and self-cleaning surfaces (Fujishima and Zhang 2006; Fujishima et al. 2008) as well as air and water remediation (Bhatkhande et al. 2002; Gogate and Pandit 2004; Choi et al. 2007; Demeestere et al. 2007). This research represents only the second study to examine TiO_2 in an antifouling capacity (Carl et al. 2012b) and the first to do so against

the recruitment of fouling from a natural fouling community in the field. It demonstrates a clear potential for this technology to be used against a broad range of fouling organisms and as a way to enhance the antifouling properties of microtexture alone. Despite this potential, a disadvantage of photocatalysts is that they only deter fouling when activated by light of sufficient energy (Wang et al. 2007; Gaya and Abdullah 2008), and in a natural environment they are ineffective at night. In addition, activating the photocatalysts during the day will rely heavily on UV attenuation in the water column, which is limited in inland and coastal waters due to chromophoric dissolved organic matter and particulate matter (Conde et al. 2000; De Lange 2000; Hader and Sinha 2005) further reducing the photocatalytic effect. Photocatalysts provide effective antifouling in limited circumstances and were clearly effective in this study however, there is an overriding need to deliver a broad-spectrum technology that is effective across the widest diversity of marine locations and fouling communities. Currently, for most applications this can be accomplished by using metal-based biocide paint technologies however, these paints are difficult to apply to polymers. In addition, pure metals, which have the potential to prevent fouling on their own, are also difficult to incorporate into polymers using conventional methods. Therefore, a significant innovation is required to deliver a broad-spectrum antifouling solution for polymers.

7.3 Chapter 4. Cold spray metal embedment: an innovative antifouling technology

To test the antifouling efficacy of pure metal incorporated into polymers, an innovative method was required, employing the use of cold spray technology where small metal particles can be sprayed into a surface at high velocity. Two polymers, high-density polyethylene (HDPE) and nylon were metallised with copper powder using cold spray to test the practicality of this as an antifouling technology and to test whether one polymer was better suited to the process. The copper-embedded polymers were deployed in the field and after 250 days, copper-embedded HDPE and

copper plate controls were completely free of hard foulers compared to copper-embedded nylon and polymer controls which were heavily fouled with both soft and hard fouling. The success of copper-embedded polymers was related to the interaction between the properties of the polymers (elastic modulus and hardness) and the cold spray process which affect particle embedment depth, and subsequently, the release of copper ions as determined by analytical techniques. Presently, applications of cold spray are very broad but only include the improvement of electrical and heat conductivity, the formation of wear- and corrosion-resistant coatings (Gärtner et al. 2006), freeform shape production without the use of moulds and structure reinforcement (Pattison et al. 2007). This is the first time that cold spray technology has been used in the prevention of fouling and demonstrates that embedding metal particles using cold spray equipment is an effective antifouling technology for polymers, in particular, those which are difficult to treat with standard copper-based biocide paints. Therefore, in a direct application of this technology, the next chapter explores how cold spray can be used to deliver antifouling properties to polyurethane seismic streamer skins, widely used in the geophysical exploration industry where fouling causes significant negative impacts.

7.4 Chapter 5. Polyurethane seismic streamer skins: an application of cold spray metal embedment

To directly apply cold spray technology, polyurethane seismic streamer skins were embedded with different loading densities of copper particles to determine antifouling longevity under field conditions. Polyurethane embedded with a high-density of copper particles (101.1 ± 10.8 g m^{-2}) deterred all hard fouling for 210 days under intense fouling pressure in the field, and for significantly longer than polyurethane embedded with a low-density of copper particles (22.1 ± 4.8 g m^{-2}) and polyurethane controls. The density of metal particles is a critical parameter in determining the longevity of polymers embedded with copper particles using cold spray technology. This chapter represents the first application of cold spray technology and establishes

that cold spray metal embedment is an effective antifouling technology for polyurethane seismic streamer skins, under intense fouling conditions. The geophysical exploration industry uses seismic streamers to protect sensitive electronic equipment which measure seismic feedback data while being towed at moderate speeds (4–5.5 knots) at specific depths (5–7 m). Fouling on these streamers reduces their capacity to float, while increasing seismic feedback noise, hydrodynamic drag and therefore fuel consumption, as well as time lost as a result of cleaning regimes (Harper 1995; Vignaux 2010; Harrick and Stenzel 2011). Although this is a clearly identified problem with a demonstrated cost in a significant marine industry, there are no functional antifouling coatings which exist for streamer skins due to the technical constraints associated with application and the mechanical handling of the streamers during operation (Vignaux 2010). Proposed solutions are automatic cleaning devices (Hoogeveen 2006; Hoogeveen et al. 2008; Lepage and Dollon 2010) and fouling-release materials (Lobe et al. 2010; Hartshorne et al. 2011) however, neither approach provides effective fouling control. Chapters 4 and 5 have established that cold spray technology is effective at adding antifouling properties to thermoplastic polymers using copper and while these results are promising, they raise a number of important questions. The first of these is what other metals prevent fouling since other metals, apart from copper, may have the toxic properties necessary to facilitate effective prevention of fouling. The second is which species are most tolerant to these metals, as each species will be able to withstand different release rates of metal ions from a surface (Bellas et al. 2001; Piola and Johnston 2006a; Piola and Johnston 2006b; Bao et al. 2010; McKenzie et al. 2011). Consequently, the third is what are the minimum effective release rates (MERRs) that are needed to prevent the most tolerant species?

7.5 Chapter 6. Assessing the antifouling properties of cold spray metal embedment using particle concentration gradients

To establish the MERRs of metal ions needed to prevent the most tolerant fouling species within a natural fouling community, loading density gradients of metal

particles were used. Gradients of copper, bronze and zinc particles were embedded into HDPE tubes using cold spray technology, with gradients ranging from low to high densities. *Watersipora* sp. and *Simplaria pseudomilitaris* were the first and second most tolerant species within the system. Notably, copper and bronze gradient tubes were equal in their MERRs of copper ions and consequently equally effective against *Watersipora* sp. (0.058 g m^{-2} h^{-1} and 0.054 g m^{-2} h^{-1}, respectively) and *S. pseudomilitaris* (0.030 g m^{-2} h^{-1} and 0.025 g m^{-2} h^{-1}, respectively). In contrast, zinc was not an effective antifoulant with complete failure after the recruitment by *Watersipora* sp. and *S. pseudomilitaris* at week 2 and week 8, respectively. Nine additional fouling species were found only on control tubes, demonstrating that cold spray metal embedment proved an effective antifouling material for those species throughout the trial. Many studies test the tolerance of fouling organisms in no-choice laboratory assays using specific concentrations of metal ions (Bellas et al. 2001; Piola and Johnston 2006a; Piola and Johnston 2006b; Bao et al. 2010; McKenzie et al. 2011). While these studies provide a basis to determine metal ion tolerance and are a good indicator of the absolute tolerance of a species, they do not provide a perspective of what occurs in the field where organisms have many options for settlement. For example, although a species may be able to survive in water with an extremely high concentration of metal ions in the laboratory, in the field that same species may be deterred by a lower level as it can simply move away from the antifouling surface releasing the metal ions, with no requirement to tolerate the absolute maximum quantity of an active toxic component. This final Chapter demonstrates that using a loading density gradient of metal particles within the same surface provides a method to establish precise field-based minimum effective release rates of the most tolerant fouling organism in a given system.

7.6 Future considerations

This thesis has identified a number of avenues for research to develop or improve innovative antifouling technologies involving microtexture and metal. For example,

textured PDMS (Chapter 2) used alone is not an effective method to deter the recruitment of fouling organisms under natural conditions for longer periods. However, textured PDMS used in conjunction with the TiO_2 photocatalyst (Chapter 3) supports the development of more effective foul-release materials with broad spectrum antifouling properties. Specific textures can increase the foul-release capabilities of smooth PDMS while the photocatalyst has the potential to prevent larval settlement and adult recruitment in the photic zone, where fouling is greatest and most diverse. The major caveat with the use of a photocatalyst is that it will only be activated by light of sufficient energy (Wang et al. 2007; Gaya and Abdullah 2008) and in a natural environment this comes from ultraviolet radiation (UV), making these surfaces ineffective at night and in waters where UV attenuation is high. That being said, the two intensities of UV light tested in the laboratory in Chapter 3 were estimated from 11:00 am daily averages. As an alternative, future assays should be done using UV light intensities estimated from the daily averages at a specific depth in the water column where surfaces would actually be located and the UV light intensities would be lower.

This thesis made use of two thermoplastic polymers (HDPE and nylon) embedded with copper particles and examined two of their polymer properties (hardness and elastic modulus) to investigate the process of embedding metal particles into thermoplastic polymers using cold spray technology (Chapter 4). As knowledge of the cold spray process is expanded and developed as an antifouling technology, it will be important to establish baseline data for other polymers used in marine industry. Given that polymers have unique properties (Gnanou and Fontanille 2008), they will each need specific cold spray parameters to optimise effective retention of metal particles to enhance antifouling longevity. The findings surrounding the physical properties of the polymers, as shown by elastic modulus and hardness values were not exhaustive and other polymer properties (glass transition temperature, response rate to high strain and impact, moisture content, percentage crystallinity and melting point) should be investigated to determine which have the greatest effect on the capture and retention of metal particles and if there are any polymers that have the ability to capture other

materials such as TiO_2 nanoparticles. In addition, interactions between these properties and parameters that can be manipulated during the cold spray process (proximity of the cold spray nozzle, machine traverse speeds, carrier gas type and gas temperature) and metal particles used (powder size, powder type and powder flow rate) should also be examined (Pattison et al. 2007; Lupoi and O'Neill 2010; Lupoi and O'Neill 2011) to determine the most effective cold spray parameter settings and the best materials to use (polymers and powders) when producing a metal-embedded polymer for antifouling applications. Furthermore, because this technology directly disrupts the surface of a thermoplastic polymer by spraying a layer of metal particles into it, bulk polymer properties need to be compared before and after spraying to confirm that no polymer is lost during the spray process, which would result in an underestimation of the metal loading when weighing samples before and after spraying, and that properties such as flexibility are not sacrificed. This is particularly important for soft, flexible polyurethane seismic streamer skins used in geophysical exploration which are handled mechanically (Chapter 5). The streamer skins are used to protect sensitive electronic equipment which record seismic signals (Harrick and Stenzel 2011) and it will be important to establish whether the presence of a layer of metal particles interferes with the transmission of acoustic signals through the polyurethane. In Chapter 5, seismic streamers were exposed to conditions that caused heavy deposition of silt, however, under most applications these surfaces are only used under flow at a constant 4–5.5 knots (Elboth et al. 2010), thus *in situ* trials for these specific operational conditions are essential. In general, for any application of this technology within the marine industry (aquaculture, geophysical exploration, shipping), pilot-scale *in situ* trials will be critical to quantify the effects of operational and environmental conditions across geographic locations. This is especially important in the case of the seismic streamers where surfaces would be exposed to a diversity of conditions as vessels move through the ocean. Consequently, there would also be legislative issues to consider when applying this technology globally as well as the consideration of the cost of application which, until used at a larger scale, will be high.

Understanding the rates of release of metal ions that prevent the most tolerant species (Chapter 6) is critical to improving the use of this technology as an effective antifouling material. The next critical step in extending the antifouling longevity of cold spray metal-embedded polymers will be to quantify the release rates over time, an important aspect to improve, and ultimately increase, the longevity of antifouling surfaces. Since these materials are produced using pure metal, it is likely that they will exhibit high initial rates of release of metal ions followed by steep declines and then constant levels with the development of a patina (Núñez et al. 2005; Earley et al. 2014). Therefore, there should be a focus on establishing methods to increase the overall particle loading while slowing the initial release of metal ions to a rate immediately above the MERR of the most tolerant species, and maintain this level. This would reduce the waste of metal ions while effectively preventing all fouling in a system. Higher metal loadings could be achieved by improving the design of the cold spray nozzle to increase particle velocity, using smaller metal particles, manipulating cold spray conditions (increasing gas temperature, gas pressure, and powder feed rates and decreasing traverse speed). In addition, alternative receiving polymers could be used, which have properties favouring deeper embedment of metal particles, or which can withstand higher temperatures during the spray process thereby allowing increased layering in metal particles. Finally, the high initial release rates of metal ions could be controlled by coating the metal-embedded polymers with a semi-permeable layer to reduce the release of metal ions to a precise level. Ultimately, some combination of these techniques will be needed where a polymer has a higher metal loading and the release of those metal ions is lowered, generating the most effective antifouling surface.

References

Abbott A, Abel PD, Arnold DW, Milne A. 2000. Cost-benefit analysis of the use of TBT: the case for a treatment approach. Sci. Total Environ. 258:5–19.

Agell G, Turon X, De Caralt S, López-Legentil S, Uriz MJ. 2004. Molecular and organism biomarkers of copper pollution in the ascidian *Pseudodistoma crucigaster*. Mar. Pollut. Bull. 48:759–767.

Aldred N, Clare AS. 2008. The adhesive strategies of cyprids and development of barnacle-resistant marine coatings. Biofouling 24:351–363.

Aldred N, Ista LK, Callow ME, Callow JA, Lopez GP, Clare AS. 2006. Mussel (*Mytilus edulis*) byssus deposition in response to variations in surface wettability. J. R. Soc. Interface 3:37–43.

Aldred N, Scardino A, Cavaco A, de Nys R, Clare AS. 2010. Attachment strength is a key factor in the selection of surfaces by barnacle cyprids (*Balanus amphitrite*) during settlement. Biofouling 26:287–299.

Almeida E, Diamantino TC, de Sousa O. 2007. Marine paints: The particular case of antifouling paints. Prog. Org. Coatings 59:2–20.

Alzieu C. 1991. Environmental problems caused by TBT in France: assessment, regulations, prospects. Mar. Environ. Res. 32:7–17.

Amon C, Beuth J, Kirchner H, Merz R, Prinz F, Schmaltz K, Weiss L. 1993. Material issues in layered forming. In: Proceedings of the Solid Freeform Fabrication Symposium. Austin, Texas: Centre for Materials Science and Engineering, University of Austin, Texas. p. 1–10.

Anderson C, Atlar M, Callow M, Candries M, Milne A, Townsin RL. 2003. The development of foul-release coatings for seagoing vessels. J. Mar. Des. Oper. 2003:11–23.

Apolinario M, Coutinho R. 2009. Understanding the biofouling of offshore and deep-sea structures. In: Hellio C, Yebra D, editors. Advances in marine antifouling coatings and technologies. Cambridge, UK: Woodhead Publishing Ltd. p. 132–147.

Aprile C, Corma A, Garcia H. 2008. Enhancement of the photocatalytic activity of TiO_2 through spatial structuring and particle size control: from subnanometric to submillimetric length scale. Phys. Chem. Chem. Phys. 10:769–783.

ASTM. 2010. Standard test method for rubber property - durometer hardness, ASTM method D2240-05. 13 pp.

ASTM. 2011. Standard test method for determination of copper release rate from antifouling coatings in substitute ocean water, ASTM method D6442-05. 9 pp.

Babcock R, Davies P. 1991. Effects of sedimentation on settlement of *Acropora millepora*. Coral Reefs 9:205–208.

Bao W-Y, Lee O-O, Chung H-C, Li M, Qian P-Y. 2010. Copper affects biofilm inductiveness to larval settlement of the serpulid polychaete *Hydroides elegans* (Haswell). Biofouling 26:119–128.

Bauer RT. 1992. Testing generalizations about latitudinal variation in reproduction and recruitment patterns with sicyoniid and caridean shrimp species. Invertebr. Reprod. Dev. 3:193–202.

Bauer S, Arpa-Sancet MP, Finlay JA, Callow ME, Callow JA, Rosenhahn A. 2013. Adhesion of marine fouling organisms on hydrophilic and amphiphilic polysaccharides. Langmuir 29:4039–4047.

Bellas J, Vázquez E, Beiras R. 2001. Toxicity of Hg, Cu, Cd, and Cr on early developmental stages of *Ciona intestinalis* (Chordata, Ascidiacea) with potential application in marine water quality assessment. Water Res. 35:2905–2912.

Bennett SM, Finlay JA, Gunari N, Wells DD, Meyer AE, Walker GC, Callow ME, Callow JA, Bright F V, Detty MR. 2010. The role of surface energy and water wettability in aminoalkyl/fluorocarbon/hydrocarbon-modified xerogel surfaces in the control of marine biofouling. Biofouling 26:235–246.

Berntsson KM, Jonsson PR, Lejhall M, Gatenholm P. 2000. Analysis of behavioural rejection of micro-textured surfaces and implications for recruitment by the barnacle *Balanus improvisus*. J. Exp. Mar. Bio. Ecol. 251:59–83.

Bers AV, Díaz ER, da Gama BAP, Vieira-Silva F, Dobretsov S, Valdivia N, Thiel M, Scardino AJ, McQuaid CD, Sudgen HE, Thomason JC, Wahl M. 2010. Relevance of mytilid shell microtopographies for fouling defence - a global comparison. Biofouling 26:367–377.

Bers AV, Wahl M. 2004. The influence of natural surface microtopographies on fouling. Biofouling 20:43–51.

Bhatkhande DS, Pangarkar VG, Beenackers AACM. 2002. Photocatalytic degradation for environmental applications - a review. J. Chem. Technol. Biotechnol. 77:102–116.

Bloecher N, de Nys R, Poole AJ, Guenther J. 2013. The fouling hydroid *Ectopleura larynx*: a lack of effect of next generation antifouling technologies. Biofouling 29:237–246.

Brady RF, Aronson CL. 2003. Elastomeric fluorinated polyurethane coatings for nontoxic fouling control. Biofouling 19:59–62.

Brady, Jr RF, Singer IL. 2000. Mechanical factors favoring release from fouling release coatings. Biofouling 15:73–81.

Braithwaite RA, Carrascosa MCC, McEvoy LA. 2007. Biofouling of salmon cage netting and the efficacy of a typical copper-based antifoulant. Aquaculture 262:219–226.

Braithwaite RA, McEvoy LA. 2005. Marine biofouling on fish farms and its remediation. Adv. Mar. Biol. 47:215–252.

Briand J-F. 2009. Marine antifouling laboratory bioassays: an overview of their diversity. Biofouling 25:297–311.

Brooks S, Waldock M. 2009. The use of copper as a biocide in marine antifouling paints. In: Hellio C, Yebra D, editors. Advances in marine antifouling coatings and technologies. Cambridge, UK: Woodhead Publishing Ltd. p. 492–515.

Brooks SJ, Bolam T, Tolhurst L, Bassett J, La Roche J, Waldock M, Barry J, Thomas KV. 2008. Dissolved organic carbon reduces the toxicity of copper to germlings of the macroalgae, Fucus vesiculosus. Ecotoxicol. Environ. Saf. 70:88–98.

Brown RJ, Galloway TS, Lowe D, Browne MA, Dissanayake A, Jones MB, Depledge MH. 2004. Differential sensitivity of three marine invertebrates to copper assessed using multiple biomarkers. Aquat. Toxicol. 66:267–278.

Bryan GW, Gibbs PE, Burt GR, Hummerstone LG. 1987. The effects of tributyltin (TBT) accumulation on adult dog-whelks, *Nucella lapillus*: long-term field and laboratory experiments. J. Mar. Biol. Asoc. UK 67:525–544.

Callow JA, Callow ME. 2009. Advanced nanostructured surfaces for the control of marine biofouling: the AMBIO project. In: Hellio C, Yebra D, editors. Advances in marine antifouling coatings and technologies. Cambridge, UK: Woodhead Publishing Ltd. p. 647–663.

Callow JA, Callow ME. 2011. Trends in the development of environmentally friendly fouling-resistant marine coatings. Nat. Commun. 2:1–10.

Callow M. 1990. Ship fouling: problems and solutions. Chem. Ind. March:123–127.

Callow ME, Callow JA, Ista LK, Sarah E, Nolasco AC, López GP, Coleman SE. 2000. Use of self-assembled monolayers of different wettabilities To study surface selection and primary adhesion processes of green algal (*Enteromorpha*) zoospores. Appl. Environ. Microbiol. 66:3249–3254.

Callow ME, Jennings AR, Brennan AB, Seegert CE, Gibson A, Wilson L, Feinberg A, Baney R, Callow JA. 2002. Microtopographic cues for settlement of zoospores of the green fouling alga *Enteromorpha*. Biofouling 18:237–245.

Callow ME. 1986. Fouling algae from "in-service" ships. Bot. Mar. 29:351–357.

Canning-Clode J, Wahl M. 2010. Patterns of fouling on a global scale. In: Dürr S, Thomason JC, editors. Biofouling. Oxford, UK: Blackwell Publishing Ltd. p. 73–86.

Carl C, Poole AJ, Sexton BA, Glenn FL, Vucko MJ, Williams MR, Whalan S, de Nys R. 2012a. Enhancing the settlement and attachment strength of pediveligers of *Mytilus galloprovincialis* by changing surface wettability and microtopography. Biofouling 28:175–186.

Carl C, Poole AJ, Vucko MJ, Williams MR, Whalan S, de Nys R. 2011. Optimising settlement assays of pediveligers and plantigrades of *Mytilus galloprovincialis*. Biofouling 27:859-868.

Carl C, Poole AJ, Vucko MJ, Williams MR, Whalan S, de Nys R. 2012b. Enhancing the efficacy of fouling-release coatings against fouling by *Mytilus galloprovincialis* using nanofillers. Biofouling 28:1077–1091.

Carman ML, Estes TG, Feinberg AW, Schumacher JF, Wilkerson W, Wilson LH, Callow ME, Callow JA, Brennan AB. 2006. Engineered antifouling microtopographies - correlating wettability with cell attachment. Biofouling 22:11–21.

Chambers LD, Stokes KR, Walsh FC, Wood RJK. 2006. Modern approaches to marine antifouling coatings. Surf. Coat. Technol. 201:3642–3652.

Champ MA. 2000. A review of organotin regulatory strategies, pending actions, related costs and benefits. Sci. Total Environ. 258:21–71.

Champ MA. 2001. New IMO convention to control anti-fouling systems on ships. Sea Technol. 42:48–50.

Chaudhury MK, Finlay JA, Chung JY, Callow ME, Callow JA. 2005. The influence of elastic modulus and thickness on the release of the soft-fouling green alga *Ulva linza* (syn. *Enteromorpha linza*) from poly(dimethylsiloxane) (PDMS) model networks. Biofouling 21:41–48.

Chaw KC, Dickinson GH, Ang KY, Deng J, Birch WR. 2011. Surface exploration of *Amphibalanus amphitrite* cyprids on microtextured surfaces. Biofouling 27:413–422.

Cho Y, Sundaram HS, Weinman CJ, Paik MY, Dimitriou MD, Finlay JA, Callow ME, Callow JA, Kramer EJ, Ober CK. 2011. Triblock copolymers with grafted Fluorine-Free, Amphiphilic, Non-Ionic Side Chains for Antifouling and Fouling-Release Applications. Macromolecules 44:4783–4792.

Choi H, Stathatos E, Dionysiou DD. 2007. Photocatalytic TiO_2 films and membranes for the development of efficient wastewater treatment and reuse systems. Desalination 202:199–206.

Clare AS, Aldred N. 2009. Surface colonisation by marine organisms and its impact on antifouling research. In: Hellio C, Yebra D, editors. Advances in marine antifouling coatings and technologies. Cambridge, UK: Woodhead Publishing Ltd. p. 46–79.

Clarke KR, Gorley RN. 2006. PRIMER v6: user manual/tutorial. Plymouth: PRIMER-E pp. 190.

Conde D, Aubriot L, Sommaruga R. 2000. Changes in UV penetration associated with marine intrusions and freshwater discharge in a shallow coastal lagoon of the Southern Atlantic Ocean. Mar. Ecol. Prog. Ser. 207:19–31.

Cooper SP, Finlay JA, Cone G, Callow ME, Callow JA, Brennan AB. 2011. Engineered antifouling microtopographies: kinetic analysis of the attachment of zoospores of the green alga *Ulva* to silicone elastomers. Biofouling 27:881–892.

Cowie PR. 2010. Biofouling patterns with depth. In: Dürr S, Thomason JC, editors. Biofouling. Oxford, UK: Blackwell Publishing Ltd. p. 87–99.

Dafforn KA, Glasby TM, Johnston EL. 2008. Differential effects of tributyltin and copper antifoulants on recruitment of non-indigenous species. Biofouling 24:23–33.

Dahlström M, Jonsson H, Jonsson PR, Elwing H. 2004. Surface wettability as a determinant in the settlement of the barnacle *Balanus improvisus* (DARWIN). J. Exp. Mar. Bio. Ecol. 305:223–232.

De Lange HJ. 2000. The attenuation of ultraviolet and visible radiation in Dutch inland waters. Aquat. Ecol. 34:215–226.

de Nys R, Guenther J. 2009. The impact and control of biofouling in marine finfish aquaculture. In: Hellio C, Yebra D, editors. Advances in marine antifouling coatings and technologies. Cambridge, UK: Woodhead Publishing Ltd. p. 177–221.

Demeestere K, Dewulf J, Van Langenhove H. 2007. Heterogeneous photocatalysis as an advanced oxidation process for the abatement of chlorinated, monocyclic aromatic and sulfurous volatile organic compunds in air: state of the art. Crit. Rev. Environ. Sci. Technol. 37:489–538.

Devi VU. 1995. Bio-accumulation and metabolic effects of zinc on marine fouling dreissinid bivalve, *Mytilopsis sallei* (Recluz). Water. Air. Soil Pollut. 81:295–304.

Di Fino A, Petrone L, Aldred N, Ederth T, Liedberg B, Clare AS. 2014. Correlation between surface chemistry and settlement behaviour in barnacle cyprids (*Balanus improvisus*). Biofouling 30:143-152.

Dormon JM, Cottrell CM, Allen DG, Ackerman JD, Spelt JK. 1996. Copper and copper-nickel alloys as zebra mussel antifoulants. J. Environ. Eng. 122:276–283.

dos Santos AB, Cervantes FJ, van Lier JB. 2007. Review paper on current technologies for decolourisation of textile wastewaters: perspectives for anaerobic biotechnology. Bioresour. Technol. 98:2369–2385.

Drach A, Tsukrov I, DeCew J, Aufrecht J, Grohbauer A, Hofmann U. 2013. Field studies of corrosion behaviour of copper alloys in natural seawater. Corros. Sci. 76:453–464.

Dubey SK, Roy U. 2003. Review: biodegradation of tributyltins (organotins) by marine bacteria. Appl. Organomet. Chem. 17:3–8.

Earley PJ, Swope BL, Barbeau K, Bundy R, McDonald JA, Rivera-Duarte I. 2014. Life cycle contributions of copper from vessel painting and maintenance activities. Biofouling 30:51–68.

Edyvean R. 2010. Consequences of fouling on shipping. In: Dürr S, Thomason JC, editors. Biofouling. Singapore: Wiley-Blackwell. p. 217–225.

Elboth T, Lilja D, Reif BAP, Andreassen Ø. 2010. Investigation of flow and flow noise around a seismic streamer cable. Geophysics 75:1–9.

Elbourne PD, Veater RA, Clare AS. 2008. Interaction of conspecific cues in *Balanus amphitrite* Darwin (Cirripedia) settlement assays: continued argument for the single-larva assay. Biofouling 24:87–96.

Enríquez S, Rodríguez-Román A. 2006. Effect of water flow on the photosynthesis of three marine macrophytes from a fringing-reef lagoon. Mar. Ecol. Prog. Ser. 323:119–132.

Evans S, Birchenough A, Brancato M. 2000. The TBT ban: out of the frying pan into the fire? Mar. Pollut. Bull. 40:204–211.

Farro NW, Veleva L, Aguilar P. 2009. Copper marine corrosion: I. corrosion rates in atmospheric and seawater environments of Peruvian port. Open Corros. J. 2:130–138.

Finlay JA, Bennett SM, Brewer LH, Sokolova A, Clay G, Gunari N, Meyer AE, Walker GC, Wendt DE, Callow ME, Callow JA, Detty MR. 2010. Barnacle settlement and the adhesion of protein and diatom microfouling to xerogel films with varying surface energy and water wettability. Biofouling 26:657–666.

Finlay JA, Callow ME, Ista LK, Lopez GP, Callow JA. 2002. The influence of surface wettability on the adhesion strength of settled spores of the green alga *Enteromorpha* and the diatom *Amphora*. Integr. Comp. Biol. 42:1116–1122.

Finnie AA, Williams DN. 2010. Paint and coatings technology for the control of marine fouling. In: Dürr S, Thomason JC, editors. Biofouling. Oxford, UK: Wiley-Blackwell. p. 185–201.

Finnie AA. 2006. Improved estimates of environmental copper release rates from antifouling products. Biofouling 22:279–291.

Fitridge I, Dempster T, Guenther J, de Nys R. 2012. The impact and control of biofouling in marine aquaculture: a review. Biofouling 28:649–669.

Fredriksson D, Decew J, Tsukrov I. 2007. Development of structural modeling techniques for evaluating HDPE plastic net pens used in marine aquaculture. Ocean Eng. 34:2124–2137.

Fujishima A, Zhang X, Tryk DA. 2008. TiO_2 photocatalysis and related surface phenomena. Surf. Sci. Rep. 63:515–582.

Fujishima A, Zhang X. 2006. Titanium dioxide photocatalysis: present situation and future approaches. Comptes Rendus Chim. 9:750–760.

Gärtner F, Stoltenhoff T, Schmidt T, Kreye H. 2006. The cold spray process and its potential for industrial applications. J. Therm. Spray Technol. 15:223–232.

Gaya UI, Abdullah AH. 2008. Heterogeneous photocatalytic degradation of organic contaminants over titanium dioxide: a review of fundamentals, progress and problems. J. Photochem. Photobiol. C Photochem. Rev. 9:1–12.

Gervis MH, Sims NA. 1992. The biology and culture of pearl oysters (Bivalvia: Pteriidae). ICLARM Stud Rev 21:1–49.

Giacomazzi S, Cochet N. 2004. Environmental impact of diuron transformation: a review. Chemosphere 56:1021–1032.

Gilmour J. 1999. Experimental investigation into the effects of suspended sediment on fertilisation , larval survival and settlement in a scleractinian coral. Mar. Biol. 135:451–462.

Gleason DF, Edmunds PJ, Gates RD. 2006. Ultraviolet radiation effects on the behavior and recruitment of larvae from the reef coral *Porites astreoides*. Mar. Biol. 148:503–512.

Gnanou Y, Fontanille M. 2008. Organic and physical chemistry of polymers. New Jersey, USA: Wiley-Interscience pp. 629.

Gogate PR, Pandit AB. 2004. Sonophotocatalytic reactors for wastewater treatment: a critical review. Am. Inst. Chem. Eng. J. 50:1051–1079.

Goode JW, Penner WA, Ray CD, Nelson RG. Mobil Oil Corporation, assignee. 1982 Apr 6. Seismic exploration system. United States Patent 4,323,990 pp. 15.

Gopal J, George RP, Muraleedharan P, Kalavathi S, Banerjee S, Dayal RK, Khatak HS. 2007. Photocatalytic inhibition of microbial fouling by anodized Ti6Al4V alloy. J. Mater. Sci. 42:5152–5158.

Gribben PE, Jeffs AG, de Nys R, Steinberg PD. 2011. Relative importance of natural cues and substrate morphology for settlement of the New Zealand Greenshell™ mussel, *Perna canaliculus*. Aquaculture 319:240–246.

Grosell M, Blanchard J, Brix K V, Gerdes R. 2007. Physiology is pivotal for interactions between salinity and acute copper toxicity to fish and invertebrates. Aquat. Toxicol. 84:162–172.

Guenther J, Misimi E, Sunde ML. 2010. The development of biofouling, particularly the hydroid *Ectopleura larynx*, on commercial salmon cage nets in Mid-Norway. Aquaculture 300:120–127.

Hader D-P, Sinha RP. 2005. Solar ultraviolet radiation-induced DNA damage in aquatic organisms: potential environmental impact. Mutat. Res. 571:221–233.

Harper, Jr. DE. 1995. Fouling of towed seismic streamers off central Africa by the Lepadomorph barnacle *Conchoderma virgatum*. Crustaceana 68:779–781.

Harrick BW, Stenzel A. PGS Geophysical AS, assignee. 2011 Jul 27. System and method for using copper coating to prevent marine growth on towed geophysical equipment. European Patent EP 2,348,078.

Hartshorne RS, Tustin GJ, Hannah J. Geco Technology BV, Schlumberger Canada Ltd, Schlumberger Seaco Inc, assignees. 2011 Jun 16. Systems and methods for marine anti-fouling. International Patent WO 2011/070411. 29 pp.

Henderson P. 2010. Fouling and antifouling in other industries - power stations, desalination plants - drinking water supplies and sensors. In: Dürr S, Thomason JC, editors. Biofouling. Singapore: Wiley-Blackwell. p. 288–305.

Hickman RW. 1992. Mussel cultivation. In: Gosling E, editor. The mussel *Mytilus*: ecology, physiology, genetics and culture. Amsterdam: Elvesier. p. 465–511.

Hoogeveen J, Hoeg A, Overskeid O, Overeng S, Nowakowski W, Karlsen K. PGS Geophysical AS, assignee. 2008 Jun 5. Self propelled cleaning device for marine seismic streamers. United States Patent 7,145,833. 12 pp.

Hoogeveen J. PGS Geophysical AS, assignee. 2006 Dec 6. Cleaning device for marine seismic streamer. United States Patent 7,145,833. 8 pp.

Howell D, Behrends B. 2010. Consequences of antifouling coatings - the chemist's perspective. In: Dürr S, Thomason JC, editors. Biofouling. Singapore: Wiley-Blackwell. p. 226–242.

Huang S, Hadfield MG. 2003. Composition and density of bacterial biofilms determine larval settlement of the polychaete *Hydroides elegans*. Mar. Ecol. Prog. Ser. 260:161–172.

Huggett MJ, Nedved BT, Hadfield MG. 2009. Effects of initial surface wettability on biofilm formation and subsequent settlement of *Hydroides elegans*. Biofouling 25:387–399.

Iketani K, Sun R-D, Toki M, Hirota K, Yamaguchi O. 2003. Sol – gel-derived TiO_2/poly(dimethylsiloxane) hybrid films and their photocatalytic activities. J. Phys. Chem. Solids 64:507–513.

Jenkins SR, Martins GM. 2010. Succession on hard substrata. In: Dürr S, Thomason JC, editors. Biofouling. Oxford, UK: Blackwell Publishing Ltd. p. 60–72.

Jerlov NG. 1950. Ultra-violet radiation in the sea. Nature 166:111–112.

Johnston EL, Keough MJ. 2000. Field assessment of effects of timing and frequency of copper pulses on settlement of sessile marine invertebrates. Mar. Biol. 137:1017–1029.

Joshi RG, Goel A, Mannari VM, Finlay JA, Callow ME, Callow JA. 2009. Evaluating fouling-resistance and fouling-release performance of smart polyurethane surfaces: an outlook for efficient and environmentally benign marine coatings. J. Appl. Polym. Sci. 114:3693–3703.

Kavanagh CJ, Quinn RD, Swain GW. 2005. Observations of barnacle detachment from silicones using high-speed video. J. Adhes. 81:843–868.

Kiil S, Weinell CE, Pedersen MS, Dam-Johansen K. 2001. Analysis of self-polishing antifouling paints using rotary experiments and mathematical modeling. Ind. Eng. Chem. Res. 40:3906–3920.

King PC, Poole AJ, Horne S, de Nys R, Gulizia S, Jahedi MZ. 2013. Embedment of copper particles into polymers by cold spray. Surf. Coatings Technol. 216:60–67.

Knight-Jones P. 1984. A new species of *Protoleodora* (Spirorbidae: Polychaeta) from Eastern U.S.S.R., with a brief revision of related genera. Zool. J. Linn. Soc. 80:109–120.

Köhler J, Hansen P, Wahl M. 1999. Colonization patterns at the substratum-water interface: how does surface microtopography influence recruitment patterns of sessile organisms? Biofouling 14:237–248.

Lepage Y, Dollon L. CGGveritas SA, assignee. 2010 Jul 13. Method and apparatus for cleaning a mobile immersed structure. United States patent US 7,754.018.

Liu D, Pacepavicius G, Maguire R, Lau Y, Okamura H, Aoyama I. 1999. Survey for the occurrence of the new antifouling compound Irgarol 1051 in the aquatic environment. Water Res. 33:2833–2843.

Lobe HJ, Tolman TK, Das AK, Knapp JR, Moffat G. Severn Marine Technologies LLC, Mid-Mountain Materials Inc., assignees. 2010 Nov 16. Anti-biofouling seismic streamer casing and method of manufacture. United States Patent 7,835,222. 11 pp.

Long CJ, Finlay JA, Callow ME, Callow JA, Brennan AB. 2010. Engineered antifouling microtopographies: mapping preferential and inhibitory microenvironments for zoospore attachment. Biofouling 26:941–952.

Long TC, Tajuba J, Sama P, Saleh N, Swartz C, Parker J, Hester S, Lowry GV, Veronesi B. 2007. Nanosize titanium dioxide stimulates reactive oxygen species in brain microglia and damages neurons in vitro. Environ. Health Perspect. 115:1631–1637.

Lonnen J, Kilvington S, Kehoe SC, Al-Touati F, McGuigan KG. 2005. Solar and photocatalytic disinfection of protozoan, fungal and bacterial microbes in drinking water. Water Res. 39:877–883.

Lopes TM, Barcarolli IF, de Oliveira CB, de Souza MM, Bianchini A. 2011. Effect of copper on ion content in isolated mantle cells of the marine clam *Mesodesma mactroides*. Environ. Toxicol. Chem. 30:1582–1585.

Lu Y, Allen HE. 2001. Partitioning of copper onto suspended particulate matter in river waters. Sci. Total Environ. 277:119–132.

Lupoi R, O'Neill W. 2010. Deposition of metallic coatings on polymer surfaces using cold spray. Surf. Coatings Technol. 205:2167–2173.

Lupoi R, O'Neill W. 2011. Powder stream characteristics in cold spray nozzles. Surf. Coatings Technol. 206:1069–1076.

Luscombe J, Braham RM, Maples ML. Credit Suisse, assignee. 1999 Aug 24. Seismic streamer. United States Patent 5,943,293 pp.10.

MacGuire JR. 2000. Review of the persistence, bioaccumulation and toxicity of tributyltin in aquatic environments in relation to Canada's toxic substances management policy. Water Qual. Res. J. Canada 35:633–679.

Madaeni SS, Ghaemi N. 2007. Characterization of self-cleaning RO membranes coated with TiO_2 particles under UV irradiation. J. Memb. Sci. 303:221–233.

Mance G. 1987. Toxicity of metals to marine life. In: Mance G, editor. Pollution threat of heavy metals in aquatic environments. Essex, UK: Elsevier Applied Science. p. 174–232.

Marshall DJ, Keough MJ. 2003. Variation in the dispersal potential of non-feeding invertebrate larvae: the desperate larva hypothesis and larval size. Mar. Ecol. Prog. Ser. 255:145–153.

Martin RC, George Dixon D, James Maguire R, Hodson PV, Tkacz RJ. 1989. Acute toxicity, uptake, depuration and tissue distribution of tri-n-butyltin in rainbow trout, *Salmo gairdneri*. Aquat. Toxicol. 15:37–51.

Martinelli E, Sarvothaman MK, Galli G, Pettitt ME, Callow ME, Callow JA, Conlan SL, Clare AS, Sugiharto B, Davies C, et al. 2012. Poly(dimethyl siloxane) (PDMS) network blends of amphiphilic acrylic copolymers with poly (ethylene glycol)-fluoroalkyl side chains for fouling-release coatings. II. Laboratory assays and field immersion trials. Biofouling 28:571–582.

Mawatari S. 1951. The natural history of a common fouling bryozoan, *Bugula neritina* (Linnaeus). Misc. Reports from Res. Inst. Nat. Resour. 20:47–54.

McKenzie LA, Brooks R, Johnston EL. 2011. Heritable pollution tolerance in a marine invader. Environ. Res. 111:926–932.

Mendez-Hermida F, Ares-Mazas E, McGuigan KG, Boyle M, Sichel C, Fernandez-Ibanez P. 2007. Disinfection of drinking water contaminated with *Cryptosporidium parvum* oocysts under natural sunlight and using the photocatalyst TiO_2. J. Photochem. Photobiol. B Biol. 88:105–111.

Mirabedini SM, Mohseni M, PazokiFard S, Esfandeh M. 2008. Effect of TiO_2 on the mechanical and adhesion properties of RTV silicone elastomer coatings. Colloids Surfaces A Physicochem. Eng. Asp. 317:80–86.

Moe H, Gaarder RH, Olsen A, Hopperstad OS. 2009. Resistance of aquaculture net cage materials to biting by Atlantic Cod (*Gadus morhua*). Aquac. Eng. 40:126–134.

Molino PJ, Campbell E, Wetherbee R. 2009a. Development of the initial diatom microfouling layer on antifouling and fouling-release surfaces in temperate and tropical Australia. Biofouling 25:685–694.

Molino PJ, Childs S, Eason Hubbard MR, Carey JM, Burgman MA, Wetherbee R. 2009b. Development of the primary bacterial microfouling layer on antifouling and fouling release coatings in temperate and tropical environments in Eastern Australia. Biofouling 25:149–162.

Molino PJ, Wetherbee R. 2008. The biology of biofouling diatoms and their role in the development of microbial slimes. Biofouling 24:365–379.

Muyssen BTA, De Schamphelaere KAC, Janssen CR. 2006. Mechanisms of chronic waterborne Zn toxicity in *Daphnia magna*. Aquat. Toxicol. 77:393–401.

Núñez L, Reguera E, Corvo F, González E, Vazquez C. 2005. Corrosion of copper in seawater and its aerosols in a tropical island. Corros. Sci. 47:461–484.

Omae I. 2003. Organotin antifouling paints and their alternatives. Appl. Organomet. Chem. 17:81–105.

Page HM, Dugan JE, Piltz F. 2010. Fouling and antifouling in oil and other offshore industries. In: Dürr S, Thomason JC, editors. Biofouling. Singapore: Wiley-Blackwell. p. 252–266.

Papyrin A, Kosarev V, Klinkov S, Alkimov A, Fomin V. 2007. Cold spray technology. Oxford, UK: Elsevier Science pp. 328.

Paspaltsis I, Berberidou C, Poulios I, Sklaviadis T. 2009. Photocatalytic degradation of prions using the photo-Fenton reagent. J. Hosp. Infect. 71:149–156.

Pattison J, Celotto S, Morgan R, Bray M, O'Neill W. 2007. Cold gas dynamic manufacturing: a non-thermal approach to freeform fabrication. Int. J. Mach. Tools Manuf. 47:627–634.

Pawlik JR. 1992. Chemical ecology of the settlement of benthic marine-invertebrates. Oceanogr. Mar. Biol. 30:273–335.

Petrone L, Di Fino A, Aldred N, Sukkaew P, Ederth T, Clare AS, Liedberg B. 2011. Effects of surface charge and Gibbs surface energy on the settlement behaviour of barnacle cyprids (*Balanus amphitrite*). Biofouling 27:1043–1055.

Phang IY, Aldred N, Clare AS, Vancso GJ. 2008. Towards a nanomechanical basis for temporary adhesion in barnacle cyprids (*Semibalanus balanoides*). J. R. Soc. Interface 5:397–401.

Pineda MC, McQuaid CD, Turon X, López-Legentil S, Ordóñez V, Rius M. 2012. Tough adults, frail babies: an analysis of stress sensitivity across early life-history stages of widely introduced marine invertebrates. PLoS One 7:e46672.

Pinho GLL, Pedroso MS, Rodrigues SC, de Souza SS, Bianchini A. 2007. Physiological effects of copper in the euryhaline copepod *Acartia tonsa*: waterborne versus waterborne plus dietborne exposure. Aquat. Toxicol. 84:62–70.

Piola RF, Dafforn KA, Johnston EL. 2009. The influence of antifouling practices on marine invasions. Biofouling 25:633–644.

Piola RF, Johnston EL. 2006a. Differential resistance to extended copper exposure in four introduced bryozoans. Mar. Ecol. Prog. Ser. 311:103–114.

Piola RF, Johnston EL. 2006b. Differential tolerance to metals among populations of the introduced bryozoan *Bugula neritina*. Mar. Biol. 148:997–1010.

Piola RF, Johnston EL. 2008. Pollution reduces native diversity and increases invader dominance in marine hard-substrate communities. Divers. Distrib. 14:329–342.

Poole AJ, de Nys R, King P, Gulizia S, Jahedi M. Commonwealth Scientific and Industrial Research Organisation, James Cook University, assignees. 2012 Jan 19. Surface treatment. International Patent WO 2012/006687. 56 pp.

Prendergast GS. 2010. Settlement and behaviour of marine fouling organisms. In: Dürr S, Thomason JC, editors. Biofouling. Oxford, UK: Blackwell Publishing Ltd. p. 30–51.

Qian P-Y, Xu Y, Fusetani N. 2010. Natural products as antifouling compounds: recent progress and future perspectives. Biofouling 26:223–234.

R Core Team. 2013. R: a language and environment for statistical computing. Vienna, Austria: R Foundation for Statistical Computing. Available from: http://www.r-project.org.

Ramus J, Venable M. 1987. Temporal ammonium patchiness and growth rate in *Codium* and *Ulva* (Ulvophyceae). J. Phycol. 23:518–523.

Rasmussen K, Østgaard K. 2001. Adhesion of the marine fouling diatom *Amphora coffeaeformis* to non-solid gel surfaces. Biofouling 17:103–115.

Rittschof D, Forward Jr RB, Cannon G, Welch JM, McClary Jr M, Holm ER, Clare AS, Conova S, McKelvey LM, Bryan P, van Dover CL. 1998. Cues and context: larval responses to physical and chemical cues. Biofouling 12:31–44.

Rivera-Duarte I, Rosen G, Lapota D, Chadwick DB, Kear-Padilla L, Zirino A. 2005. Copper toxicity to larval stages of three marine invertebrates and copper complexation capacity in San Diego Bay, California. Environ. Sci. Technol. 39:1542–1546.

Rosenhahn A, Ederth T, Pettitt ME. 2008. Advanced nanostructures for the control of biofouling: the FP6 EU integrated project AMBIO. Biointerphases 3:IR1–5.

Rüdel H. 2003. Case study: bioavailability of tin and tin compounds. Ecotoxicol. Environ. Saf. 56:180-189.

Scardino AJ, Guenther J, de Nys R. 2008. Attachment point theory revisited: the fouling response to a microtextured matrix. Biofouling 24:45–53.

Scardino AJ, Harvey E, de Nys R. 2006. Testing attachment point theory: diatom attachment on microtextured polyimide biomimics. Biofouling 22:55–60.

Scardino AJ, Hudleston D, Peng Z, Paul NA, de Nys R. 2009a. Biomimetic characterisation of key surface parameters for the development of fouling resistant materials. Biofouling 25:83–93.

Scardino AJ, de Nys R. 2004. Fouling deterrence on the bivalve shell *Mytilus galloprovincialis*: a physical phenomenon? Biofouling 20:249–257.

Scardino AJ, de Nys R. 2011. Mini review: biomimetic models and bioinspired surfaces for fouling control. Biofouling 27:73–86.

Scardino AJ, Zhang H, Cookson DJ, Lamb RN, de Nys R. 2009b. The role of nano-roughness in antifouling. Biofouling 25:757–767.

Scardino AJ. 2006. Biomimetic fouling control (PhD thesis). James Cook University.

Schultz MP, Bendick JA, Holm ER, Hertel WM. 2011. Economic impact of biofouling on a naval surface ship. Biofouling 27:87–98.

Schumacher JF, Carman ML, Estes TG, Feinberg AW, Wilson LH, Callow ME, Callow JA, Finlay JA, Brennan AB. 2007a. Engineered antifouling microtopographies - effect of feature size, geometry, and roughness on settlement of zoospores of the green alga *Ulva*. Biofouling 23:55–62.

Schumacher JF, Aldred N, Callow ME, Finlay JA, Callow JA, Clare AS, Brennan AB. 2007b. Species-specific engineered antifouling topographies: correlations between the settlement of algal zoospores and barnacle cyprids. Biofouling 23:307–317.

Sexton BA, Marnock RJ. 2000. Characterization of high resolution resists and metal shims by scanning probe microscopy. Microsc. Microanal. 6:129–136.

Smith RC, Prezelin BB, Baker KS, Bidigare RR, Boucher NP, Coley T, Karentz D, Macintyre S, Matlick HA, Menzies D, et al. 1992. Ozone depletion: ultraviolet radiation and phytoplankton biology in antarctic waters. Science 255:952–959.

Sokmen M, Degerli S, Aslan A. 2008. Photocatalytic disinfection of Giardia intestinalis and *Acanthamoeba castellani* cysts in water. Exp. Parasitol. 119:44–48.

Stoltenhoff T, Kreye H, Richter HJ. 2002. An analysis of the cold spray process and its coatings. J. Therm. Spray Technol. 11:542–550.

Svane I, Cheshire A, Barnett J. 2006. Test of an antifouling treatment on tuna fish-cages in Boston Bay, Port Lincoln, South Australia. Biofouling 22:209–219.

Swain G, Herpe S, Ralston E, Tribou M. 2006. Short-term testing of antifouling surfaces: the importance of colour. Biofouling 22:425-429.

Sweat LH, Johnson KB. 2013. The effects of fine-scale substratum roughness on diatom community structure in estuarine biofilms. Biofouling 28:879–890.

Terlizzi A, Faimali M. 2010. Fouling on artificial substrata. In: Dürr S, Thomason JC, editors. Biofouling. Oxford, UK: Blackwell Publishing Ltd. p. 170–184.

Terlizzi A, Fraschetti S, Gianguzza P, Faimali M, Boero F. 2001. Environmental impact of antifouling technologies: state of the art and perspectives. Aquat. Conserv. Mar. Freshw. Ecosyst. 11:311–317.

Thiyagarajan V, Harder T, Qian P-Y. 2002. Effect of the physiological condition of cyprids and laboratory-mimicked seasonal conditions on the metamorphic successes of *Balanus amphitrite* Darwin (Cirripedia; Thoracica). J. Exp. Mar. Bio. Ecol. 274:65–74.

Thomas K V. 2009. The use of broad-spectrum organic biocides in marine antifouling paints. In: Hellio C, Yebra D, editors. Advances in marine antifouling coatings and technologies. Cambridge, UK: Woodhead Publishing Ltd. p. 522–553.

Thomas KV, Brooks S. 2010. The environmental fate and effects of antifouling paint biocides. Biofouling 26:73–88.

Thomason JC, Letissier MDA, Thomason PO, Field SN. 2002. Optimising settlement tiles: the effects of surface texture and energy, orientation and deployment duration upon the fouling community. Biofouling 18:293–304.

Tóth S, Becker-van Slooten K, Spack L, de Alencastro LF, Tarradellas J. 1996. Irgarol 1051, an antifouling compound in freshwater, sediment, and biota of Lake Geneva. Bull. Environ. Contam. Toxicol. 57:426–433.

Townsin RL, Anderson CD. 2009. Fouling control coatings using low surface energy, foul release technology. In: Hellio C, Yebra D, editors. Advances in marine antifouling coatings and technologies. Cambridge, UK: Woodhead Publishing Ltd. p. 693–708.

Townsin RL. 2003. The ship hull fouling penalty. Biofouling 19 Suppl:9–15.

Unabia CRC, Hadfield MG. 1999. Role of bacteria in larval settlement and metamorphosis of the polychaete *Hydroides elegans*. Mar. Biol. 133:55–64.

Valkirs AO, Seligman PF, Haslbeck E, Caso JS. 2003. Measurement of copper release rates from antifouling paint under laboratory and *in situ* conditions: implications for loading estimation to marine water bodies. Mar. Pollut. Bull. 46:763–779.

Vignaux J-J. Sercel, assignee. 2010 Jan 28. Seismic streamer formed of sections comprising a main sheath covered with an external sheath formed using a thermoplastic material loaded with a biocide material. United States patent US 2010/0,020,644.

Voulvoulis N, Scrimshaw MD, Lester JN. 1999. Review Alternative Antifouling Biocides. Appl. Organomet. Chem. 13:135–143.

Vucko MJ, King PC, Poole AJ, Carl C, Jahedi MZ, de Nys R. 2012. Cold spray metal embedment: an innovative antifouling technology. Biofouling 28:239–248.

Vucko MJ, King PC, Poole AJ, Jahedi MZ, de Nys R. 2013a. Polyurethane seismic streamer skins: an application of cold spray metal embedment. Biofouling 29:1–9.

Vucko MJ, Poole AJ, Carl C, Sexton BA, Glenn FL, Whalan S, de Nys R. 2014. Using textured PDMS to prevent settlement and enhance release of marine fouling organisms. Biofouling 30:1–16.

Vucko MJ, Poole AJ, Sexton BA, Glenn FL, Carl C, Whalan S, de Nys R. 2013b. Combining a photocatalyst with microtopography to develop effective antifouling materials. Biofouling 29:751–762.

Wang S, Ang HM, Tade MO. 2007. Volatile organic compounds in indoor environment and photocatalytic oxidation: state of the art. Environ. Int. 33:694–705.

Watts RJ, Kong S, Orr MP, Miller GC, Henry BE. 1995. Photocatalytic inactivation of coliform bacteria and viruses in secondary wastewater effluent. Water Res. 29:95–100.

Webster DC, Chisholm BJ. 2010. New directions in antifouling technology. In: Dürr S, Thomason JC, editors. Biofouling. Oxford, UK: Blackwell Publishing Ltd. p. 366–387.

Weidenhaupt A, Arnold C, Müller SR, Haderlein SB, Schwarzenbach RP. 1997. Sorption of organotin biocides to mineral surfaces. Environ. Sci. Technol. 31:2603–2609.

Wendt DE, Kowalke GL, Kim J, Singer IL. 2006. Factors that influence elastomeric coating performance: the effect of coating thickness on basal plate morphology, growth and critical removal stress of the barnacle *Balanus amphitrite*. Biofouling 22:1–9.

Woods Hole Oceanographic Institute. 1952a. The history of the prevention of fouling. In: Marine fouling and its prevention. Annapolis, MD: U. S. Naval Institute. p. 211–223.

Woods Hole Oceanographic Institute. 1952b. The fouling of metallic surfaces. In: Marine fouling and its prevention. Annapolis, MD: U. S. Naval Institute. p. 349–364.

Xu J, Sun Y, Zhao Y, Huang J, Chen C, Jiang Z. 2007. Photocatalytic inactivation effect of gold-doped TiO_2 (Au/TiO_2) nanocomposites on human colon carcinoma LoVo cells. Int. J. Photoenergy 2007:1–7.

Yebra DM, Kiil S, Dam-Johansen K. 2004. Antifouling technology - past, present and future steps towards efficient and environmentally friendly antifouling coatings. Prog. Org. Coatings 50:75–104.

Zargiel KA, Coogan JS, Swain GW. 2011. Diatom community structure on commercially available ship hull coatings. Biofouling 27:955–965.

Zhang H, Lamb R, Lewis J. 2005. Engineering nanoscale roughness on hydrophobic surface—preliminary assessment of fouling behaviour. Sci. Technol. Adv. Mater. 6:236–239.

Zhang Y-F, Kitano Y, Nogata Y, Zhang Y, Qian P-Y. 2012. The mode of action of isocyanide in three aquatic organisms, *Balanus amphitrite*, *Bugula neritina* and *Danio rerio*. PLoS One 7:e45442.

Zhao J, Krishna V, Hua B, Moudgil B, Koopman B. 2009. Effect of UVA irradiance on photocatalytic and UVA inactivation of *Bacillus cereus* spores. J. Photochem. Photobiol. B Biol. 94:96–100.

Zhu X, Huang G, Lin L, Liu D. 2008. Long term corrosion characteristics of metallic materials in marine environments. Corros. Eng. Sci. Technol. 43:328–334.

Appendix

Biofouling, 2014
Vol. 30, No. 1, 1–16, http://dx.doi.org/10.1080/08927014.2013.836507

Taylor & Francis
Taylor & Francis Group

Using textured PDMS to prevent settlement and enhance release of marine fouling organisms

M.J. Vucko[a]*, A.J. Poole[b], C. Carl[a], B.A. Sexton[c], F.L. Glenn[c], S. Whalan[d] and R. de Nys[a]

[a]*School of Marine & Tropical Biology, James Cook University, Townsville, Australia;* [b]*CSIRO Materials Science and Engineering, Geelong, Australia;* [c]*CSIRO Materials Science and Engineering, Clayton, Australia;* [d]*School of Environment, Science and Engineering, Marine Ecology Research Centre, Southern Cross University, Lismore, Australia*

(*Received 1 July 2013; accepted 16 August 2013*)

The antifouling efficacy of a series of 18 textured (0.2–1000 μm) and non-textured (0 μm) polydimethylsiloxane surfaces with the profiles of round- and square-wave linear grating was tested by recording the settlement of fouling organisms in the laboratory and in the field by monitoring the recruitment of a multi-species fouling community. In laboratory assays, the diatoms *Nitzschia closterium* and *Amphora* sp. were deterred by all surface topographies regardless of texture type. Settlement of propagules *of Ulva* sp. was lower on texture sizes less than the propagule size, and settlement of larvae of *Saccostrea glomerata* and *Bugula neritina* was lower on texture sizes closest to, but less than, the sizes of larvae. After a six month field trial, all textured surfaces lost their deterrent effect; however, the foul-release capabilities of textures were still present. High initial attachment was correlated with most fouling remaining after removal trials, indicating that fouling organisms recruited in higher numbers to surfaces upon which they attached most strongly.

Keywords: polydimethylsiloxane; silicone; texture; antifouling; topography

*Corresponding author: Email: matthew.vucko@my.jcu.edu.au

Biofouling, 2013
Vol. 29, No. 7, 751–762, http://dx.doi.org/10.1080/08927014.2013.803193

Taylor & Francis
Taylor & Francis Group

Combining a photocatalyst with microtopography to develop effective antifouling materials

M.J. Vucko[a]*, A.J. Poole[b], B.A. Sexton[c], F.L. Glenn[c], C. Carl[a], S. Whalan[d] and R. de Nys[a]

[a]*Centre for Sustainable Tropical Fisheries and Aquaculture, School of Marine & Tropical Biology, James Cook University, Townsville, Australia;* [b]*CSIRO Materials Science and Engineering, Waurn Ponds, Australia;* [c]*CSIRO Materials Science and Engineering, Clayton, Australia;* [d]*Marine Ecology Research Centre, School of Environment, Science and Engineering, Southern Cross University, Lismore, Australia*

(*Received 24 February 2013; final version received 29 April 2013*)

Polydimethylsiloxane surfaces textured with a square-wave linear grating profile (0, 20, 200, 300 and 600 μm), and embedded with a range of photocatalytic titanium dioxide (TiO_2) nanoparticle loadings (3.75, 7.5, 11.25 and 15 wt.%), were used to test the combined efficacy of these technologies as antifouling materials. Settlement of the fouling bryozoan species *Bugula neritina* was quantified in the laboratory under two intensities of UV light. The lowest settlement rates were observed on 20 μm surfaces. However, texture effects were not as critical to larval settlement as the presence of TiO_2. In conjunction with UV light, TiO_2 completely inhibited larval metamorphosis even at the lowest loading (3.75 wt.%) and the lowest intensity of UV light (24 W m^{-2}). Recruitment of *B. neritina* was also quantified in field trials and showed similar results to laboratory assays. The lowest recruitment was observed on 20 and 200 μm surfaces, with recruitment being significantly lower on all surfaces containing TiO_2. Therefore for *B. neritina,* although all TiO_2 loadings were effective, 3.75 wt.% can be used as a minimum inhibitory concentration to deter larval settlement and the addition of a 20 μm texture further increases the deterrent effect.

Keywords: bryozoan; *Bugula neritina*; *Hydroides elegans*; PDMS; titanium dioxide; photocatalysis

*Corresponding author. Email: matthew.vucko@my.jcu.edu.au

Biofouling
Vol. 28, No. 3, March 2012, 239–248

Taylor & Francis
Taylor & Francis Group

Cold spray metal embedment: an innovative antifouling technology

M.J. Vucko[a]*, P.C. King[b], A.J. Poole[c], C. Carl[a], M.Z. Jahedi[b] and R. de Nys[a]

[a]*School of Marine & Tropical Biology, James Cook University, Townsville, Queensland, Australia;* [b]*CSIRO Materials Science and Engineering, Clayton, Victoria, Australia;* [c]*CSIRO Materials Science and Engineering, Belmont, Victoria, Australia*

(*Received 21 December 2011; final version received 13 February 2012*)

The study demonstrates that embedment of copper particles into thermoplastic polymers (polymers) using cold spray technology is an effective deterrent against fouling organisms. Two polymers, high-density polyethylene (HDPE) and nylon were metallised with copper powder using cold spray technology. After 250 days in the field, Cu-embedded HDPE and copper plate controls were completely free of hard foulers compared to Cu-embedded nylon and polymer controls which were heavily fouled with both soft and hard fouling. Antifouling (AF) success is related to the interaction between the properties of the polymers (elastic modulus and hardness) and the cold spray process which affect particle embedment depth, and subsequently, the release of copper ions as determined by analytical techniques. Embedding metal using cold spray equipment is shown to be an effective AF technology for polymers, in particular those that are difficult to treat with standard AF coatings, with efficacy being a function of the interaction between the cold spray metal and the polymer recipient.

Keywords: antifouling; biofouling; copper; polymer; HDPE; nylon

*Corresponding author. Email: matthew.vucko@my.jcu.edu.au

ISSN 0892-7014 print/ISSN 1029-2454 online

http://dx.doi.org/10.1080/08927014.2012.670849
http://www.tandfonline.com

Biofouling, 2013
Vol. 29, No. 1, 1–9, http://dx.doi.org/10.1080/08927014.2012.741682

Taylor & Francis
Taylor & Francis Group

Polyurethane seismic streamer skins: an application of cold spray metal embedment

M.J. Vucko[a]*, P.C. King[b], A.J. Poole[c], M.Z. Jahedi[b] and R. de Nys[a]

[a]*Centre for Sustainable Tropical Fisheries and Aquaculture, School of Marine and Tropical Biology, James Cook University, Townsville, Queensland, Australia;* [b]*CSIRO Materials Science and Engineering, Clayton, Victoria, Australia;* [c]*CSIRO Materials Science and Engineering, Belmont, Victoria, Australia*

(*Received 9 July 2012; final version received 15 October 2012*)

Cold spray metal embedment is an innovative antifouling (AF) technology that delivers metal particles with AF properties into many thermoplastic polymers. AF efficacy was quantified for low (22.1 ± 4.8 g m^{-2}) and high (101.1 ± 10.8 g m^{-2}) densities of copper particles embedded into polyurethane (PU) seismic streamer skins, which are used in geophysical exploration. Failure of each Cu-embedded treatment was defined as settlement of hard foulers. Low-density streamers failed after 42 days while high-density streamers failed after 210 days. Most importantly, the high-density streamers were completely free of hard foulers including the barnacle *Amphibalanus reticulatus* during this time period. In conclusion, cold-spray metal embedment is an effective AF technology for PU seismic streamer skins, under intense fouling conditions. Higher copper particle densities enhance AF longevity and the effect of density provides a tool to extend efficacy and enhance AF performance for specific polymers.

Keywords: antifouling; biofouling; cold spray metals; copper; thermoplastic polymers

*Corresponding author. Email: matthew.vucko@my.jcu.edu.au

Biofouling, 2014
Vol. 30, No. 6, 651–666, http://dx.doi.org/10.1080/08927014.2014.906584

Taylor & Francis
Taylor & Francis Group

Assessing the antifouling properties of cold-spray metal embedment using loading density gradients of metal particles

M.J. Vucko[a]*, P.C. King[b], A.J. Poole[c], Y. Hu[d], M.Z. Jahedi[b] and R. de Nys[a]

[a]*Centre for Sustainable Tropical Fisheries and Aquaculture, School of Marine and Tropical Biology, James Cook University, Townsville, Australia;* [b]*CSIRO Materials Science and Engineering, Clayton, Australia;* [c]*CSIRO Materials Science and Engineering, Waurn Ponds, Geelong, Australia;* [d]*Advanced Analytical Centre, James Cook University, Townsville, Australia*

(*Received 28 January 2014; accepted 11 March 2014*)

Particles of copper, bronze and zinc were embedded into a polymer using cold-spray technology to produce loading density gradients of metal particles. The gradients were used to identify the species with the highest tolerance to the release of copper and zinc ions. The gradients also established the minimum effective release rates (MERRs) of copper and zinc ions needed to prevent the recruitment of fouling under field conditions. *Watersipora* sp. and *Simplaria pseudomilitaris* had the highest tolerances to the release of metal ions. Copper and bronze gradient tubes were similar in their MERRs of copper ions against *Watersipora* sp. (0.058 g m^{-2} h^{-1} and 0.054 g m^{-2} h^{-1}, respectively) and against *S. pseudomilitaris* (0.030 g m^{-2} h^{-1} and 0.025 g m^{-2} h^{-1}, respectively). Zinc was not an effective antifoulant, with failure within two weeks. In conclusion, cold-spray gradients were effective in determining MERRs and these outcomes provide the basis for the development of cold-spray surfaces with pre-determined life-spans using controlled MERRs.

Keywords: minimum effective release rate; metal ion tolerance; polymer; *Watersipora* sp.; copper; bronze

*Corresponding author. Email: matthew.vucko@my.jcu.edu.au